

DOCTORAL DISSERTATION

**Development of high-performance SiC-based membranes
derived from preceramic precursors and application to gas
separation and pervaporation**

(プレセラミック前駆体を用いた高性能 SiC 膜の開発とガス分離および浸透気化分離への応用)

Qing Wang

Supervisors: Toshinori Tsuru

Department of Chemical Engineering,

Graduate school of Engineering, Hiroshima University

(広島大学大学院工学研究科 化学工学専攻)

September, 2020

CONTENTS

Chapter 1 General introduction	1
1.1 Membrane separation technology	1
1.2 Types of membranes	2
1.3 Membrane processes	4
1.4 Transport mechanisms in gas separation and PV processes	6
1.4.1 General mechanisms in gas separation	6
1.4.2 General mechanisms in PV	9
1.5 Inorganic membranes	11
1.5.1 Silica-based membranes	12
1.5.2 Silicon carbide-based membranes	14
1.6 Scope of this thesis	25
References	31
Chapter 2 Development and microstructure tuning of conventional SiC-based membranes derived from polycarbosilane	44
2.1 Introduction	44
2.2 Experimental	46
2.2.1 Preparation of cured and pyrolyzed PCS powders	46
2.2.2 Fabrication of the PCS-derived membrane	47
2.2.3 Characterization of PCS powders and PCS membranes	48
2.3 Results and discussion	49
2.3.1 Physicochemical properties of PCS	49
2.3.2 PCS-derived membranes	66
2.4 Conclusions	80
References	82
Chapter 3 Development of high-performance sub-nanoporous SiC-based membranes derived from polytitanocarbosilane: Effect of pyrolysis temperature	90
3.1 Introduction	90
3.2 Experimental	93
3.2.1 Preparation of TiPCS powders	93
3.2.2 Fabrication of the TiPCS-derived membranes	94
3.2.3 Characterization of TiPCS powders and membranes	94
3.2.4 Gas permeation measurement	95
3.3 Results and discussion	97
3.3.1 Physicochemical characterization of the TiPCS precursor	97
3.3.2 Fabrication and reproducibility of TiPCS-derived membranes	108
3.3.3 PV Performance of the TiPCS-derived membrane	114
3.4 Conclusions	121
References	123
Chapter 4 Study on the effect of oxidative cross-linking on the structure and performance of polytitanocarbosilane-derived SiC-based membranes	132
4.1 Introduction	132
4.2 Experimental	135

4.2.1 Preparation of cross-linked TiPCS powders.....	135
4.2.2 Fabrication of a TiPCS-derived membrane.....	135
4.2.3 Characterization of TiPCS powders and membranes.....	136
4.2.4 Single-gas permeation, pervaporation, and H ₂ O/N ₂ separation measurements	137
4.3 Results and Discussion.....	138
4.3.1 Cross-linking behavior of the TiPCS polymer.....	138
4.3.2 Characterization of TiPCS powders fired at different temperatures.....	140
4.3.3 Membrane fabrication.....	150
4.3.4 Pervaporation performance of cross-linked TiPCS membranes.....	157
4.3.5 H ₂ O/N ₂ separation at high temperature.....	162
4.4 Conclusions.....	165
References.....	167
Chapter 5 Conclusions.....	178
5.1 Summary of this study.....	178
5.2 Recommendations.....	181
List of Publications.....	184
Acknowledgements.....	185

Chapter 1

General introduction

1.1 Membrane separation technology

Today, membrane-based separation processes are widely used in our day-to-day activities from the petrochemical, food, biotechnology, and pharmaceutical industries, and in a range of environmental uses, including water treatment, desalination, and gas separations. Their simplicity and cost efficiency have made them very popular and widely spread in their applications [1]. For instance, membrane technology offers superior economics compared to conventional separation techniques, and it is estimated that the use of membranes can decrease energy costs by as much as 30% when compared with conventional, energy-intensive technologies [2]. Because the cost-effectiveness of membrane technology, for example, in the case of gas separation, is attributed to the ability to allow gasses to be treated in a single-stage/-phase as opposed to the multiple stages (e.g., pressurizing, depressurizing and purging) needed for conventional pressure swing adsorption systems or different phases (gas and liquid), which are common in commercialized cryogenic separation methods.

A membrane, described as a semi-permeable active or passive barrier that selectively permits specific species to pass through to the permeate stream, while being able to retain most of the impermeable species in the retentate/feed stream with characteristic advantages of low energy consumption, low operation cost and small

foot print [3]. A general definition of membrane for binary mixtures is as demonstrated in Fig. 1-1.

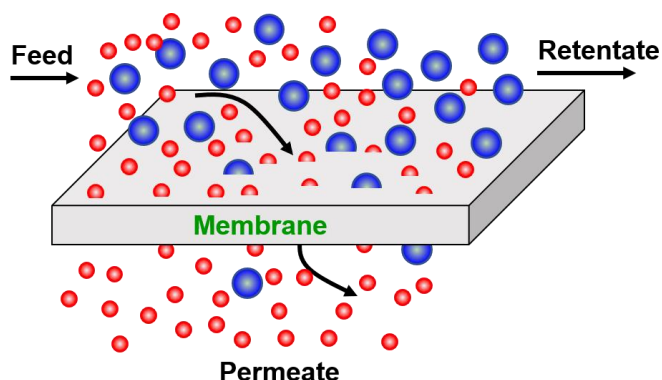


Fig. 1-1 Schematic of membrane separation for binary mixtures.

1.2 Types of membranes

Generally speaking, membranes can be roughly categorized into two classes based on their morphology (isotropic or anisotropic) and the material (inorganic or organic) used for their synthesis as shown in Fig. 1-2 [1]. According to the morphology of the membranes, it is further divided into two groups, namely, isotropic and anisotropic membranes. The typical schematic diagrams of the isotropic and anisotropic membranes are shown in Fig. 1-3 [4, 5]. The isotropic membranes have a homogenous composition and their structure is composed of a single material. On the contrary, anisotropic membranes have a heterogeneous composition both in their chemical composition as well as in their structure. Anisotropic membranes consist of an extremely thin surface layer (separation layer) supported on a thicker, porous substructure, which usually also has a heterogeneous chemical composition and

structure (multilayer structure, e.g., the intermediate layer, particle layer, and porous support). The separation properties and permeability of the membrane are determined only by the surface layer/separation layer; the substructure serves as mechanical support. Anisotropic membranes have the advantage of higher fluxes, so that almost all commercial processes use this type of membrane [4].

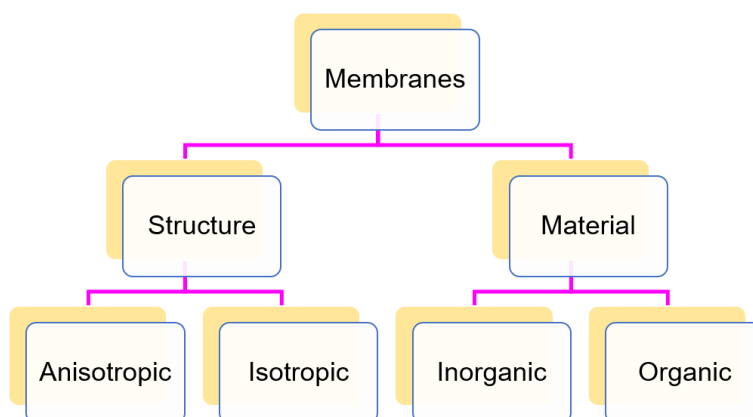


Fig. 1-2 Membrane categories based on their structure and material [1].

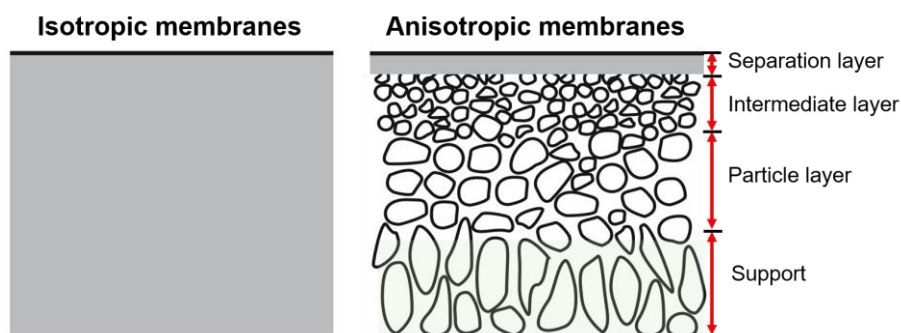


Fig. 1-3 Schematic diagrams of the isotropic and anisotropic membranes [4].

On the other hand, membranes can be classified into organic membranes (polymeric membranes) and inorganic membranes based on synthetic materials. Organic membranes are usually made of polymers such as polysulfone, cellulose

acetate, polyimide, polyetherimide, polycarbonate, and polydimethylsiloxane. In a broad term, inorganic membranes consist of ceramic, carbon, and metal membranes [6, 7]. Among them, ceramic membranes are usually made from typical metal oxides (e.g., alumina (Al_2O_3), titania (TiO_2), zirconia (ZrO_2) and silica (SiO_2)), zeolite, MOFs, non-oxides (such as silicon carbide (SiC)) as well as the composites of combinations of oxides and non-oxides (e.g., SiCO) [1]. Since polymeric membranes often suffer from low mechanical stability and fouling problems, while inorganic membranes possess better properties such as high chemical, thermal and mechanical stabilities, which make them suitable for use under harsh conditions, such as corrosive and high-temperature environments [8, 9]. Due to the advantages of inorganic membranes, this thesis is primarily concerned with their synthesis techniques and their applications in gas separation and pervaporation (PV).

1.3 Membrane processes

In a broad term, membrane separation processes could be categorized into several types based on the phase species (e.g., liquid or gaseous) of the components in both feed and permeate side and based on the pore size of the membranes. For one case where both the feed and permeate streams are a liquid phase and the driving force is a pressure difference (e.g., application in saline water treatment), the separation processes involved are as follows: microfiltration (MF), ultrafiltration (UF), nanofiltration (NF) and reverse osmosis (RO) membranes. Fig. 1-4 shows the general

description of these four membrane processes with their pore sizes and pore types. RO process enjoys many advantages which make it an attractive technology for seawater desalination because of its high-water recovery rate and salt rejection rate, which is attributed to their narrow pore sizes of 0.3-0.6 nm [10].

In addition to RO, most pervaporation (PV) and gas separation membranes also use the membranes with pore sizes of < 0.6 nm to perform the separation. The PV process is typically identified as that the feed stream is in the liquid phase while the permeate stream is a gaseous/vapor phase by evacuation. Pervaporation provides the possibility of separating closely boiling mixtures (or azeotropes) that are difficult to separate by distillation or other means. For the case of gas separation where both feed and permeate streams are in the gas phases. MF, UF, NF, and RO processes in terms of water treatment have been extensively studied, well developed, and the market is served by a number of experienced companies [4]. However, gas separation and PV are relatively new membrane processes, which are developing rapidly with increasing attention. Therefore, gas separation and PV processes were the main fields involved in this study.

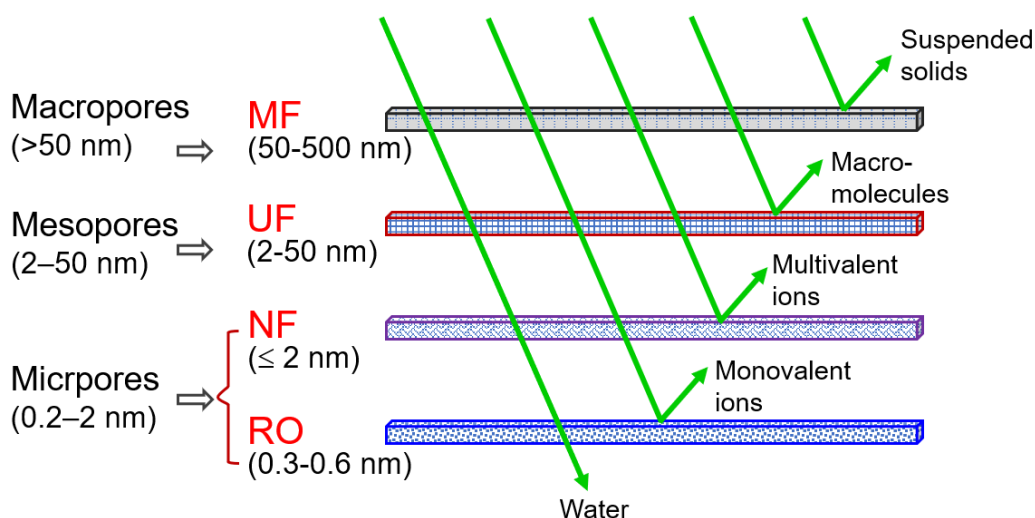


Fig. 1-4 General descriptions of RO, NF, UF, and MF membrane processes with their pore sizes and pore types.

1.4 Transport mechanisms in gas separation and PV processes

In the past decades, the successful synthesis of a variety of good quality membranes promoted extensive experimental and theoretical studies on the transport mechanism through these membranes. The theory of transportation mechanism, which is essential not only for a better understanding of the process itself but also for design purposes. Considering the scope of this thesis, here we introduce the general transport mechanisms in gas separation and PV processes for inorganic membranes.

1.4.1 General mechanisms in gas separation

In membrane science, performance is most commonly associated with two properties, permeance (or permeability) and selectivity. The permeability refers to the

intrinsic ability of a membrane to allow passage of a gas specie and relates the molar flux to the driving force, which is usually expressed by the difference in pressure or concentration across the membrane. The ideal selectivity is obtained most simply by the ratio of the single-gas permeances (or permeabilities) that are measured on the same conditions. However, gas permeation through a microporous inorganic membrane is a process combining adsorption and diffusion. The permeation process even for the single gas permeation is complex involving a variety of phenomena. On the other hand, the actual selectivity in a gas mixture could strongly deviate from the ideal selectivity due to interactions between species with each other or with the membrane walls. Therefore, the ideal selectivity should be considered as a limiting case approximation.

Gas transport in membranes can occur through a number of possible mechanisms [11]. According to the properties of both permeants and membranes, various transport mechanisms have been proposed for gas transport across membranes [11, 12]. Fig. 1-5 illustrates a schematic representation of the mechanisms for the permeation of gases through porous as well as dense membranes. For the porous membranes, it includes Knudsen diffusion, surface diffusion, and molecular sieving, while for the dense membranes, it is the solution-diffusion mechanism [13-15].

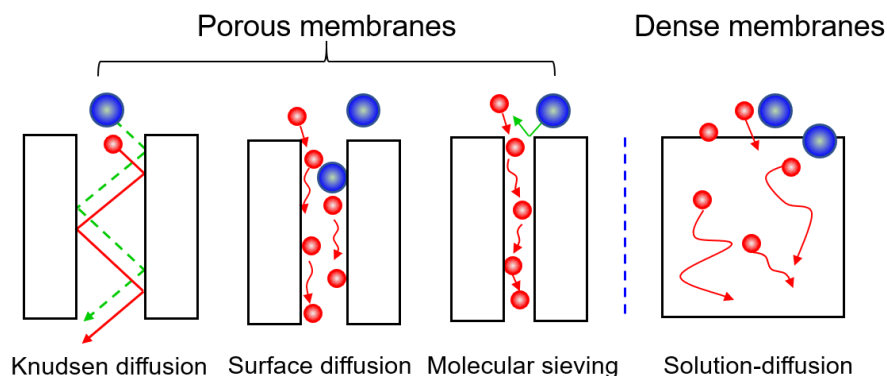


Fig. 1-5 Schematic presentation of mechanisms for permeation of gases through membranes.

Knudsen diffusion occurs when the pore size diameter of the membrane is smaller than the mean free path (i.e., the distance between collisions that primarily occurs between gas molecules and the pore walls) of the gas species [12, 16]. Depending on the types of gases, the free path is fixed using the molecular weight, temperature, and pressure. Different gas species move at different velocities; therefore, the separation is achieved. The selectivity in Knudsen diffusion can be estimated from the square root of the ratio of the molecular weights. From a practical application point of view, gas separation membranes only based on the Knudsen diffusion mechanism are not commercially attractive due to their low selectivity.

Surface diffusion occurs at low temperatures when gas molecules cannot escape from the surface potential field. It occurs in three steps: (1) gas molecules adsorb onto the surface of the membrane at the pore entrance, (2) diffuse through the membrane, adsorbed molecules migrate along the pore walls, and (3) desorb at the pore exit [11, 16]. This diffusion can usually occur together with Knudsen diffusion. The gas adsorption reduces the effective pore diameter, consequently, the transport of

nonadsorbing gas molecules is reduced. Surface diffusion can enhance the permeability and selectivity for the gas that can be strongly adsorbed to the pore walls.

Molecular sieving operates on a size-exclusion principle. If the pore sizes of membranes are small enough (in the range of 0.3-0.6 nm), molecular sieving can be used to separate molecules with different kinetic diameters, and only small molecular gases can be allowed to pass through the membrane. However, as the pore sizes decrease, the porosity of the membrane is expected to decrease, resulting in increased resistance across the membrane and reduced gas flux. Therefore, the pore size and porosity should be balanced to produce an efficient membrane.

The mechanism of gas separation using a non-porous membrane is different from that using a porous membrane. The solution-diffusion mechanism is the most commonly used model to explain gas transport through dense membranes. The solution-diffusion mechanism is described as follows: gas molecules or atoms adsorbed on the upstream boundary permeate through the membrane and desorb on the other side of the membrane. This separation mechanism is based on both solubility and mobility of gas molecules in membranes.

Generally, molecules diffuse through the membrane by more than one mechanism based on the properties of both permeants and membranes.

1.4.2 General mechanisms in PV

Pervaporation (PV) has been widely used to separate close-boiling point

mixtures or azeotropes. PV process has better separation capacity and energy efficiency than competing distillation, adsorption, and extraction technologies and their applications could lead to 40-60% energy reductions [17].

In PV, a liquid mixture contacts one side of a membrane (feed side), and the permeate is removed as a vapor from the other (permeate side). Transport through the membrane is induced by the vapor pressure difference between the feed solution and the permeate vapor, which is maintained by the low vapor pressure on the permeate side generated by cooling and condensing the permeate vapor [4, 18, 19]. Because the PV process involves changes in the liquid-vapor phase, the process is usually accompanied by stable heating [20].

In a pervaporation process, transport through the porous membranes is generally described by a so-called 'adsorption-diffusion mechanism' which can also be simply described by 3 consecutive steps (as represented schematically in Fig. 1-6) [19, 21]:

- (1) Selective sorption of the species in the liquid mixture at the interface between feed and the membrane;
- (2) Diffusion of the permeating components through the membrane due to concentration gradient;
- (3) Desorption of the permeating components at the interface between the membrane and permeate into the vapor phase permeate side.

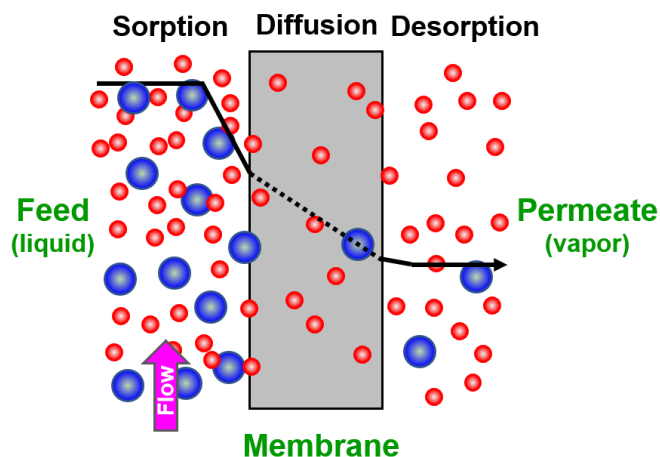


Fig. 1-6 Schematic pervaporation process of a binary mixture through a porous membrane based on the solution-diffusion mechanism.

According to this mechanism, the dominant steps are the sorption and the diffusion (or one of the two), whereas the desorption step is very fast since vacuum or sweeping gas is applied to remove the diffused components [19, 21]. The first two steps are also responsible for the final permselectivity [22].

1.5 Inorganic membranes

Polymeric membranes have been developed for a variety of industrial applications due to the lower cost. However, polymeric membranes suffer from low mechanical stability and fouling problems. Compared to polymeric materials, inorganic membranes receive significant attention from both academia and industry as they possess better properties such as high chemical, thermal and mechanical stabilities, and show great potential in several important applications, such as MF, UF, NF, RO, gas separation and PV [4, 23]. In this thesis, we mainly introduce the

extensively investigated amorphous Silica (SiO_2)-based membranes as well as the emerging amorphous SiC-based membranes.

1.5.1 Silica-based membranes

Silica-based/silica membranes have been widely utilized in gas separation and pervaporation applications because the appropriate cavity size can be successfully controlled through chemical vapor deposition or sol-gel techniques. Their amorphous structure is a great advantage in the formation of highly permeable thin-films [24, 25]. One advantage is that the pore structure of the silica membrane is controllable, and the permeation performance can correspondingly be adjusted [26]. According to molecular dynamic simulation, conventional amorphous SiO_2 membranes consist of pores ranging from 0.3-0.4 nm, which makes them suitable for the separation of small molecule mixtures such as H_2/N_2 and H_2/CO_2 , but may not be suitable for the separation of small-to-medium-sized molecules from large molecules such as N_2/SF_6 due to the high resistance caused by the small pores [24, 25, 27-30]. In the hydrogen separation, silica membranes generally show H_2 permeances ranging from 10^{-6} - 10^{-8} mol/(m^2 s Pa) with selectivities (e.g., H_2/N_2 , H_2/CH_4 , and H_2/CO_2) over hundreds to thousands, which are sufficient for the demands of industrial separations.

However, silica membranes are reportedly densified under a hydrothermal atmosphere, particularly at high temperatures [24, 25, 27, 28]. This is because water molecules can degrade the silica network by hydrolysis of Si-O-Si even at low

temperatures, resulting in severe degradation with a loss of separation ability [31, 32]. To address this problem, researchers have attempted to modify the surface properties of the silica, to minimize the interaction of water molecules with the membrane structure [33]. One strategy to solve this challenging problem is introducing organic groups into the pure silica structure [32, 34]. Castricum et al. developed a new type of membranes categorized as silsesquioxane ($\text{RSiO}_{1.5}$) derived from organoalkoxysilanes to enhance the hydrothermal stability and allow tuning of the network structures that could overcome the drawbacks of silica membranes [34].

These types of membranes with organosilica networks were given names such as organic-inorganic silica membrane, organosilica membranes, or silica-based membrane. For example, the addition of organic groups of $-\text{CH}_2-$, $-(\text{CH}_2)_2-$, $-(\text{CH}_2)_3-$, $-(\text{CH}_2)_6-$, $-(\text{CH}_2)_8-$, and phenyl as bridged types have been reported to increase the hydrothermal stability and tune the pore size of membranes [30, 35-37]. These types of organosilica membranes showed good performance in gas separation, PV, and RO applications. Furthermore, recently, our group reported an organosilica membrane (BTESE) for the separation of steam/non-condensable gas mixtures at temperatures ranging from 80 to 200 °C, which confirmed the hydrothermal stability and showed promise for their future applications in humid gas separation [38]. However, organosilica membranes also have their inherent limitations, for example, when they are used at high temperatures or in the presence of oxygen, the effectiveness of organosilica membranes could be limited due to decomposition or oxidation of the organic linking units [39].

1.5.2 Silicon carbide-based membranes

1.5.2.1 Silicon carbide-based ceramics

Silicon carbide (SiC) attracts much attention as key engineering components in many advanced technology programs, primarily due to its high levels of mechanical strength, structural stability, and chemical stability, and also its reliability at room and elevated temperatures [40-43]. The traditional method for the preparation of ceramics involves powder technology [44]. However, significant progress in the fabrication of SiC-based ceramic was achieved by the pioneering work of Yajima et al. [45] via the pyrolysis of a preceramic polymer polycarbosilane (PCS, a typical polyorganocarbosilane) with the molecular formula $[-(\text{CH}_3)\text{SiH}-\text{CH}_2-]_n$. Since then, industrial technologies for fiber production have rapidly developed. For example, Ube Industries and Nippon Carbon, two Japanese companies, successfully commercialized SiC fibers in the late 1970s [46, 47]. Polymer-derived SiC-based ceramic fibers have become important industrial materials [47]. Preceramic polymers can be processed or shaped, using simply polymer-forming techniques (such as melt-spinning, coating, foaming, impregnating, and even 3D printing), curing for cross-linking, and then converted to ceramic components by pyrolysis [44]. Therefore, SiC-based fibers, SiC-based layers, SiC-based foams, and SiC complex architectures were produced from preceramic polymers, which cannot be easily obtained using the powder technology [44, 46, 48-50]. SiC materials have been applied in many key fields such as electronics, aerospace, nuclear, automotive, as well as membrane

separation, protective coating, and catalysis [44, 46, 51].

The fabrication of SiC-based ceramics by the polymer-pyrolysis process strongly influenced by the chemistry and architecture of the precursors, their processing route, and the parameters used for their pyrolysis [52]. First of all, the molecular structure and type of the preceramic polymer influences not only the composition but also the number of phases as well as the phase distribution and the microstructure of the final ceramic produced therefrom. The general classes of silicon-based polymers used as precursors for ceramics, i.e., polyorganosilanes, polyorganocarbosilanes, polyorganosiloxanes, polyorganosilazanes and polyorganosilylcarbodiimides and their corresponding classes of ceramics are shown in Fig. 1-7 [46, 53]. The nano/microstructure of the resulting types of polymer-derived ceramics (i.e., silicon carbides, silicon oxycarbides, and silicon carbonitrides) is indicated as well. The macroscopic chemical and physical properties of polymer-derived ceramics can be varied and adjusted to a huge extent by the design of the molecular precursor.

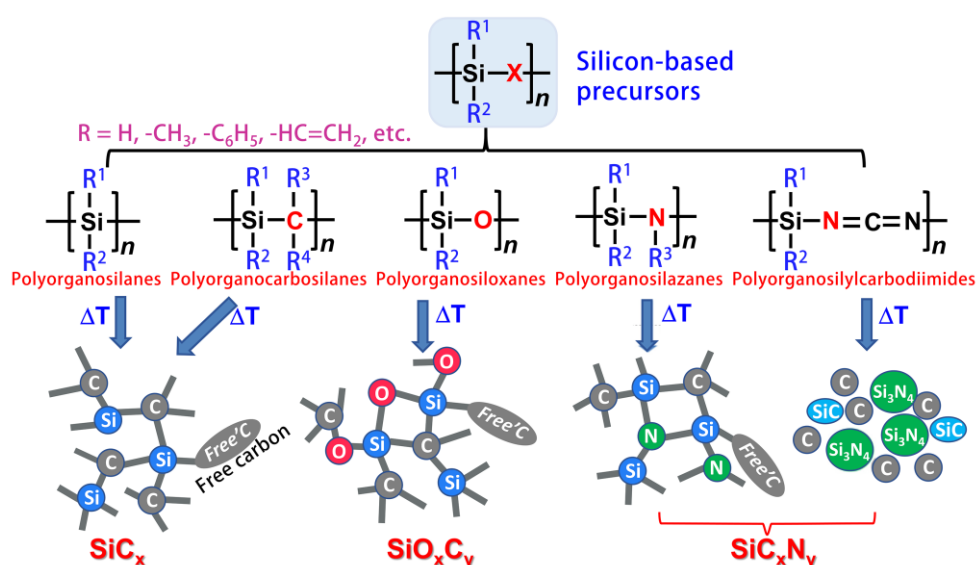


Fig. 1-7 Silicon-containing preceramic polymers and resulting ceramics [46, 53].

On the other hand, different pyrolysis temperatures also lead to different ceramic structures. Fig. 1-8 shows the general polymer-to-ceramic transformation process of preceramic polymers depending on the temperature. Generally, pyrolysis of polycarbosilanes leads to amorphous SiC-based ceramics at moderate temperatures between 600 °C and 1000 °C. With a further increase in the pyrolysis temperature, the amorphous SiC-based ceramics may crystallize, however, crystallization is not necessary or even undesired because it could damage the structure of the ceramics [54].

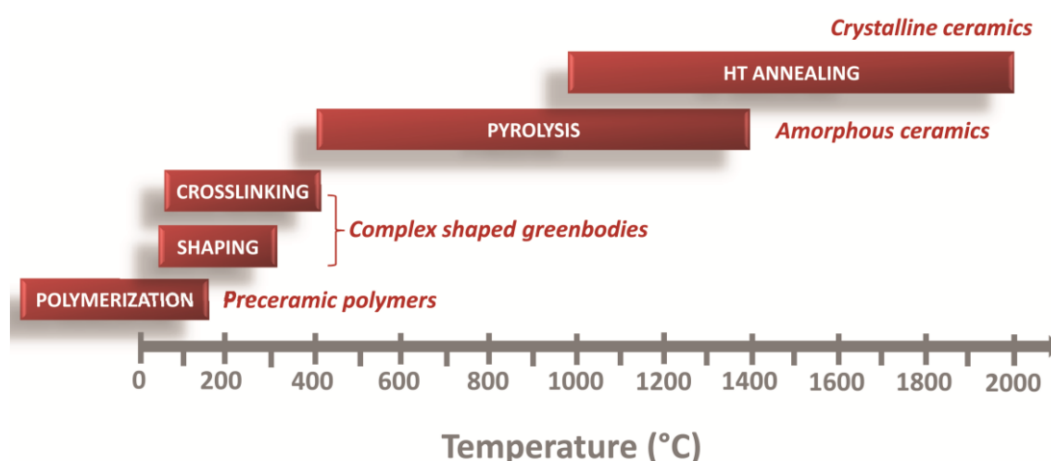


Fig. 1-8 Polymer-to-ceramic transformation of preceramic polymers [52].

Among the above mentioned, the curing stage of the fabrication process plays an important role in determining the final quality of the SiC-based ceramic, because it not only prevents the shapes/coating-layers of green-precursors from fusing together during the pyrolysis process, but also has a significant impact on their microstructural properties [55]. Cross-linking of PCS can be achieved by thermal curing in air atmosphere or irradiation (UV, γ -ray, or e-beam) curing under inert atmosphere

[56-60]. Cross-linking of PCS in the presence of oxygen has been found to occur via radical mechanisms: oxidation of Si-H and Si-CH₃ bonds occurs with the formation of Si-OH, Si-O-Si and C=O groups [61, 62]. On the other hand, cross-linking of PCS in the absence of oxygen involves reactions of Si-H bonds with Si-CH₃ groups leading to Si-CH₂-Si linkages [52, 63]. Different cross-linking methods and pyrolysis atmospheres produce different types of SiC-based ceramics, as shown in Fig. 1-9 [64]. Three types of SiC-based ceramics are produced from PCS. Si-C-O ceramic is produced by oxygen-curing of PCS; Si-C and Si-N ceramics are produced by radiation crosslinking of PCS. Particularly, Si-N ceramic is produced by pyrolysis under the NH₃ atmosphere [64, 65].

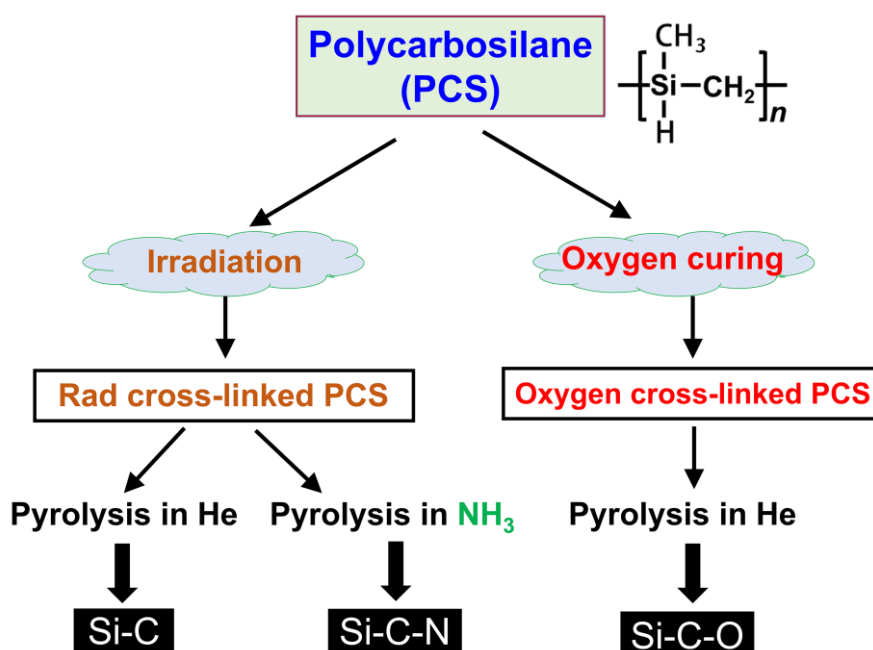


Fig. 1-9 Production process of SiC-based ceramic under different atmospheres [64].

So far, many silicon-based polymers have been used as preceramic precursors for the SiC-based ceramics [52]. SiC-based ceramics have been extensively investigated and applied to various fields. However, PCS-derived ceramics still have drawbacks in

their mechanical properties that cause them to deteriorate at high temperatures [66]. With the development of science and technology, the main method for preparation of high-performance SiC-based ceramics is the introduction of transition metals (e.g., Ti, Al, Zr, B, etc.) into SiC-based ceramics via the pyrolysis of polymetallo-carbosilanes, which is a chemical modification of PCS and can enhance the comprehensive performance of the SiC-based ceramics [67, 68]. Among these metal-containing PCS, a Ti-incorporated PCS precursor, polytitanocarbo-silane (TiPCS), has been developed. This polymer precursor can be synthesized via a reaction with titanium alkoxide (Ti(OR)_4) using PCS as shown in Fig. 1-10 [47, 66, 69]. Introduction of a small amount of titanium component, Ti-containing SiC-based ceramic exhibits more enhanced properties such as inhibiting crystalline grain growth of β -SiC up to high temperature [69]. Moreover, using this polymer, a Si-Ti-C-O (TiOSiC) fiber, commercialized under the name Tyranno Fiber and marketed by Ube industries LTD. (Japan), has now been synthesized [70, 71]. The Si-Ti-C-O fiber has many desirable mechanical properties and excellent heat resistance by comparison with SiC fibers obtained from PCS [66]. The metal-containing SiC-based ceramics are prepared by a similar process to that used for the fabrication of SiC-based ceramics derived from PCS as illustrated in Fig. 1-9.

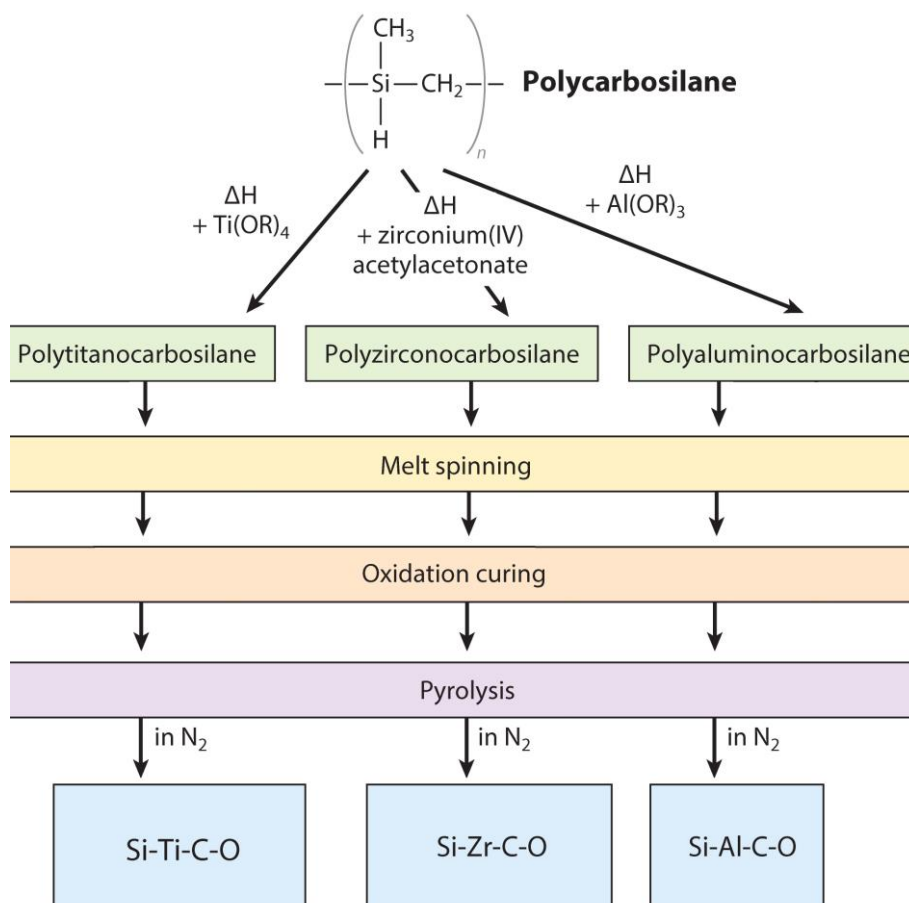


Fig. 1-10 Typical preparation process of metal-containing SiC-based ceramics derived from polymetallocarbosilane (Ti, Zr, and Al) precursors [47].

1.5.2.2 Silicon carbide-based membranes

For H₂ separation membranes, silica, carbon, and polymeric membranes cannot withstand either the higher operating temperatures or the presence of steam [72, 73]. Palladium membranes that are 100% selective towards hydrogen are expensive and sensitive to sulfur and carbon monoxide poisoning and coking [73]. Silicon carbide-based (e.g., SiC, SiOC, SiNC) ceramics have shown promise for use in H₂ separation due to excellent mechanical and chemical stability, high oxidation resistance, hydrothermal stability, high-temperature corrosion resistance, and high

thermal shock resistance. Thus far, SiC-based membranes have primarily been used for water treatment [74, 75], hot gas filtration [76, 77], catalytic substrates [78], and gas separation applications [73, 79].

The two approaches commonly utilized for the fabrication of SiC-based membranes include chemical-vapor deposition/infiltration (CVD/CVI), and pyrolysis of pre-ceramic polymer precursors [61]. For example, Sea et al. [80] prepared a SiC membrane via the CVD of triisopropylsilane (TPS) at 700-800 °C on an α -alumina tube with post-heat treatment under Ar at 1,000 °C. They achieved a H₂ permeance in the range of $(5-6) \times 10^{-7}$ mol/(m² s Pa) with a Knudsen-dominant gas permeation mechanism. Ciora et al. [43] also reported microporous SiC membranes using the CVD/CVI technique. However, the preparation procedure using TPS involved multiple steps that increased the cost and required post-treatment for further structural tailoring at temperatures reaching 1,000 °C. From a membrane manufacturing standpoint, therefore, the advantage of the CVD/CVI technique is lost.

In the formation of SiC-based membranes, the preceramic polymer method has been employed as an effective route by comparison with CVD/CVI methods [42]. The greatest advantage of this method is its simplicity and the fact that the processing can be carried out either batchwise or continuously [54]. To obtain SiC-based ceramic products, the precursors usually must undergo a sequence of shaping (coating), curing for cross-linking, and pyrolysis for polymer-to-ceramic transformation [61, 81].

As mentioned earlier, some curing methods for cross-linking have been used to produce SiC-based ceramics/membranes such as γ -ray/electron beam irradiation and conventional thermal oxidation (air-curing). Among the preceramic precursors, PCS is

the most commonly used for the formation of SiC-based membranes. For instance, Wach *et al.* [82, 83] reported the preparation of a SiC-based (Si-O-C) membrane via the electron-beam irradiation curing of a polycarbosilane (PCS) and polyvinylsilane blend. Their membrane achieved H₂ permeance of 10⁻¹⁰-10⁻⁸ mol/(m² s Pa) and excellent H₂/N₂ selectivity of 254 at 250 °C [83]. Li *et al.*[84] used PCS as a precursor to prepare SiC-based (Si-O-C) membranes via thermal-oxidative cross-linking (i.e., cured at 200 °C under air atmosphere). The Li membrane showed a H₂ permeance of 10⁻⁸ mol/(m² s Pa) with a H₂/N₂ selectivity of 18-63. The thermal oxidation was the most popular owing to its simplicity and cost-effectiveness. Furthermore, The Tsotsis group [42, 73] used an intramolecular thermal cross-linking method via allyl groups (C=C-C) without oxygen in allyl-hydridopolycarbosilane (AHPCS) to produce a SiC-based membrane. The Tsotsis membrane showed an ideal He/Ar separation factor of ~1,100 with He permeance of ~1 × 10⁻⁸ mol/(m² s Pa) at 200 °C [42].

Transition metallic elements such as Al, Ti, and Zr could improve the heat resistance, structure stability, and electrical properties of the final ceramic product as well as SiC-based membranes [85, 86]. However, to date, few reports have focused on metal-containing SiC-based membranes for molecular separation. Chao *et al.* reported a Al-containing SiC-based (Si-Al-C) membrane [87] that was prepared via air-curing at 200 °C and then pyrolyzed at 700 °C. One Si-Al-C membrane showed a H₂ permeance of 1 × 10⁻⁹ mol/(m² s Pa) with a H₂/N₂ selectivity of 2.25 (~Knudsen selectivity) at 200 °C. Also, a multilayered B-containing Si-B-C-N/γ-Al₂O₃/α-Al₂O₃

membrane with gradient porosity was prepared and investigated with respect to gas separation behavior [88, 89]. The typical micromorphology of a Si-B-C-N/ γ -Al₂O₃/ α -Al₂O₃ membrane was an asymmetric membrane as shown in Fig. 1-11. A H₂ permeance of 1.05×10^{-8} mol/(m² s Pa) and a H₂/CO selectivity of 10.5 were determined, showing its potential for applications such as hydrogen purification [88].

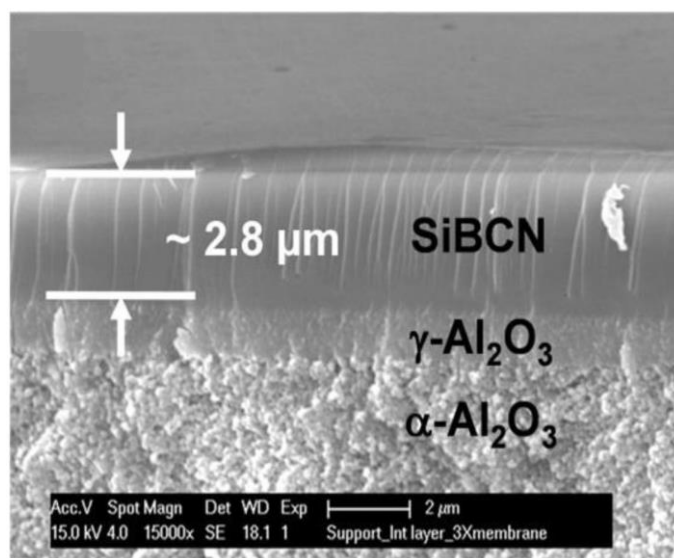


Fig. 1-11 Cross-section of a multilayered Si-B-C-N/ γ -Al₂O₃/ α -Al₂O₃ membrane [88].

Table 1-1 lists the synthesis conditions and performance of representative SiC-based membranes for gas separation, and the molecular structure of the preceramic precursors was also shown in Fig. 1-12. In addition, Fig. 1-13 summarizes the gas separation performance for SiC-based (SiC, SiOC, and SiAlC; including the data in Table 1-1) and other membranes. Silica membranes, which were prepared by sol-gel or CVD, generally showed high performance in H₂/N₂ separation because of narrow pore size, but their performance was reportedly poor under a hydrothermal atmosphere, particularly at high temperatures [32]. Most SiC-based membranes have

shown a low level of gas permeance. H_2 permeance of these membranes ranges from $\sim 10^{-9}$ - 10^{-8} mol/(m² s Pa) though H_2/N_2 selectivities varied greatly (Fig. 1-13a). SF_6 , which is the gas with the largest molecular size, is often used for evaluating the existence of large pores, and N_2/SF_6 is used as a benchmark for the separation of mid-sized molecules from large molecules such as the removal of methanol from organic mixtures [90, 91], and is also used as an index to evaluate membrane quality [92]. Fig. 1-13b revealed permeation properties that dictate lower permselectivity for N_2/SF_6 compared with MFI membranes. This indicates that most SiC-based membranes had a small pore size distribution and probably accompanied some defects such as pinholes. The small pore size distribution is why most SiC-based membranes were used for H_2 separation. Therefore, molecular separation SiC-based membranes need to optimize the preparation process and adjust their pore structures, which is also one of the important objectives of this thesis.

Table 1-1. Summary of synthesis conditions and membrane performance of SiC-based membranes for gas separation.

Precursor	Pyrolysis temp. [°C]	Type	Permeation temp. [°C] [$\times 10^{-8}$ mol/(m ² s Pa)]	H ₂ permeance [$\times 10^{-8}$ mol/(m ² s Pa)]	H ₂ /N ₂ selectivity	H ₂ /SF ₆ selectivity	Ref.
TPS	700-800	SiC	200	39.7	4.2	10-11	[80]
	750	SiC	200	0.54-1.18	29-78 (H ₂ /CH ₄)		[93]
AHPCS	750	SiC	200	1.05-2	101-258 (H ₂ /Ar)		[79]
	750	SiC	200	0.9 (He)	1,100 (He/Ar)		[42]
PCS	450	SiC	200	52.6	6.1		[94]
PCS	500	SiC	100	5.6	5.6	591	[95]
PCS	750	SiCO	200	4.7	9		[84]
PCS/PS	950		300	6.4	7.09		
PMS	600	SiC	200	0.27	20		[96]
PMS/Al-AcAc	500	SiAlC	200	0.65	4.8		[87]
PCS/PS	950	SiCO	200	2.4	10		[97]
PCS	850	SiC	250	2	146		[83]
PCS/PVS			250	1.2	254		
PMS	600	SiCO	200	0.49	40		[98]
VTMS/TRIES/TMDSO	700	SiCO	200	80	6.2	2,920	[27]
XP RV 200	700	SiCO	200	1	20	152	[99]

(TPS: triisopropylsilane; AHPCS: allylhydridopolycarbosilane; PCS: polycarbosilane; PS: polystyrene; PMS: polydimethylsilane; Al-AcAc: aluminum acetylacetonate; PVS: polyvinylsilane; VTMS/TRIES/TMDSO: vinyltrimethoxysilane/triethoxysilane/tetramethyldisiloxane; XP RV 200: vinyl-functionalized polysiloxane; the molecular structure of the preceramic precursors was shown in Fig. 1-12).

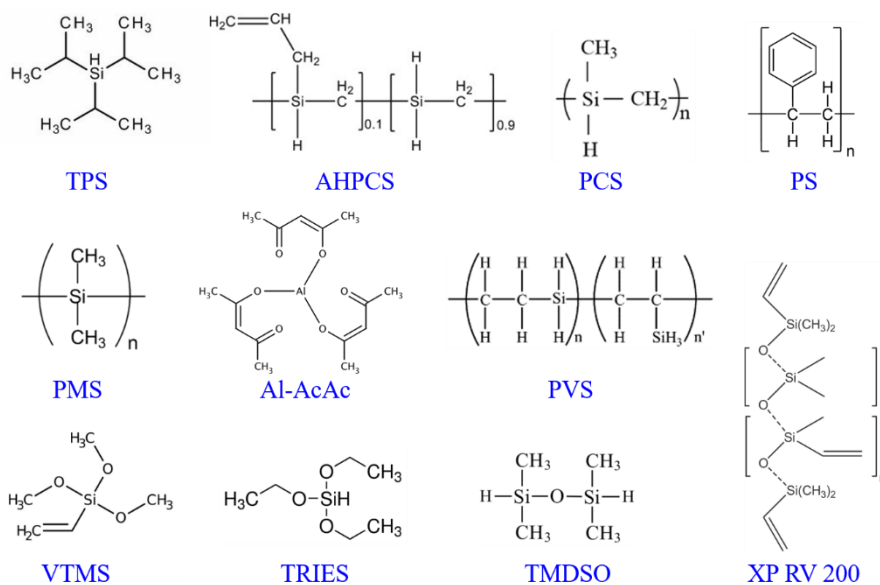


Fig. 1-12 The molecular structure of examples of silicon-containing precursors for SiC-based membranes (TPS-derived SiC-based membranes were formed by CVD method).

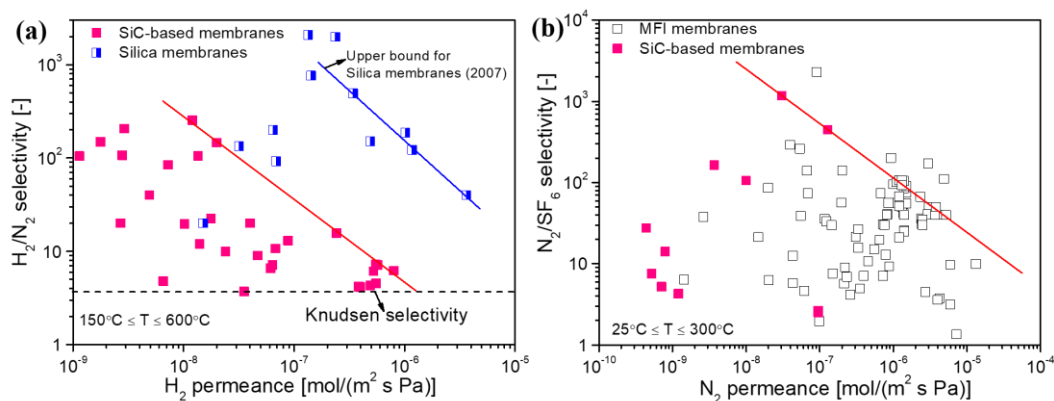


Fig. 1-13 Comparison of the selectivities for (a) H_2/N_2 and (b) N_2/SF_6 of SiC-based membranes and other membranes [39, 61].

1.6 Scope of this thesis

Membrane separation process has become one of the emerging technologies that undergo a rapid growth for the past few decades. The development of advanced

membranes for molecular separation with excellent separation performances, a simple fabrication process, and low-cost is always being pursued by membrane developers. The overall of this dissertation research is focused on the development and microstructure tuning of SiC-based membranes for gas separation and PV application. Two types of preceramic precursors, PCS and TiPCS were chosen for the fabrication of SiC-based membranes and Ti-containing SiC-based membranes, respectively. Conventional SiC-based membranes derived from PCS are mainly used for H₂/N₂ separation due to their narrow and small pore sizes. However, few studies have investigated the microporosity of ceramic products pyrolyzed at moderate temperatures (350-800 °C), and the relationship between the microporous structure and curing process for molecular separation remains unclear. Furthermore, Ti-containing SiC-based ceramics have many superior properties, however, the research on them is limited to fibers and bulk ceramics at high temperatures ($\geq 1,000$ °C). Here, we are the first to propose the fabrication of SiC-based membranes to obtain sub-nanopores by doping with Ti for molecular separation of small/mid-sized molecules from large molecules.

The high separation performance which could be obtained by adjusting the pore size of the SiC-based membranes, is expected to make SiC-based membranes suitable for separation not limited to H₂/N₂ separation but also in a wide range of applications for molecular separation. From these requirements, the main work of this research is as follows:

- (i) Tuning the microstructure of PCS-derived SiC-based separation membranes

via thermal-oxidative cross-linking;

(ii) Investigation of physicochemical properties and microstructural variations of TiPCS under different curing and pyrolysis conditions;

(iii) Development of high-performance sub-nanoporous SiC-based membranes derived from TiPCS for gas separation and PV applications.

This thesis consists of 5 chapters, the brief descriptions are shown below:

Chapter 1 is “**General introduction**” which involves the background and motivation of the current research.

Chapter 2 is “**Development and microstructure tuning of conventional SiC-based membranes derived from polycarbosilane**”. The main interest was focused on tuning the microstructure of the PCS-derived membranes via air-curing temperature. The elemental composition and microstructure of the final ceramic material could be precisely tailored via the air curing process. The most promising PCS-derived membranes, which were cured at 250 °C and then pyrolyzed at 750 °C, had high thermal stability and oxidation resistance at 500 °C in addition to excellent permeation properties: H₂ permeance of $1\text{-}2 \times 10^{-6}$ mol/(m² s Pa) at 500 °C with H₂/N₂ selectivity of 31 and H₂/C₃H₈ selectivity of 1,740; and, CO₂ permeance of 1.8×10^{-6} mol/(m² s Pa) at 27 °C with CO₂/CH₄ selectivity of 40. This is the first study to propose the concept of tailoring the microstructure of SiC-based membranes by controlling the curing process.

Chapter 3 is “**Development of high-performance sub-nanoporous SiC-based membranes derived from polytitanocarbosilane**”. Many studies have characterized

TiPCS-derived ceramics by firing at high temperatures ($> 1,000$ °C), however, few studies have investigated the microporosity of ceramic products pyrolyzed at moderate temperatures. This work marks the first fabrication of TiPCS-derived SiC-based membranes with sub-nanopores via the pyrolysis of a commercial polytitanocarbosilane polymer, Tyranno Coat, at temperature ranges of 350-850 °C. The dependence of the polymer-to-ceramic transformation process of TiPCS on pyrolysis temperature was systematically investigated. The pore characteristics and the surface areas of TiPCS-derived ceramic powders were strongly dependent on the pyrolysis temperatures. The evolution of the network structure of TiPCS during the pyrolysis process began with a dense polymer structure (≤ 350 °C) that was then passed through a loose transitional structure (350-650 °C), and then transformed into a relatively denser ceramic structure (> 650 °C). Additionally, the titanium components in TiPCS effectively inhibited and/or reduced the densification of the network structures at elevated temperatures. The network structure of TiPCS-derived SiC-based membranes showed trends similar to those of TiPCS-derived ceramic powders. The membrane prepared at 750 °C featured sub-nanopores, reproducibility, and attractive selectivities (H_2/SF_6 , 16,600; and N_2/SF_6 , 2,100) with a high H_2 permeance at a magnitude of 10^{-6} mol/(m² s Pa). These SiC-based membranes demonstrated great potential for the separation of small and mid-sized molecules from large molecules such as N_2/SF_6 separation and PV removal of water or methanol from liquid mixtures. The TiPCS membranes exhibited separation performance for methanol/methyl acetate mixtures with a total flux of 0.38 kg/(m² h) and a

methanol/methyl acetate separation factor of 35 for 10 wt% MeOH in a MeOH/MeOAc binary mixture at 60 °C.

Chapter 4 is “**Study on the effect of oxidative cross-linking on the structure and performance of polytitanocarbosilane-derived SiC-based membranes**”. In this section, special attention was focused on a process of thermal-oxidative curing that was used to induce cross-linking and the effect of this process on the ceramic yield, thermal stability, oxidation resistance, and microstructure of TiPCS. The cross-linked TiPCS powders showed a ceramic yield and thermal stability that were higher than that from the non-cross-linked version. In addition, the cross-linked TiPCS with uniform micropores showed higher levels of N₂ and CO₂ adsorption capacity, BET surface area, and micropore volume than the non-cross-linked versions, and the cross-linking process enhanced the stability of the pore structure at high temperature. The pore formation behavior induced by the cross-linking process of TiPCS chains was closely related to the gas permeation properties in SiC-based membranes. The cross-linked TiPCS membranes showed higher oxidation resistance than their non-cross-linked counterparts at 300 °C under air. Furthermore, the influence of the concentration of the TiPCS precursor coating solution was optimized. The cross-linked, optimized membranes demonstrated great performance for the pervaporation removal of methanol in binary azeotropic systems of either MeOH/butyl acetate or MeOH/toluene. Moreover, the membranes showed high hydrothermal stability together with an H₂O permeance of 1.64×10^{-6} mol/(m² s Pa).

and a high H₂O/N₂ selectivity of 40 in an equimolar H₂O/N₂ mixture (50 kPa: 50 kPa) at 300 °C. The TiPCS membrane is a promising candidate for gas dehumidification in membrane contactor systems that must operate at high temperatures.

Chapter 5 is “**Conclusions**”. The main conclusions of this study are summarized and recommendations for further study are presented here.

References

- [1] A. Kayvani Fard, G. McKay, A. Buekenhoudt, H. Al Sulaiti, F. Motmans, M. Khraishah, M. Atieh, Inorganic membranes: Preparation and application for water treatment and desalination, *Materials*, 11 (2018) 74.
- [2] V.M.A. Melgar, J. Kim, M.R. Othman, Zeolitic imidazolate framework membranes for gas separation: a review of synthesis methods and gas separation performance, *Journal of Industrial and Engineering Chemistry*, 28 (2015) 1-15.
- [3] D.L. Gin, R.D. Noble, Designing the next generation of chemical separation membranes, *Science*, 332 (2011) 674-676.
- [4] R.W. Baker, Membrane technology and applications, 3rd ed.; John Wiley & Sons, 2012.
- [5] G. Ji, M. Zhao, Membrane separation technology in carbon capture, *Recent Advances in Carbon Capture and Storage; Yun, Y., Ed*, (2017) 59-90.
- [6] P. Goh, A. Ismail, A review on inorganic membranes for desalination and wastewater treatment, *Desalination*, 434 (2018) 60-80.
- [7] Y. Lin, I. Kumakiri, B. Nair, H. Alsyouri, Microporous inorganic membranes, *Sep. Purif. Methods*, 31 (2002) 229-379.
- [8] R.S. Faibish, Y. Cohen, Fouling and rejection behavior of ceramic and polymer-modified ceramic membranes for ultrafiltration of oil-in-water emulsions and microemulsions, *Colloids Surf. Physicochem. Eng. Aspects*, 191 (2001) 27-40.

- [9] Y. Yoshino, T. Suzuki, B.N. Nair, H. Taguchi, N. Itoh, Development of tubular substrates, silica based membranes and membrane modules for hydrogen separation at high temperature, *J. Membr. Sci.*, 267 (2005) 8-17.
- [10] M.M. Pendergast, E.M. Hoek, A review of water treatment membrane nanotechnologies, *Energy & Environmental Science*, 4 (2011) 1946-1971.
- [11] S.T. Oyama, Review on mechanisms of gas permeation through inorganic membranes, *Journal of the Japan Petroleum Institute*, 54 (2011) 298-309.
- [12] P. Pandey, R. Chauhan, Membranes for gas separation, *Prog. Polym. Sci.*, 26 (2001) 853-893.
- [13] W.J. Koros, R. Mahajan, Pushing the limits on possibilities for large scale gas separation: which strategies?, *J. Membr. Sci.*, 175 (2000) 181-196.
- [14] S.J. Khatib, S.T. Oyama, K.R. de Souza, F.B. Noronha, Chapter 2 - Review of Silica Membranes for Hydrogen Separation Prepared by Chemical Vapor Deposition, in: S.T. Oyama, S.M. Stagg-Williams (Eds.) *Membrane Science and Technology*, Elsevier, 2011, pp. 25-60.
- [15] E.P. Favvas, CO₂ Permeation Behavior through Carbon Membranes: A Short Review of the Progress during the Last Decade, *Journal of Membrane and Separation Technology*, 5 (2016) 3-15.
- [16] X. Huang, H. Yao, Z. Cheng, Hydrogen Separation Membranes of Polymeric Materials, in: *Nanostructured Materials for Next-Generation Energy Storage and Conversion*, Springer, 2017, pp. 85-116.
- [17] J. Sekulić, J.E. ten Elshof, D.H. Blank, Separation mechanism in dehydration of

- water/organic binary liquids by pervaporation through microporous silica, *J. Membr. Sci.*, 254 (2005) 267-274.
- [18] S.P. Nunes, K.-V. Peinemann, Membrane technology: in the chemical industry, John Wiley & Sons, 2006.
- [19] G.M. Shi, D. Hua, T.S. Chung, Pervaporation and Vapor Separation, in: Membrane Separation Principles and Applications, Elsevier, 2019, pp. 181-231.
- [20] J. Neel, R. Huang, Introduction to pervaporation, pervaporation membrane separation processes, *edited by RYM Huang, Membrane Science and Technology Series*, 1 (1991) 23-31.
- [21] S.-L. Wee, C.-T. Tye, S. Bhatia, Membrane separation process-Pervaporation through zeolite membrane, *Sep. Purif. Technol.*, 63 (2008) 500-516.
- [22] T.C. Bowen, S. Li, R.D. Noble, J.L. Falconer, Driving force for pervaporation through zeolite membranes, *J. Membr. Sci.*, 225 (2003) 165-176.
- [23] H. Li, K. Haas-Santo, U. Schygulla, R. Dittmeyer, Inorganic microporous membranes for H₂ and CO₂ separation-Review of experimental and modeling progress, *Chem. Eng. Sci.*, 127 (2015) 401-417.
- [24] T. Tsuru, Nano/subnano-tuning of porous ceramic membranes for molecular separation, *J. Sol-Gel Sci. Technol.*, 46 (2008) 349-361.
- [25] X. Yu, H. Nagasawa, M. Kanezashi, T. Tsuru, Improved thermal and oxidation stability of bis (triethoxysilyl) ethane (BTESE)-derived membranes, and their gas-permeation properties, *Journal of Materials Chemistry A*, 6 (2018) 23378-23387.

- [26] S.J. Khatib, S.T. Oyama, K.R. de Souza, F.B. Noronha, Review of silica membranes for hydrogen separation prepared by chemical vapor deposition, in: *Membrane Science and Technology*, Elsevier, 2011, pp. 25-60.
- [27] H. Inde, M. Kanezashi, H. Nagasawa, T. Nakaya, T. Tsuru, Tailoring a Thermally Stable Amorphous SiOC Structure for the Separation of Large Molecules: The Effect of Calcination Temperature on SiOC Structures and Gas Permeation Properties, *ACS Omega*, 3 (2018) 6369-6377.
- [28] N.W. Ockwig, T.M. Nenoff, Membranes for hydrogen separation, *Chem. Rev.*, 107 (2007) 4078-4110.
- [29] K.-S. Chang, T. Yoshioka, M. Kanezashi, T. Tsuru, K.-L. Tung, A molecular dynamics simulation of a homogeneous organic-inorganic hybrid silica membrane, *Chem. Commun.*, 46 (2010) 9140-9142.
- [30] X. Ren, T. Tsuru, Organosilica-Based Membranes in Gas and Liquid-Phase Separation, *Membranes*, 9 (2019) 107.
- [31] M. Asaeda, S. Yamasaki, Separation of inorganic/organic gas mixtures by porous silica membranes, *Sep. Purif. Technol.*, 25 (2001) 151-159.
- [32] T. Tsuru, Silica-Based Membranes with Molecular-Net-Sieving Properties: Development and Applications, *J. Chem. Eng. Jpn.*, 51 (2018) 713-725.
- [33] M. Elma, C. Yacou, D.K. Wang, S. Smart, J.C. Diniz da Costa, Microporous silica based membranes for desalination, *Water*, 4 (2012) 629-649.
- [34] H.L. Castricum, A. Sah, R. Kreiter, D.H. Blank, J.F. Vente, E. Johan, Hydrothermally stable molecular separation membranes from organically linked

- silica, *J. Mater. Chem.*, 18 (2008) 2150-2158.
- [35] M. Kanezashi, Y. Yoneda, H. Nagasawa, T. Tsuru, K. Yamamoto, J. Ohshita, Gas permeation properties for organosilica membranes with different Si/C ratios and evaluation of microporous structures, *AIChE J.*, 63 (2017) 4491-4498.
- [36] X. Ren, K. Nishimoto, M. Kanezashi, H. Nagasawa, T. Yoshioka, T. Tsuru, CO₂ permeation through hybrid organosilica membranes in the presence of water vapor, *Industrial & engineering chemistry research*, 53 (2014) 6113-6120.
- [37] H.L. Castricum, G.G. Paradis, M.C. Mittelmeijer-Hazeleger, R. Kreiter, J.F. Vente, J.E. Ten Elshof, Tailoring the separation behavior of hybrid organosilica membranes by adjusting the structure of the organic bridging group, *Adv. Funct. Mater.*, 21 (2011) 2319-2329.
- [38] N. Moriyama, H. Nagasawa, M. Kanezashi, T. Tsuru, Selective water vapor permeation from steam/non-condensable gas mixtures via organosilica membranes at moderate-to-high temperatures, *J. Membr. Sci.*, 589 (2019) 117254.
- [39] Q. Wang, L. Yu, H. Nagasawa, M. Kanezashi, T. Tsuru, High-performance molecular-separation ceramic membranes derived from oxidative cross-linked polytitanocarbosilane, *J. Am. Ceram. Soc.*, 103 (2020) 4473-4488.
- [40] V. Proust, M.C. Bechelany, R. Ghisleni, M.-F. Beaufort, P. Miele, S. Bernard, Polymer-derived Si-C-Ti systems: From titanium nanoparticle-filled polycarbosilanes to dense monolithic multi-phase components with high hardness, *J. Eur. Ceram. Soc.*, 36 (2016) 3671-3679.

- [41] M. Kanezashi, H. Sazaki, H. Nagasawa, T. Yoshioka, T. Tsuru, Preparation and gas permeation properties of thermally stable organosilica membranes derived by hydrosilylation, *Journal of Materials Chemistry A*, 2 (2014) 672-680.
- [42] S. Dabir, W.X. Deng, M. Sahimi, T. Tsotsis, Fabrication of silicon carbide membranes on highly permeable supports, *J. Membr. Sci.*, 537 (2017) 239-247.
- [43] R.J. Ciora, B. Fayyaz, P.K.T. Liu, V. Suwanmethanond, R. Mallada, M. Sahimi, T.T. Tsotsis, Preparation and reactive applications of nanoporous silicon carbide membranes, *Chem. Eng. Sci.*, 59 (2004) 4957-4965.
- [44] X. Li, X. Pei, X. Zhong, G. Mo, L. He, Z. Huang, Q. Huang, Highly effective free-radical-catalyzed curing of hyperbranched polycarbosilane for near stoichiometric SiC ceramics, *J. Am. Ceram. Soc.*, 102 (2019) 1041-1048.
- [45] S. Yajima, K. Okamura, J. Hayashi, M. Omori, Synthesis of continuous SiC fibers with high tensile strength, *J. Am. Ceram. Soc.*, 59 (1976) 324-327.
- [46] P. Colombo, G. Mera, R. Riedel, G.D. Soraru, Polymer-derived ceramics: 40 years of research and innovation in advanced ceramics, *J. Am. Ceram. Soc.*, 93 (2010) 1805-1837.
- [47] H. Ichikawa, Polymer-derived ceramic fibers, *Annual Review of Materials Research*, 46 (2016) 335-356.
- [48] T. Ishikawa, Y. Kohtoku, K. Kumagawa, T. Yamamura, T. Nagasawa, High-strength alkali-resistant sintered SiC fibre stable to 2200°C, *Nature*, 391 (1998) 773-775.
- [49] F. Xue, K. Zhou, N. Wu, H. Luo, X. Wang, X. Zhou, Z. Yan, I. Abrahams, D.

- Zhang, Porous SiC ceramics with dendritic pore structures by freeze casting from chemical cross-linked polycarbosilane, *Ceram. Int.*, 44 (2018) 6293-6299.
- [50] H. Zhong, Z. Wang, H. Zhou, D. Ni, Y. Kan, Y. Ding, S. Dong, Properties and microstructure evolution of Cf/SiC composites fabricated by polymer impregnation and pyrolysis (PIP) with liquid polycarbosilane, *Ceram. Int.*, 43 (2017) 7387-7392.
- [51] Z. He, P. Lian, Y. Song, Z. Liu, J. Song, J. Zhang, X. Ren, J. Feng, X. Yan, Q. Guo, Protecting nuclear graphite from liquid fluoride salt and oxidation by SiC coating derived from polycarbosilane, *J. Eur. Ceram. Soc.*, 38 (2018) 453-462.
- [52] G. Mera, M. Gallei, S. Bernard, E. Ionescu, Ceramic Nanocomposites from Tailor-Made Pre ceramic Polymers, *Nanomaterials*, 5 (2015) 468-540.
- [53] E. Ionescu, G. Mera, R. Riedel, Polymer-derived ceramics (PDCs): Materials design towards applications at ultrahigh-temperatures and in extreme environments, in: *Nanotechnology: Concepts, Methodologies, Tools, and Applications*, IGI Global, 2014, pp. 1108-1139.
- [54] G. Barroso, Q. Li, R.K. Bordia, G. Motz, Polymeric and ceramic silicon-based coatings—a review, *Journal of Materials Chemistry A*, 7 (2019) 1936-1963.
- [55] J. Hong, K.Y. Cho, D.G. Shin, J.I. Kim, D.H. Riu, Iodine diffusion during iodine-vapor curing and its effects on the morphology of polycarbosilane/silicon carbide fibers, *J. Appl. Polym. Sci.*, 132 (2015).
- [56] X. Zhong, X. Pei, Y. Miao, L. He, Q. Huang, Accelerating the crosslinking process of hyperbranched polycarbosilane by UV irradiation, *J. Eur. Ceram. Soc.*,

- 37 (2017) 3263-3270.
- [57] A. Takeyama, M. Sugimoto, M. Yoshikawa, Gas Permeation Property of SiC Membrane Using Curing of Polymer Precursor Film by Electron Beam Irradiation in Helium Atmosphere, *Materials Transactions*, advpub (2011) 1276-1280.
- [58] M. Shibuya, T. Yamamura, Characteristics of a continuous Si-Ti-C-O fibre with low oxygen content using an organometallic polymer precursor, *JMatS*, 31 (1996) 3231-3235.
- [59] H.M. Williams, E.A. Dawson, P.A. Barnes, B. Rand, R.M.D. Brydson, A.R. Brough, High temperature ceramics for use in membrane reactors: the development of microporosity during the pyrolysis of polycarbosilanes, *J. Mater. Chem.*, 12 (2002) 3754-3760.
- [60] Y.L. Li, H. Fan, D. Su, C. Fasel, R. Riedel, Synthesis, structures, and properties of bulk Si(O)C ceramics from polycarbosilane, *J. Am. Ceram. Soc.*, 92 (2009) 2175-2181.
- [61] Q. Wang, L. Yu, H. Nagasawa, M. Kanezashi, T. Tsuru, Tuning the microstructure of polycarbosilane-derived SiC(O) separation membranes via thermal-oxidative cross-linking, *Sep. Purif. Technol.*, 248 (2020) 117067.
- [62] L. Anhua, C. Jianming, D. Shaonan, Y. Yanbo, L. Ling, L. Fengping, C. Lifu, Processing and characterization of cobalt silicide nanoparticle-containing silicon carbide fibers through a colloidal method and their underlying mechanism, *Journal of Materials Chemistry C*, 2 (2014) 4980-4988.

- [63] Y. Hasegawa, K. Okamura, Synthesis of continuous silicon carbide fibre. III- Pyrolysis process of polycarbosilane and structure of the products, *JMatS*, 18 (1983) 3633-3648.
- [64] K. Makuuchi, S. Cheng, New Application of Radiation Crosslinking, in: Radiation Processing of Polymer Materials and its Industrial Applications, John Wiley & Sons, 2012, pp. 166-200.
- [65] C. Schitco, M.S. Bazarjani, R. Riedel, A. Gurlo, NH₃-assisted synthesis of microporous silicon oxycarbonitride ceramics from preceramic polymers: a combined N₂ and CO₂ adsorption and small angle X-ray scattering study, *Journal of Materials Chemistry A*, 3 (2015) 805-818.
- [66] T. Yamamura, T. Ishikawa, M. Shibuya, T. Hisayuki, K. Okamura, Development of a new continuous Si-Ti-C-O fibre using an organometallic polymer precursor, *JMatS*, 23 (1988) 2589-2594.
- [67] Z. Yu, L. Yang, J. Zhan, C. Zhou, H. Min, Q. Zheng, H. Xia, Preparation, cross-linking and ceramization of AHPCS/Cp₂ZrCl₂ hybrid precursors for SiC/ZrC/C composites, *J. Eur. Ceram. Soc.*, 32 (2012) 1291-1298.
- [68] R.K. Gupta, R. Mishra, R.K. Tiwari, A. Ranjan, A.K. Saxena, Studies on the Rheological Behavior of Polycarbosilane Part I: Effect of Time, Temperature and Atmosphere, *Silicon*, 3 (2011) 27-35.
- [69] T. Ishikawa, T. Yamamura, K. Okamura, Production mechanism of polytitanocarbosilane and its conversion of the polymer into inorganic materials, *JMatS*, 27 (1992) 6627-6634.

- [70] G. Chollon, B. Aldacourrou, L. Capes, R. Pailler, R. Naslain, Thermal behaviour of a polytitanocarbosilane-derived fibre with a low oxygen content: The Tyranno Lox-E fibre, *JMatS*, 33 (1998) 901-911.
- [71] N.S. Jacobson, S.E. Kline, A Thermoanalytical Study of the Conversion of Amorphous Si-Ti-C-O Fibers to SiC, *International Journal of Applied Ceramic Technology*, 9 (2012) 816-822.
- [72] A.R. Maddocks, D.J. Cassidy, A.S. Jones, A.T. Harris, Synthesis of nanoporous silicon carbide via the preceramic polymer route, *Mater. Chem. Phys.*, 113 (2009) 861-867.
- [73] B. Elyassi, W.X. Deng, M. Sahimi, T.T. Tsotsis, On the Use of Porous and Nonporous Fillers in the Fabrication of Silicon Carbide Membranes, *Industrial & Engineering Chemistry Research*, 52 (2013) 10269-10275.
- [74] S.C. Kim, H.J. Yeom, Y.W. Kim, I.H. Song, J.H. Ha, Processing of alumina-coated glass-bonded silicon carbide membranes for oily wastewater treatment, *International Journal of Applied Ceramic Technology*, 14 (2017) 692-702.
- [75] K. König, V. Boffa, B. Buchbjerg, A. Farsi, M.L. Christensen, G. Magnacca, Y. Yue, One-step deposition of ultrafiltration SiC membranes on macroporous SiC supports, *J. Membr. Sci.*, 472 (2014) 232-240.
- [76] M. Herrmann, G. Standke, S. Höhn, G. Himpel, T. Gestrich, High-temperature corrosion of silicon carbide ceramics by coal ashes, *Ceram. Int.*, 40 (2014) 1471-1479.
- [77] F. Han, Z. Zhong, Y. Yang, W. Wei, F. Zhang, W. Xing, Y. Fan, High gas

- permeability of SiC porous ceramics reinforced by mullite fibers, *J. Eur. Ceram. Soc.*, 36 (2016) 3909-3917.
- [78] Y.A. Kim, J.H. Choi, J. Scott, K. Chiang, R. Amal, Preparation of high porous Pt–V₂O₅–WO₃/TiO₂/SiC filter for simultaneous removal of NO and particulates, *Powder Technol.*, 180 (2008) 79-85.
- [79] B. Elyassi, M. Sahimi, T.T. Tsotsis, A novel sacrificial interlayer-based method for the preparation of silicon carbide membranes, *J. Membr. Sci.*, 316 (2008) 73-79.
- [80] B.-K. Sea, K. Ando, K. Kusakabe, S. Morooka, Separation of hydrogen from steam using a SiC-based membrane formed by chemical vapor deposition of triisopropylsilane, *J. Membr. Sci.*, 146 (1998) 73-82.
- [81] Q. Wang, Y. Kawano, L. Yu, H. Nagasawa, M. Kanezashi, T. Tsuru, Development of high-performance sub-nanoporous SiC-based membranes derived from polytitanocarbosilane, *J. Membr. Sci.*, 598 (2020) 117688.
- [82] R.A. Wach, M. Sugimoto, M. Yoshikawa, Formation of Silicone Carbide Membrane by Radiation Curing of Polycarbosilane and Polyvinylsilane and its Gas Separation up to 250°C, *J. Am. Ceram. Soc.*, 90 (2007) 275-278.
- [83] R.A. Wach, M. Sugimoto, A. Idesaki, M. Yoshikawa, Molecular sieve SiC-based membrane for hydrogen separation produced by radiation curing of preceramic polymers, *Materials Science and Engineering: B*, 140 (2007) 81-89.
- [84] L. Zhongyang, K. Kusakabe, S. Morooka, Preparation of thermostable amorphous Si-C-O membrane and its application to gas separation at elevated

- temperature, *J. Membr. Sci.*, 118 (1996) 159-168.
- [85] T. Ishikawa, H. Yamaoka, Y. Harada, T. Fujii, T. Nagasawa, A general process for in situ formation of functional surface layers on ceramics, *Nature*, 416 (2002) 64-67.
- [86] K. Suzuki, K. Kumagawa, T. Kamiyama, M. Shibuya, Characterization of the medium-range structure of Si-Al-C-O, Si-Zr-C-O and Si-Al-C Tyranno fibers by small angle X-ray scattering, *JMatS*, 37 (2002) 949-953.
- [87] C.C. Chao, D.S. Tsai, Si-Al-C gas separation membranes derived from polydimethylsilane and aluminum acetylacetonate, *J. Membr. Sci.*, 192 (2001) 209-216.
- [88] R.M. Prasad, Y. Iwamoto, R. Riedel, A. Gurlo, Multilayer Amorphous-Si-B-C-N/ γ -Al₂O₃/ α -Al₂O₃ Membranes for Hydrogen Purification, *Adv. Eng. Mater.*, 12 (2010) 522-528.
- [89] R. Hauser, S. Nahar-Borchard, R. Riedel, Y.H. Ikuhara, Y. Iwamoto, Polymer-Derived SiBCN Ceramic and their Potential Application for High Temperature Membranes, *J. Ceram. Soc. Jpn.*, 114 (2006) 524-528.
- [90] M. Kanezashi, M. Murata, H. Nagasawa, T. Tsuru, Fluorine Doping of Microporous Organosilica Membranes for Pore Size Control and Enhanced Hydrophobic Properties, *ACS Omega*, 3 (2018) 8612-8620.
- [91] M. Drobek, J. Motuzas, M. van Loon, R.W.J. Dirrix, R.A. Terpstra, A. Julbe, Coupling microwave-assisted and classical heating methods for scaling-up MFI zeolite membrane synthesis, *J. Membr. Sci.*, 401 (2012) 144-151.

- [92] Q. Wang, A. Wu, S. Zhong, B. Wang, R. Zhou, Highly (*h0h*)-oriented silicalite-1 membranes for butane isomer separation, *J. Membr. Sci.*, 540 (2017) 50-59.
- [93] B. Elyassi, M. Sahimi, T.T. Tsotsis, Silicon carbide membranes for gas separation applications, *J. Membr. Sci.*, 288 (2007) 290-297.
- [94] K. Kusakabe, Z. Yan Li, H. Maeda, S. Morooka, Preparation of supported composite membrane by pyrolysis of polycarbosilane for gas separation at high temperature, *J. Membr. Sci.*, 103 (1995) 175-180.
- [95] H. Suda, H. Yamauchi, Y. Uchimar, I. Fujiwara, K. Haraya, Structural Evolution during Conversion of Polycarbosilane Precursor into Silicon Carbide-Based Microporous Membranes, *J. Ceram. Soc. Jpn.*, 114 (2006) 539-544.
- [96] L.-L. Lee, D.-S. Tsai, Synthesis and Permeation Properties of Silicon-Carbon-Based Inorganic Membrane for Gas Separation, *Industrial & Engineering Chemistry Research*, 40 (2001) 612-616.
- [97] Z. Li, K. Kusakabe, S. Morooka, Pore Structure and Permeance of Amorphous Si-C-O Membranes with High Durability at Elevated Temperature, *Sep. Sci. Technol.*, 32 (1997) 1233-1254.
- [98] L.-L. Lee, D.-S. Tsai, A Hydrogen-Permselective Silicon Oxycarbide Membrane Derived from Polydimethylsilane, *J. Am. Ceram. Soc.*, 82 (1999) 2796-2800.
- [99] R.M. Prasad, Y. Jüttke, H. Richter, I. Voigt, R. Riedel, A. Gurlo, Mechanism of Gas Separation through Amorphous Silicon Oxycarbide Membranes *Adv. Eng. Mater.*, 18 (2016) 721-727.

Chapter 2

Development and microstructure tuning of conventional SiC-based membranes derived from polycarbosilane

2.1 Introduction

Hydrogen as a clean energy carrier is considered one of the key alternatives for the replacement of petroleum as fuel, and is expected to play a significant role in the reduction of greenhouse gas emissions [1]. Efficient production and separation of hydrogen are the main obstacles limiting its widespread application. A membrane reactor has been proposed in order to achieve the objectives of membrane separation and catalytic reaction in one unit [1]. Most dehydrogenation reactions (e.g., dehydrogenation in methylcyclohexane and propane) are limited by thermodynamic equilibrium, and the membranous removal of H₂ could improve the conversion process beyond static equilibrium. However, the difficulty of manufacturing pores with a suitable diameter and the lack of stability at high temperatures are the main challenges for membrane materials [2, 3].

Regarding H₂ separation membranes, silica, carbon, and polymeric membranes cannot withstand either the higher operating temperatures or the presence of steam [4, 5]. Palladium membranes that are 100% selective towards hydrogen are expensive and sensitive to sulfur and carbon monoxide poisoning and coking [4, 5]. These factors have created the need to develop new materials. Silicon carbide-based (SiC

and SiC-related, e.g., SiC, SiOC, SiNC) ceramics have shown promise for use in H₂ separation. Thus far, SiC-based membranes have primarily been used for water treatment [6, 7], hot gas filtration [8, 9], catalytic substrates [10], pervaporation [11], and gas separation applications [5, 12] due to excellent mechanical and chemical stability, high oxidation resistance, hydrothermal stability, high-temperature corrosion resistance, and high thermal shock resistance.

In the formation of SiC-based membranes, the preceramic polymer method has been employed as an effective route by comparison with chemical-vapor deposition/infiltration (CVD/CVI) methods. The greatest advantage of this method is its simplicity and the fact that the processing can be carried out either batchwise or continuously. In order to obtain SiC-based ceramic products, the precursors usually must undergo a sequence of shaping (coating), curing for cross-linking, and pyrolysis for polymer-to-ceramic transformation [13]. The curing stage of the fabrication process plays an important role in determining the final quality of the SiC-based ceramic, because it not only prevents the shapes/coating-layers of green-precursors from fusing together during the pyrolysis process, but also has a significant impact on their microstructural properties [14]. Thus far, a number of different curing methods have been used to produce SiC-based membranes such as γ -ray/electron beam irradiation [15, 16] and conventional thermal oxidation [3, 17]. Among these, thermal oxidation (air) curing has been the most popular owing to its simplicity and cost-effectiveness.

Polycarbosilane (PCS) is the most commonly used preceramic polymer for the

formation of SiC-based materials (e.g., SiC and SiOC) since Yajima et al. first reported its use for SiC fibers with the trade name Nicalon [18]. Thus far, many studies have characterized PCS-derived materials (powders, fibers) by firing at high temperatures ($> 1,000\text{ }^{\circ}\text{C}$), which usually results in almost no porosity. With respect to separation membrane research, however, few studies have investigated the microporosity of ceramic products pyrolyzed at moderate temperatures ($350\text{-}800\text{ }^{\circ}\text{C}$), and the relationship between the microporous structure and curing process for molecular separation remains unclear. In the present study, our interest was focused on tuning the microstructure of the PCS membrane via air-curing temperature in order to accomplish the separation of $\text{H}_2/\text{C}_3\text{H}_8$ for potential applications to propane dehydrogenation membrane reactors under high temperatures. Thus, the physicochemical properties and microstructural variations of PCS-derived ceramic powders were systematically studied under different curing and pyrolysis temperatures. The optimized PCS-derived membranes had excellent permeation properties with high thermal stability and good oxidation resistance. The present study is the first to propose the concept of tailoring the microstructure and permeation properties of SiC-based membranes via a process of thermal-oxidative curing.

2.2 Experimental

2.2.1 Preparation of cured and pyrolyzed PCS powders

To study the conversion behavior from organic polymer to ceramic,

polycarbosilane (PCS, Type-UH, main structure $[-(\text{CH}_3)\text{HSi-CH}_2-]_n$, mean molecular weight = 3694, NGS Advanced Fibers Co., Ltd., Japan) powder with a melting point higher than 300 °C was used in this work. The air curing process for cross-linking using raw PCS powder was carried out for 2 h at temperatures of 150-350 °C with a 50 °C interval under an air flow (500 mL min⁻¹). The cured PCS powders were then separately pyrolyzed at 350, 550, 650, 700, 750 and 850 °C for 2 h under a N₂ flow (500 mL min⁻¹). During the above processes, the furnace was heated at 35 °C min⁻¹ and cooled to room temperature naturally.

2.2.2 Fabrication of the PCS-derived membrane

An α -Al₂O₃ porous tube with an average pore diameter of 1 μm (porosity, 50%; outer diameter, 10 mm; inner diameter, 8 mm; tube length, 100 mm; Nikkato, Co., Japan) was used as a support. On the outer surface of this porous support, two types of α -alumina particles (0.2 μm and 2 μm) with 1 wt% SiO₂-ZrO₂ (Si/Zr = 5/5) colloidal sols as a binder were coated and followed by calcination at 750 °C for 20 min under air. Subsequently, 0.5 wt% SiO₂-ZrO₂ (Si/Zr = 5/5) colloidal sol was coated onto the α -alumina particle layer and calcinated at 750 °C for 15 min as an intermediate layer to minimize the defects of the membrane. Details of the procedure used to modify the support are similar to that used in our previous work [19-21].

As a precursor solution for fabrication of the PCS-derived top layer, a *p*-xylene solution of PCS was prepared. A solution of 3 wt% PCS was coated onto the intermediate layer. Subsequently, the coated membrane was cured under an air flow

for 2 h at 150-300 °C and then pyrolyzed at 750 °C for 0.5 h under a N₂ atmosphere at a heating rate of ~35 °C/min. The flow rates of air and N₂ were both set at 500 mL/min. The coating-curing-pyrolysis process was performed twice to reduce the possible defects in the SiC-based membranes.

2.2.3 Characterization of PCS powders and PCS membranes

The PCS powders prepared via each air curing and pyrolysis process were used for ATR-FTIR, EDS, XRD, and N₂ and CO₂ adsorption-desorption isotherm analyses. FTIR analysis was conducted using an FTIR-4100 (JASCO Co., Japan) and the attenuated total reflection (ATR) technique on all samples. Thermogravimetric analysis (TGA) was performed using a Shimadzu TG-50 with thermo-balance at a heating rate of 35 °C/min under either a N₂ or air atmosphere at a flow rate of 50 ml min⁻¹. To minimize the effect of buoyancy, the initial mass of each sample was about 10 mg, and the final residual weight was based on the weight under the same temperature and atmosphere as that at the beginning and end of each measurement. N₂ (-196 °C) and CO₂ (25 °C) adsorption-desorption isotherms for PCS powders were carried out using a BELMAX (BELL Co., Japan). Before the measurement, all the powder samples were pre-treated to promote degassing at 150-200 °C under vacuum for 12 h. The BET surface area was evaluated using N₂ adsorption data at relative pressures (P/P_0) that ranged between 0.001 and 0.15, and the micropore volume was calculated using *t*-plot analysis. The micropore volume based on CO₂ adsorption was also obtained via the NLDFT method. The chemical elements of the PCS powders were examined using a scanning electron microscope equipped with an EX-37001 EDS accessory (JCM 5700, JEOL, Japan). XRD patterns of PCS powders were obtained using Cu K α as the X-ray radiation source (1.54 Å) for a D2 PHASER X-ray

diffractometer (Bruker, Germany).

The permeance of single gases with different kinetic diameters (He, 0.26 nm; H₂, 0.289 nm; CO₂, 0.33 nm; N₂, 0.364 nm; CH₄, 0.38 nm; C₃H₈, 0.43 nm) was measured using a soap film meter and an experimental setup that is schematically shown elsewhere [22]. The gas was fed to the outside of a cylindrical membrane at 27-500 °C. The feed gas was pressurized at ~0.1 MPa, while the permeate stream was maintained at atmospheric pressure. Mixed-gas separation in an equimolar H₂/C₃H₈ mixture (50: 50 vol%) was conducted at 500 °C without sweep gas. The pressure at feed side was pressurized at 250 kPa (absolute pressure) using a back-pressure regulator, while the permeate side was maintained at atmospheric pressure (100 kPa). The gas composition was analyzed by using a Shimadzu GC-14B with a thermal conductivity detector. A log-mean pressure drop was used to calculate the permeance for mixtures. And the selectivity is defined as the permeance ratio [23].

2.3 Results and discussion

2.3.1 Physicochemical properties of PCS

2.3.1.1 Cross-linking of PCS

Fig. 2-1a shows the time course of TGA for PCS precursor powders during air curing at 250 °C for 2 h under air, which was followed by pyrolysis at 1,000 °C for 0.5 h under N₂. The typical time-versus-temperature profile was as follows: air curing at a certain temperature for 2 h, which then was switched to a pure N₂ atmosphere and held for ~30 min to flush the system and remove residual air. The temperature was then raised to 1,000 °C and held for 0.5 h. During air curing, the results of TGA

gradually increased due to the oxidative reaction of cross-linking, which will be discussed later in detail. During the pyrolysis process the results decreased due to the decomposition of the organic groups. Fig. 2-1b summarizes the TGA results of the PCS following the air curing and the pyrolysis processes, which were also normalized with the weight of the initial state of the PCS powder, as a function of the curing temperatures together with an uncured powder for comparison. Generally, cross-linking is performed at low and narrow temperature ranges of from 160-220 °C [17, 24]. In the present study, the PCS precursor powders were cured at temperatures that ranged between 150 and 400 °C at a 50 °C interval for 2 h under air. With increases in the curing temperature, the weight gain of the curing stage increased rapidly below 250 °C, then increased slightly and reaching a maximum value of 14.2 wt% at 300 °C, and finally was slightly decreased. This is because the activity of the Si-H group was increased with increases in temperature, which resulted in more oxygen being introduced into the precursor. With further increases in the curing temperature, however, some of the organic groups were burned off, which resulted in a decrease in the mass residue. Generally, the ceramic yield is an important factor that is used to evaluate a polymer precursor. After pyrolysis, the weight residue increased gradually with increases in the curing temperature until a platform was attained at 300 °C. It is worth noting that there was almost no weight gain in the cured PCS at 150 °C, but the weight of the residue at 150 °C was a significant improvement of 79 to 93 wt% compared with that of the uncured PCS. This indicates that curing for cross-linking enhanced the thermal stability of the PCS.

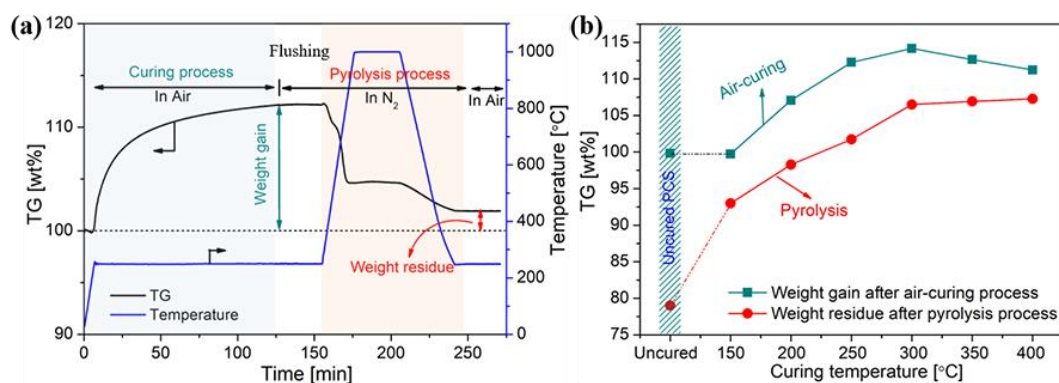


Fig. 2-1 (a) Time course of TGA for PCS precursor powders during air curing and pyrolysis processes (the temperature history is also shown to the right of the y-axis), (b) the TGA results of PCS during the air curing and pyrolysis processes as a function of the curing temperatures together with an uncured powder for comparison. The cured PCS powders were pretreated for 2 h under air before pyrolysis at 1,000 °C for 0.5 h under N₂.

Fig. 2-2 shows the ATR-FTIR spectra and elemental composition analysis via EDS for cured PCS powders at different curing temperatures together with that of raw powder for comparison. The ATR-FTIR vibration bands of the raw PCS marked in Fig. 2-2a are based on previous studies [17, 25, 26] and the detailed assignment was as follows: 2,950 cm⁻¹ (CH₃); 2,900 cm⁻¹ (CH₂); 2,100 cm⁻¹ (Si-H); 1,010 cm⁻¹ (Si-CH₂-Si); 1,250 cm⁻¹ (Si-CH₃); and, ~800 cm⁻¹ (vs, Si-C stretching). According to previous studies [17, 26], both of the Si-H and Si-CH₃ side groups in PCS can be attacked by oxygen and the effect of oxygen becomes larger at higher temperatures because the higher kinetic energy enables oxygen to attack atoms more effectively.

When the raw PCS was subjected to thermal oxidation curing at 150 °C, the peaks of Si-H and Si-CH₃ bonds were either unchanged and/or decreased only slightly, but when the curing temperature was raised to 200 °C, the Si-H peak was significantly decreased and/or almost disappeared, and both Si-CH₃ and the Si-C stretching peaks also were decreased significantly with the appearance of a weak peak at 1,710 cm⁻¹ (C=O bonds). The formation of C=O bonds suggested the side Si-CH₃ groups were oxidized [25]. Furthermore, the peak at around 1,010 cm⁻¹ increased and became broader owing to the formation of Si-O-Si (1,080 cm⁻¹) bonds that overlapped with the absorption of the Si-CH₂-Si (1,010 cm⁻¹) bonds.

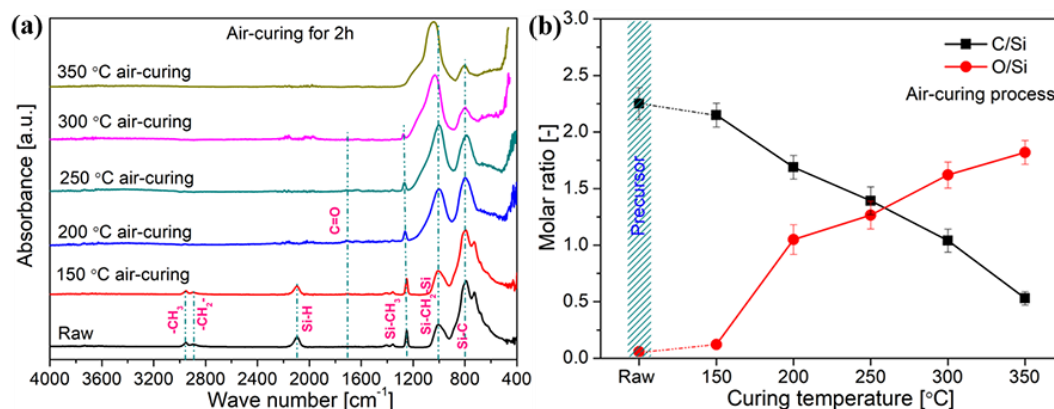


Fig. 2-2 (a) ATR-FTIR spectra and (b) elemental composition analysis for cured PCS powders via EDS at different curing temperatures for 2 h under air with raw powder analyzed for comparison (the molar ratio is based on Si).

Fig. 2-2b shows the EDS analysis of the elemental composition ratios (molar ratio based on Si) for cured PCS powders as a function of curing temperature. The ratio of O/Si increased rapidly when the curing temperature was increased higher than

150 °C, whereas that of C/Si exhibited the opposite trend. Compared with the raw PCS, when PCS was cured at 150 °C, the ratio of C/Si showed no changes and/or only a slight decrease, which was probably due to the vaporization of oligomers, whereas that of O/Si was increased only slightly due to a few oxidized Si-H groups forming Si-O-Si bonds. It is worth noting that the theoretical ratio of C/Si is 2 for raw PCS according to the molecular formula $[-(\text{CH}_3)\text{HSi-CH}_2-]_n$. When PCS was cured at 350 °C, the C/Si was only 0.54 (less than 1) with an O/Si value of 1.82, which is similar to silica (O/Si: 2). That result suggests that curing at high temperatures (≥ 350 °C) removes most of the side Si-CH₃ groups and carbon atoms in the main chain [-Si-CH₂-]. On the other hand, a certain number of organic groups in the precursor could have assisted in the formation of intermolecular bonding among the cross-linked precursor molecules/particles during pyrolysis. Thus, the air curing for cross-linking must be carefully controlled.

2.3.1.2 Pyrolysis of PCS

Fig. 2-3 shows the TGA curves of cured (air curing at 250 °C for 2 h) and uncured PCS powders with a heating rate of 35 °C/min to 1,000 °C. The weights of the residue materials were normalized at 250 °C for convenience of comparison. Clearly, at 93%, the cured powders had a higher residue weight than the uncured version at 81%. Furthermore, two curves for the weights of the residue reached plateaus at around 750 °C, indicating that the polymer-to-ceramic transformation was completed. Moreover, the examination of both cured and uncured PCS powders

revealed that the mass loss started at ~ 350 °C, or higher, but the slope at 350-750 °C in the TG curve was gentler for cured PCS than that for uncured PCS. This again confirmed that cross-linking stabilized the PCS structure, and, thus, the ceramic yield was increased.

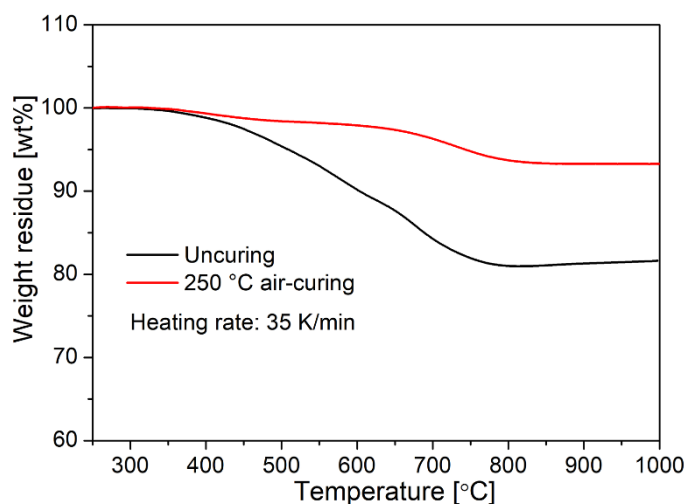


Fig. 2-3 TGA curves of the thermal decomposition behavior for cured and uncured PCS powders under a N_2 atmosphere. The cured powder was cured under air at 250 °C for 2 h, and the weights of the residue materials were normalized at 250 °C (i.e., deducting the mass gain during the curing process) for convenience of comparison.

The structure evolution during polymer-to-ceramic conversion was investigated by ATR-FTIR (Fig. 2-4). The absorption of Si-CH₃ ($1,250\text{ cm}^{-1}$) for both cured and uncured PCS was decreased with an increase in the pyrolysis temperature, and these groups had vanished at 750 °C. After that point, there was almost no change in the absorption bands, which confirmed that the polymer-to-ceramic transformation was completed at that temperature. This result was in good agreement with the results of

TG analysis shown in Fig. 2-3, i.e., the curves of weight residue reached plateaus at around 750 °C.

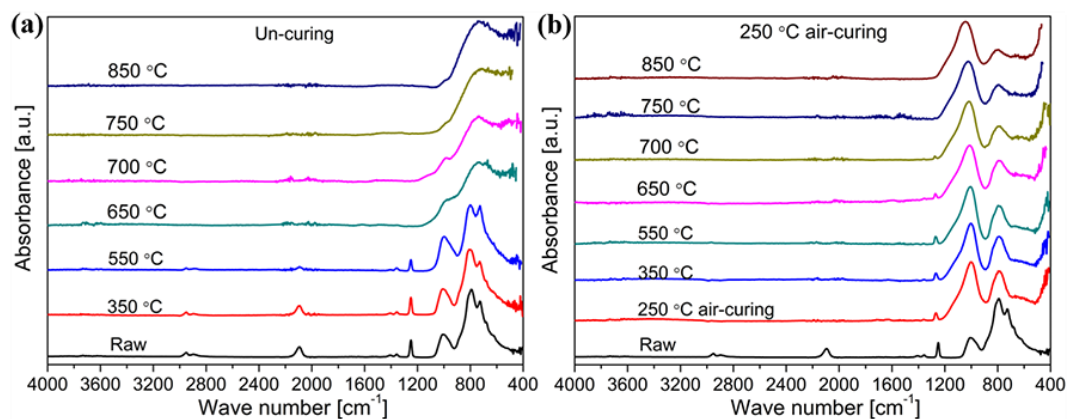


Fig. 2-4 ATR-FTIR spectra of (a) uncured and (b) cured (air curing at 250 °C for 2 h) PCS powders pyrolyzed under a N₂ flow for 2 h at different temperatures.

A small amount of Si-Si (620 cm^{-1}) bonds were believed to have formed in the uncured PCS during the decomposition via the dehydrocoupling reaction ($2\text{ }\equiv\text{Si-H} \rightarrow \equiv\text{Si-Si}\equiv + \text{H}_2$) to release H₂ and during the demethanation reaction ($\equiv\text{Si-H} + \equiv\text{Si-CH}_3 \rightarrow \equiv\text{Si-Si}\equiv + \text{CH}_4$) to release CH₄ [27-29]. The final ceramic powders of uncured PCS displayed a major absorption band at 800 cm^{-1} (attributed to the SiC₄ linkages [27]) with an overlapping and weak absorption band at $\sim 1,000\text{ cm}^{-1}$ that was attributed to the asymmetric stretching vibrations of Si-O owing to the reactions with oxygen and/or moisture that had adsorbed onto the surface of the powders. In addition to the absorption peak at 800 cm^{-1} (SiC₄), the final ceramic powders of cured PCS had a strong, broad peak between $1,250$ and 900 cm^{-1} , which was attributed to the stretching vibrations of Si-O-Si and O-Si-C mixture linkages [30, 31]. It is worth noting that the

Si-CH₃ bonds decreased rapidly at 350-650 °C for uncured PCS powders since the organic groups were mostly removed by the decomposition reaction with gas evolution, which generated a transitional structure [11].

Fig. 2-5 shows the EDS analysis of the elemental composition ratios for cured (air curing at 250 °C for 2 h) and uncured PCS powders as a function of pyrolysis temperature at 350-850 °C. With an increase in the pyrolysis temperature, the C/Si ratios for both cured and uncured PCS decreased slightly at temperatures below 550 °C, then decreased rapidly and reached platforms at 750 °C, but the falling slope was gentler for cured PCS than for uncured PCS, which agrees with the conclusions that the cross-linking enhances the thermal stability of the PCS structure and that the polymer-to-ceramic transformation was completed at 750 °C, which is consistent with the results of ATR-FTIR (Fig. 2-4). It should be noted that when the temperature was higher than 550 °C, the ratio of O/Si was increased slightly, which probably was due to the absorbed oxygen and/or moisture. In particular, for the uncured PCS, the O/Si ratio dropped again when the temperature reached higher than 650 °C. This may have been due to oxygen and/or moisture adsorbed by the unstable micropores of uncured PCS that were generated by the decomposition of organic groups at 550-650 °C. These micropores either collapsed or were closed at higher temperatures (> 650 °C), which resulted in densification [11].

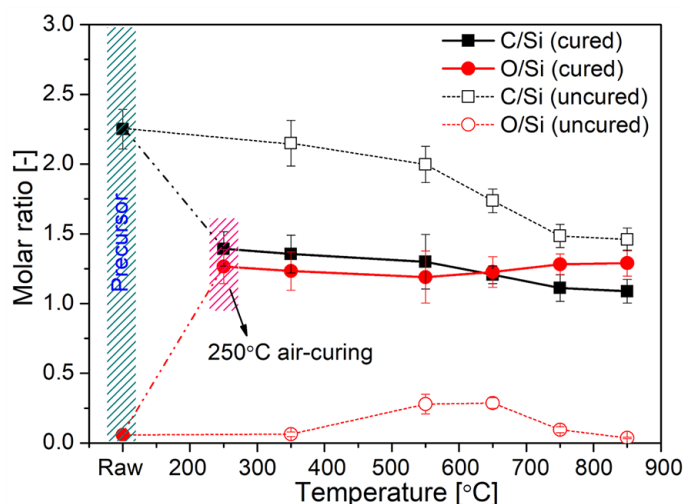


Fig. 2-5 Elemental composition analysis via EDS for cured (air curing at 250 °C for 2 h) and uncured PCS powders pyrolyzed at different temperatures for 2 h under N₂ flow together with raw powder for comparison (the molar ratio is based on Si).

The dependence of the chemical structure and elemental composition of the final ceramics on the curing temperature was also investigated. Fig. 2-6 shows the ATR-FTIR spectra and elemental composition analysis (together with the curing process for comparison) via EDS for the cured PCS powders pyrolyzed at 750 °C. With an increase in the curing temperature, the absorption peak between 1,250 and 900 cm⁻¹, which is attributed to the stretching vibrations of Si-O-Si and O-Si-C mixture linkages, increased, and become broader, which was ascribed to the increased number of Si-O bonds due to an increase in the oxygen content, as shown in Fig. 2-6b. Clearly, the centers of this peak shifted to a higher wave number (blueshift), from 1,000 cm⁻¹ to 1,055 cm⁻¹, with increases in the curing temperature, which was ascribed to the enhanced degree of cross-linking for the cured PCS via the introduction of more oxygen. A frequency shift in the FTIR spectra was also assigned

to changes in the bond angles for Si-O-Si, and the Si-O-Si bond angles were increased with the wave numbers [32, 33]. In this case, the blueshift indicated an increase in the bond angles (θ) of Si-O-Si between the strands derived from the linear skeleton of PCS, which resulted in an increase in the distance between the strands, as illustrated in Fig. 2-7.

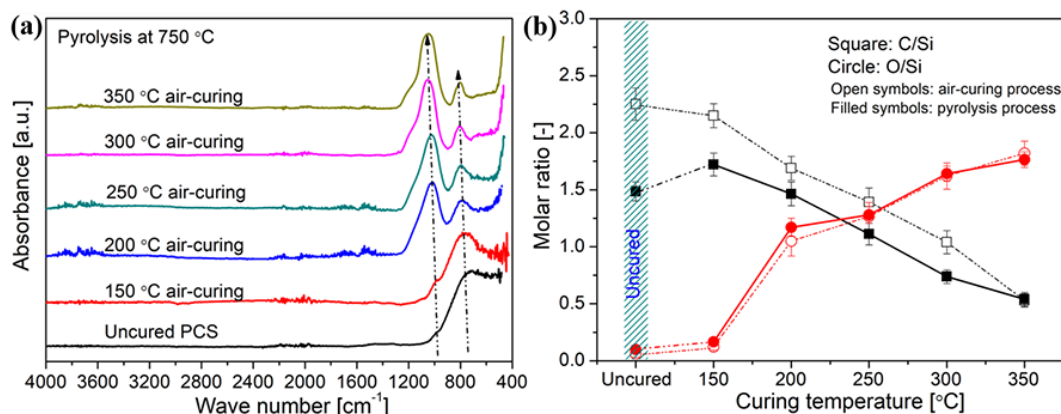


Fig. 2-6 (a) ATR-FTIR spectra and (b) elemental composition analysis via EDS (together with the curing process for comparison) of pyrolyzed PCS powders. The air curing process was carried out at different temperatures for 2 h under air, and the pyrolysis process was carried out at 750 °C for 2 h under N₂.

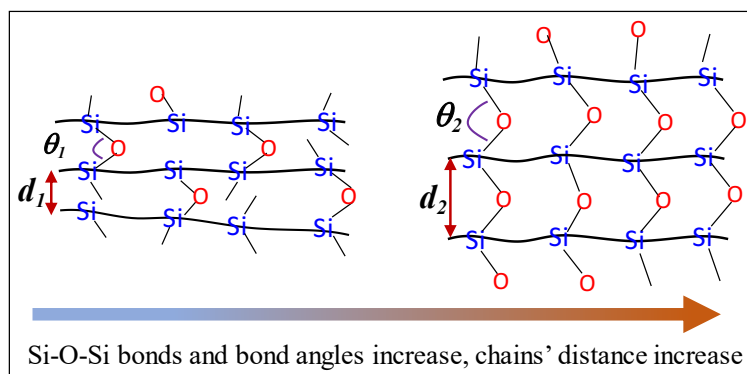


Fig. 2-7 Schematic illustration of the relationship between Si-O-Si bond angles and

the distance between strands for the final ceramic material with an increase in introduced oxygen.

On the other hand, the absorption peak centered at $\sim 800\text{ cm}^{-1}$ (Si-C) was decreased due to the positive correlation with the carbon content of the cured polymers and the decomposition of the organic groups during pyrolysis, as revealed by the EDS (Fig. 2-6b) and ATR-FTIR spectra (Fig. 2-4). Furthermore, the blue-shifted Si-C bonds with increases in the curing temperature, as shown in Fig. 2-6a, may also have corresponded to the increase in the C-Si-C bond angles [32]. Consequently, the cross-linking that resulted in an increase in the Si-O-Si and C-Si-C bond angles together with these rigid bonds were expected to form a more stable, uniform and three-dimensional microporous structure.

In addition, variations in the O/Si and C/Si ratios in the final ceramic powders followed the same trends as that in the cured (un-pyrolysis) PCS with respect to the curing temperature, as shown in Fig. 2-6b. This result indicates that the elemental composition of the final ceramic PCS was positively correlated with the cured polymers, and that the elemental composition could be precisely tailored via thermal oxidation curing. Different ceramic compositions would have different structural properties, which will be discussed in the next section.

2.3.1.3 Microstructure evolution of PCS

During the structure evolution of PCS, the XRD patterns can supply very useful

information on the packaging of inter-chains/strands via the spacing distance (d -spacing), which was determined using θ in Bragg's equation (i.e., $n\lambda=2d\sin\theta$) [34, 35]. The crystallization behaviors for the PCS powders during curing and pyrolysis processes were investigated via XRD, as shown in Fig. 2-8. As expected, the XRD patterns clearly showed entirely amorphous structures for all cured and pyrolyzed samples. As shown in Fig. 2-8a for the curing process, as the curing temperature increased to 350 °C, the peak centered at $\sim 35^\circ$ (d -spacing: ~ 0.25 nm) for the raw PCS and cured PCS at 150 °C, which was associated with the amorphous SiC environment, was shifted to a lower diffraction angle of $\sim 23^\circ$ (d -spacing: ~ 0.38 nm), which was associated with the amorphous SiOC environment. The observed shift in the main peak indicated that the spacing of the inter-chains/strands was remarkably increased with increases in the curing temperature due to the formation of more Si-O-Si bonds, which is consistent with trends documented in the blueshift of Si-O-Si peaks, in which increases in the bond angles revealed an increase in the d -spacing (ATR-FTIR, Fig. 2-6a). This tendency has also been reported in the radiation cross-linking of poly(lactic acid) [34] and poly(L-lactic acid)/poly(D-lactic acid) mixtures [35], as confirmed via XRD patterns.

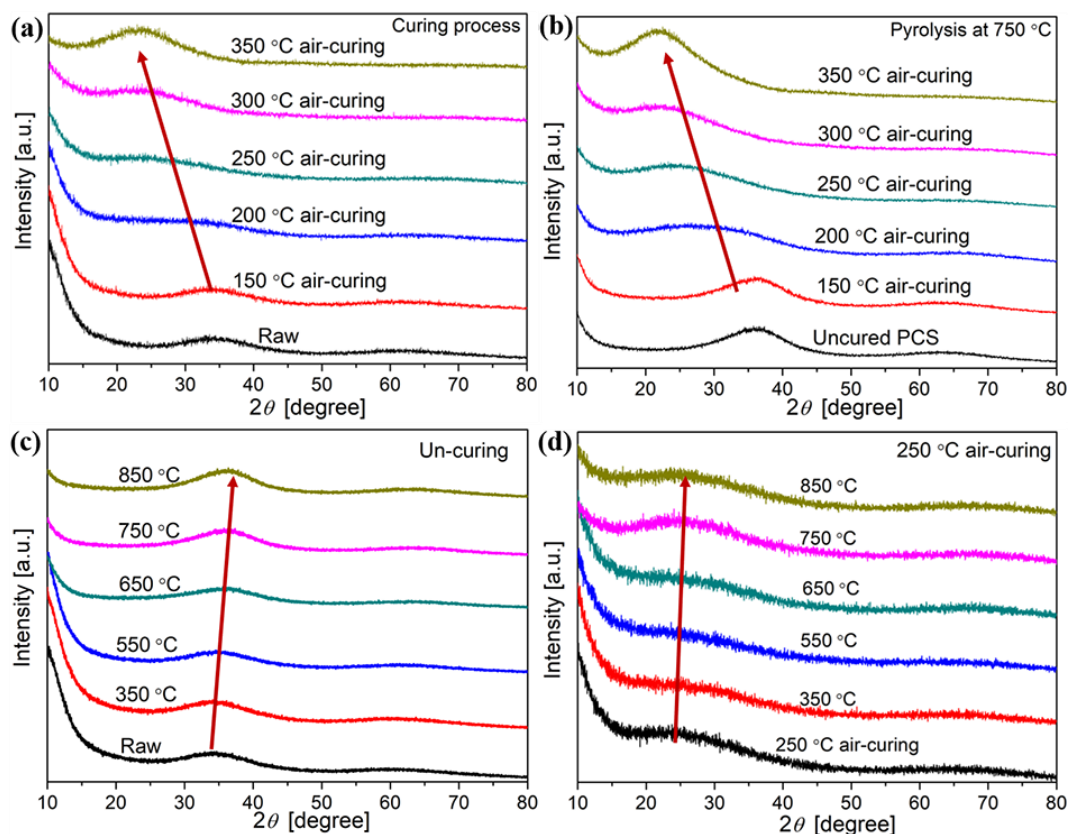


Fig. 2-8 XRD patterns of (a) cured PCS powders with different curing temperatures, (b) pyrolyzed PCS (deriving from the cured PCS) at a pyrolysis temperature of 750 °C, (c) uncured PCS powders with different pyrolysis temperatures, (d) cured PCS powders at a curing temperature of 250 °C with different pyrolysis temperatures. (The curing and pyrolysis processes were carried out for 2 h under air and N_2 atmospheres, respectively. The plots are displayed alongside those of raw/uncured powder for comparison.)

Fig. 2-8b shows the XRD patterns for the cured PCS pyrolyzed at 750 °C, all samples showed a similar trend during the curing process (Fig. 2-8a). Each peak of the pyrolyzed samples, however, was moved slightly to a higher diffraction angle, and, in particular, the cured samples at 150 °C and the uncured samples with a low

cross-linking degree showed a greater shift. As shown in Figs. 8c and d, the diffraction peaks of the samples moved towards a higher diffraction angle with increases in the pyrolysis temperature, and the spacing of the inter-chains/strands was decreased, which also resulted in densification [3]. In particular, the degree of shift in the samples cured at 250 °C was much lower than that in the uncured samples. This indicated that the cross-linking promoted the structural thermal stability of the PCS, and that the structure of uncured PCS tended to become more densified as the pyrolysis temperature increased and micropores could more easily collapse or close [11].

The structural parameters (micropore volume and BET surface area) of micropores analyzed via the N₂ adsorption-desorption isotherms for the PCS powders with different curing temperatures as a function of pyrolysis temperature are listed in Tables 2-1 and 2-2.

Table 2-1 Micropore volumes based on nitrogen adsorption for the uncured and cured PCS powders as a function of pyrolysis temperature.

Pyrolysis temperature [°C]	Micropore volume* [cm ³ g ⁻¹]					
	Un-curing	150 °C air-curing	200°C air-curing	250°C air-curing	300°C air-curing	350°C air-curing
350	0.0268	0.0398	0.2164	0.1819	0.149	0.05
550	0.2669	0.2546	0.2326	0.1789	0.0426	0.0023
650	0	0	0.1304	0.1345	0.0063	0
750	0	0	0	0	0	0

*The micropore volume was calculated using *t*-plot analysis.

Table 2-2 BET surface area based on nitrogen adsorption for the uncured and cured PCS powders as a function of pyrolysis temperature.

Pyrolysis temperature [°C]	BET surface area* [m ² g ⁻¹]					
	Un-curing	150 °C air-curing	200°C air-curing	250°C air-curing	300°C air-curing	350°C air-curing
350	36	68	449	404	358	121
550	592	579	520	400	108	4.8
650	0.6	1.26	316	332	11.9	0.84
750	0.52	0.62	0.754	0.97	0.37	0.68

*BET surface area was obtained from the linear BET plots over the range of $0.001 < P/P_o < 0.15$.

In particular, the micropore volumes of cured (air curing at 250 °C) and uncured PCS as a function of pyrolysis temperature are also plotted in Fig. 2-9a. With an increase in the pyrolysis temperature, the micropore volumes for the samples derived from low curing temperatures of 150 and 200 °C (as shown in Table 2-1) and the uncured sample (as plotted in Fig. 2-9a) first increased and reached a maximum at 550 °C, at which point an abundant number of organic groups were decomposed producing transitional structures. With a further increase in the pyrolysis temperature, the micropore volumes were decreased due to the rearrangement and densification reactions [11, 36]. For samples derived from the high curing temperatures (≥ 250 °C, as shown in Table 2-1, and the sample cured at 250 °C plotted in Fig. 2-9a), the

micropore volume was decreased gradually with an increase in the pyrolysis temperature, which indicated a large number of micropores could have been generated during the curing process.

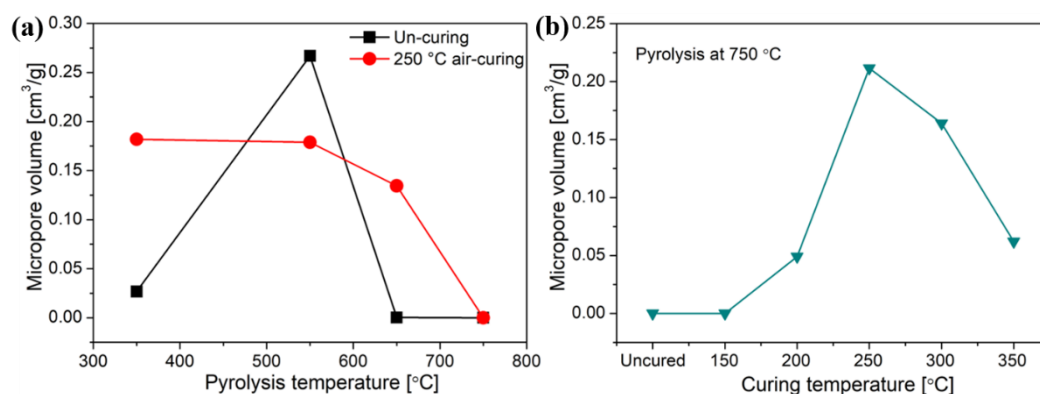


Fig. 2-9 (a) Micropore volume based on N₂ adsorption-desorption isotherms at -196 °C for uncured and cured (air curing at 250 °C) PCS powders pyrolyzed at different temperatures, and (b) micropore volume based on CO₂ adsorption-desorption isotherms at 25 °C for cured PCS powders pyrolyzed at 750 °C (together with an uncured powder for comparison). The air curing and pyrolysis processes were performed for 2 h under air and under N₂ flow, respectively.

Variations in the BET surface area (Table 2-2) exactly followed the same trends as those of the micropore volumes. It is worth noting that at a pyrolysis temperature of 650 °C, the micropore volumes and BET surface areas were non-zero only for the samples cured between 200-300 °C, and the maximum values were obtained at a curing temperature of 250 °C. However, when the pyrolysis temperature reached 750 °C, the micropore volumes of all samples dropped to zero, and no micropores

were presented in the samples. Generally, N₂ (0.364 nm) molecules cannot access the ultra-micropores (< 0.7 nm) at extremely low temperatures (-196 °C). By contrast, the smaller CO₂ (0.33 nm) molecules are able to enter these pores with a high level of kinetic energy at high temperatures (25 °C) [37]. Fig. 2-9b shows the micropore volume based on the CO₂ adsorption at 25 °C for PCS powders pyrolyzed at 750 °C. The variations in the micropore volumes by CO₂ adsorption are similar to the N₂ data of the samples pyrolyzed at 650 °C, and the maximum values of micropore volume also existed at a curing temperature of 250 °C. Moreover, samples with a low degree of cross-linking (i.e., uncured and cured at 150 °C) showed no micropores even for the more sensitive CO₂ as the adsorbed molecules. These results indicate that appropriate cross-linking can promote structural stability, and that either excessive (main chain may be oxidized) or insufficient cross-linking could cause the micropores to collapse or disappear.

Based on the characteristics described thus far, the evolution of the network structures for both the cross-linked and non-cross-linked PCS pyrolyzed at 750 °C is schematically illustrated in Fig. 2-10. The ceramic structures of both uncured and low cross-linked PCS were derived from the stacks of random “strands” of the linear polymer molecules. Some small micropores could be formed by the weak cross-linking caused by the dehydrocoupling and demethanation reactions with the formation of Si-Si bonds, in which the Si-Si bonds are responsible for very short spacing between the strands. Also, large “slit-like” micropores were possibly formed by the imperfect packing of the aforementioned strands, which is similar to the

formation of pores in carbon molecular sieve materials [38]. On the contrary, the ceramic structures of cured PCS with a suitable cross-linking were derived from the cross-linked polymer molecules with uniform cross-linked strands created by Si-O-Si bonds, which made the final structure both more stable and more stationary under high temperatures.

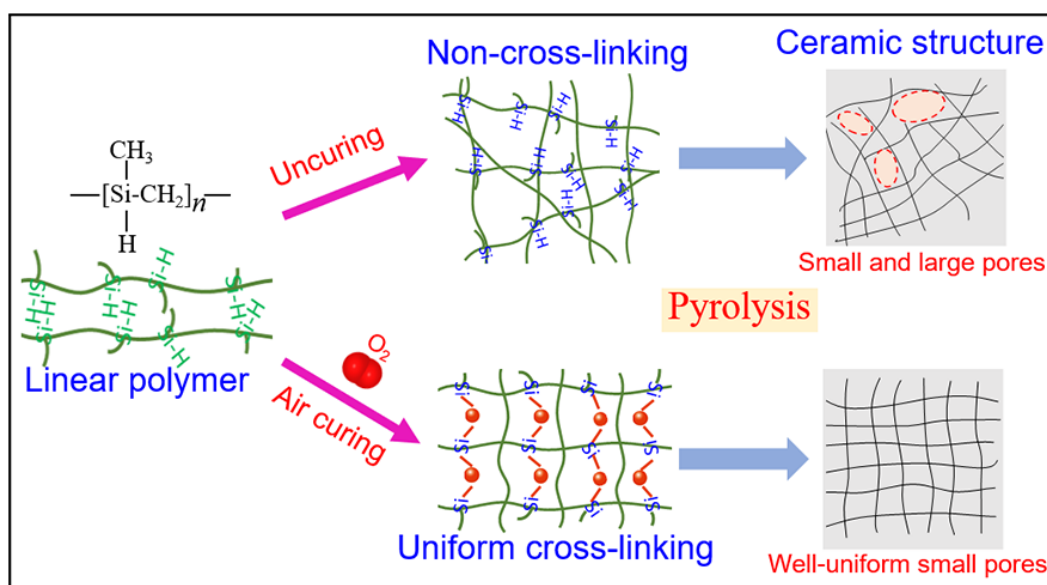


Fig. 2-10 Schematic illustration showing the evolution of the network structure for the cured and uncured PCS.

2.3.2 PCS-derived membranes

2.3.2.1 Membrane fabrication and gas permeation

PCS membranes were prepared by coating a 3% PCS solution onto intermediate layers followed by curing under air at 150, 200, 250 and 300 °C and then pyrolysis under a N₂ atmosphere at 750 °C, which hereafter will be used to refer to the membranes: M150, M200, M250 and M300, respectively. Fig. 2-11a shows the single-gas permeance at 200 °C for PCS membranes cured at 150-300 °C as a

function of the molecular size, and Fig. 2-11b shows the H_2/N_2 , H_2/CH_4 and H_2/C_3H_8 selectivity with the H_2 permeance as a function of the curing temperature. With the exception of H_2 , the permeance was decreased with the kinetic increases in the diameters of the molecules for a permeance order of $H_2 > He > CO_2 > N_2 > CH_4 > C_3H_8$. Moreover, the selectivity of small molecules (e.g., He, and H_2) over the large ones (e.g., N_2 , CH_4 and C_3H_8) was higher than Knudsen selectivity, indicating that the membranes exhibited molecular sieving properties.

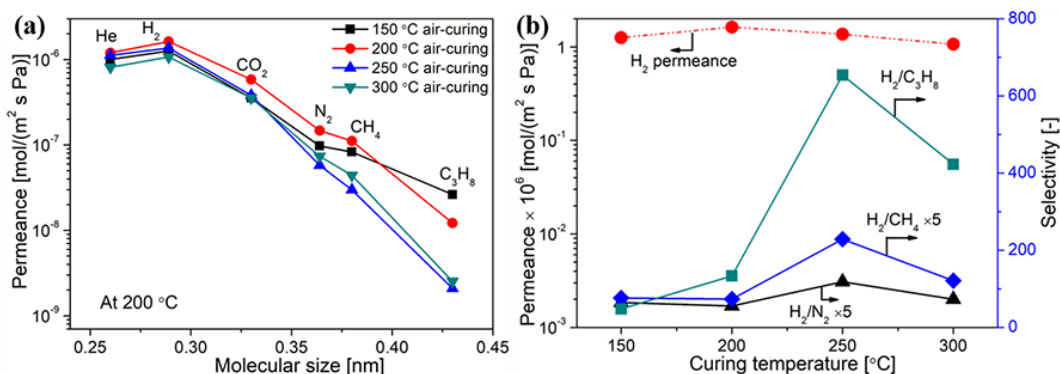


Fig. 2-11 (a) Single-gas permeance at 200 °C as a function of molecular size through PCS membranes formed by different curing temperatures and pyrolyzed at 750 °C, (b) relationship between the gas permeation performance of PCS membranes and curing temperature.

The small molecular gases (0.26 ~ 0.33 nm, i.e., He, H_2 and CO_2) have similar permeation properties despite the use of membranes derived from different curing temperatures. For example, the H_2 permeance of all membranes exhibited satisfactory H_2 permeance of $1\sim 2 \times 10^{-6}$ mol/(m² s Pa). This is because the small molecules are allowed to permeate through both small and large pores of the membranes. On the

contrary, the gas permeabilities of the larger molecules (≥ 0.364 nm) showed different trends depending on the curing temperature. As shown in Fig. 2-11b, the membranes M150 and M200 derived from cured PCS with a low degree of cross-linking showed selectivities for H_2/N_2 , H_2/CH_4 and $\text{H}_2/\text{C}_3\text{H}_8$ that were lower than that of the M250 and M300 membranes that are derived from a higher degree of cross-linking. This result indicates that a low degree of cross-linking creates difficulties in obtaining small pores or defect-free membranes compared with that of extensively cross-linked PCS with pores that are precisely uniform and small. In addition, the M250 membrane exhibited the maximum selectivities for H_2/N_2 (24), H_2/CH_4 (47) and $\text{H}_2/\text{C}_3\text{H}_8$ (654), and exhibited a satisfactory H_2 permeance of 1.37×10^{-6} mol/(m^2 s Pa) at 200 °C. This performance of the M250 membrane could be ascribed to a unique stoichiometric composition ($\text{Si}_{1.0}\text{O}_{1.28}\text{C}_{1.11}$ shown in Fig. 2-6) and a very stable microstructure (largest micropore volume shown in Fig. 2-9) attributed to an appropriately cross-linked and three-dimensional network via the hybrid rigid bonds of Si-O-Si, O-Si-C, and Si-C. Therefore, the M250 was selected as the most promising membrane.

Fig. 2-12 shows the single-gas permeation properties at 200 °C as a function of molecular size through PCS M250 membranes prepared under the same conditions. The averages for H_2 permeance and H_2/N_2 selectivity of the four membranes were $(1.20 \pm 0.13) \times 10^{-6}$ mol (m^2 s Pa) $^{-1}$ and 19 ± 3.5 , respectively. The relative standard deviations of H_2 permeance and H_2/N_2 selectivity were 10.6 and 19%, respectively, which indicated that synthesis of these membranes is reproducible.

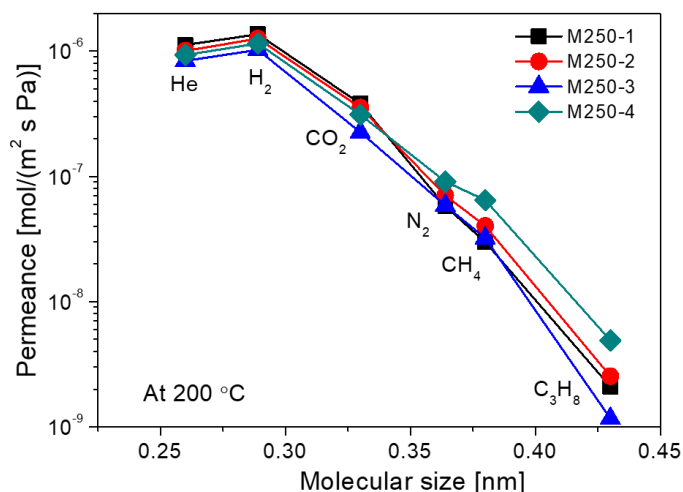


Fig. 2-12 Single-gas permeance at 200 °C as a function of molecular size through PCS membranes. PCS membranes were prepared by coating a 3% PCS solution onto intermediate layers followed by curing under air at 250 °C, and were pyrolyzed under a N₂ atmosphere at 750 °C.

2.3.2.2 Thermal stability and oxidation resistance of PCS membranes

Fig. 2-13 shows the molecular size dependence of single-gas permeance at 200 °C for a PCS-derived membrane (M250-1) before and after the thermal stability test at 500 °C. Clearly, the membrane (M250-1) showed a high level of thermal stability at 500 °C under a He atmosphere for 12 h, and no appreciable change in permeance was confirmed for any gas.

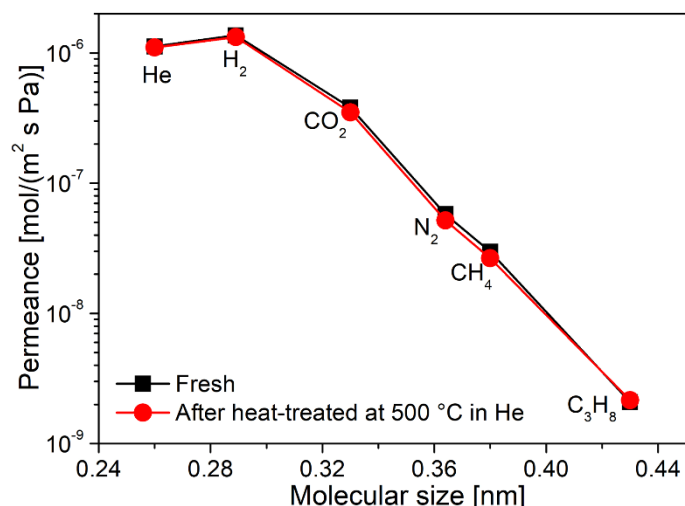


Fig. 2-13 Single-gas permeance at 200 °C as a function of molecular size for a PCS membrane (M250-1) before and after thermal stability testing at 500 °C under a He atmosphere for 12 h.

A common problem associated with the dehydrogenation of alkanes is the formation of coke, which leads to catalyst deactivation and decreases membranes performance [39, 40]. The catalysts and membranes were usually regenerated using an oxidant agent (e.g., air) in order to burn off the coke. Therefore, the oxidation resistance of membranes is important. Fig. 2-14 shows the values recorded for the time course of air flux at 500 °C under a pressure difference of 50 kPa for a typical PCS (M250-2) membrane. The air flux was slightly increased during the initial stages due to the burning of free carbons and then reached a steady state after exposure to air for 1 h. Fig. 2-15 shows the single-gas permeance at 200 °C for the PCS M250-2 membrane before and after air treatment at 500 °C as a function of the molecular size. The membrane showed a slight increase in gas permeance after air treatment, with little change in the selectivity of the membrane, particularly in the selectivities of

H_2/N_2 and H_2/C_3H_8 . This result suggests that the PCS membranes had good resistance to oxidation, which was also confirmed by the TG analysis shown in Fig. 2-16. It is worth noting that the TG analysis of the pyrolyzed PCS powder basically showed a mass loss of 4% at 200 °C, which could possibly be attributed to adsorbed water. The residual weight of the pyrolyzed PCS powder (the pyrolyzed powder was prepared under the same conditions as the M250 membranes) showed almost no change (less than 0.5 wt%) after air treatment at 500 °C for 12 hours. This result confirmed that PCS-derived ceramics have excellent oxidation resistance and agreed with the findings of experiments using TiPCS-derived SiC-based membranes [41]. The free carbons were removed, which could reduce the steric resistance and enhance the gas permeation while maintaining selectivity due to the high-level stability of the skeleton structure.

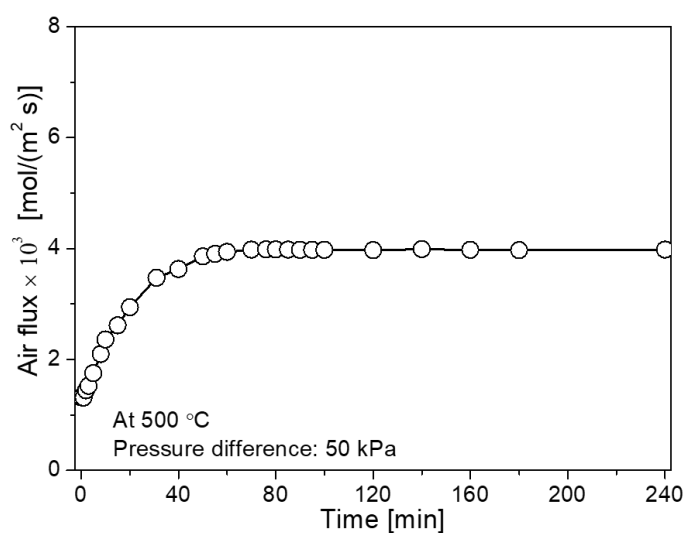


Fig. 2-14 Time course of air flux for a PCS membrane (M250-2) at 500 °C with a pressure difference of 50 kPa.

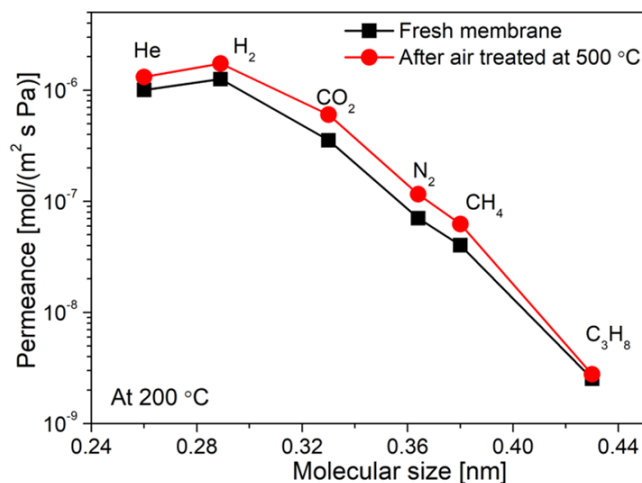


Fig. 2-15 Single-gas permeance at 200 °C for a PCS M250-2 membrane before and after air treatment at 500 °C for 4 h.

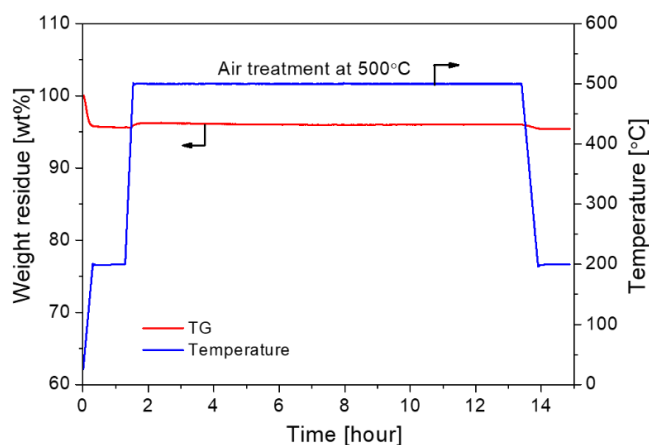


Fig. 2-16 Time-course changes in the weight of the pyrolyzed PCS powder residue under air at 500 °C following 12 h (the temperature history appears to the right of the y-axis). The pyrolyzed PCS powder was prepared by air curing at 250 °C and pyrolysis at 750 °C under N₂.

2.3.2.3 Temperature dependence of gas permeation

Testing for the temperature dependence of gas permeance for the PCS-derived membranes was carried out using two membranes (M250-1 and M250-3) at temperatures ranging from 27-500 °C. Moreover, the two M250 membranes had a

similar average pore size of ~ 0.41 nm (as shown in Fig. 2-17) based on the modified gas translation model (GT) previously proposed by our group [42, 43], and the temperature dependence of the single-gas permeation for the M250-3 membrane, as shown in Fig. 2-18, displayed behavior similar to that of the M250-1 (Fig. 2-19), which again confirmed that the synthesis of this membrane is reproducible.

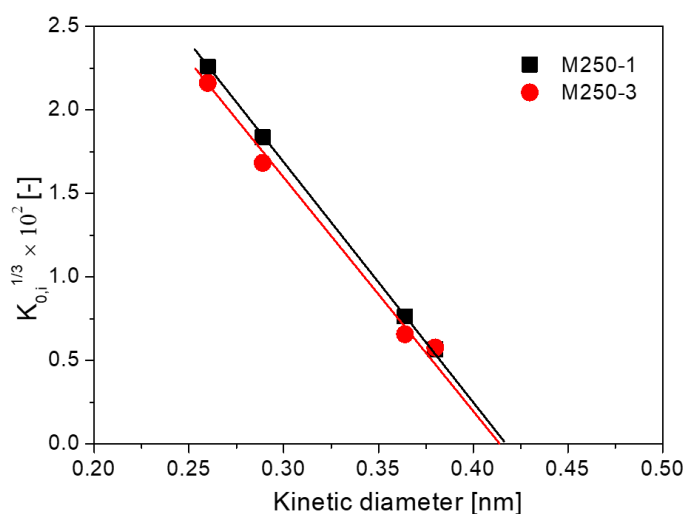


Fig. 2-17 The relationship between kinetic diameter and $K_{0,i}^{1/3}$ for PCS membranes (M250).

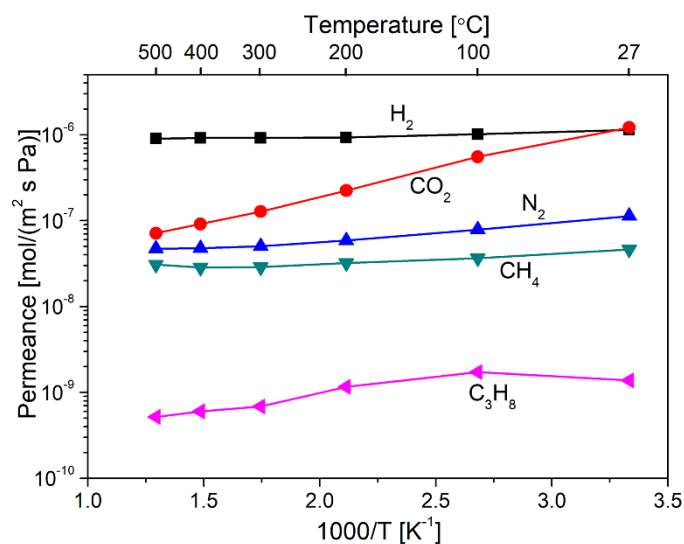


Fig. 2-18 Temperature dependence of single-gas permeance for a PCS membrane (M250-3).

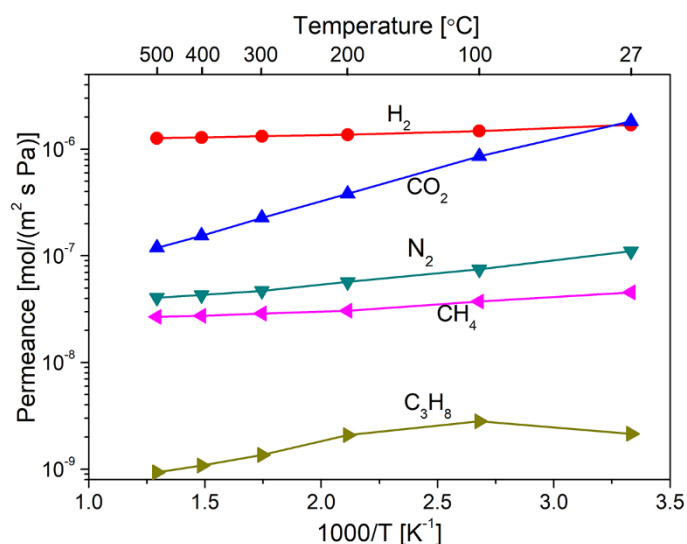


Fig. 2-19 Temperature dependence of single-gas permeance for a PCS membrane (M250-1) formed by air curing at 250 °C and pyrolysis at 750 °C.

As shown in Fig. 2-19, the permeance of H₂ was independent of temperature, which can be ascribed to the balance of activated and Knudsen permeation. Most sol-gel-derived microporous silica membranes have an average pore size of approximately 0.3-0.35 nm, in which H₂ molecules can permeate by activated permeation [44]. In the present study, the M250 showed an average pore size of ~0.41 nm, which was much larger than that of silica membranes and is consistent with its higher permeance for H₂ than for He as shown in Fig. 2-11 via the contribution of Knudsen flow.

The permeance of CO₂ was increased with decreases in the permeation temperature, which indicated a surface diffusion mechanism, because of the greater adsorption of CO₂ on the pore surface at lower temperature due to a strong affinity by comparison with other gases. At room temperature, in particular, the CO₂ (0.33 nm) permeance was higher than that of H₂ (0.289 nm) even though CO₂ has a larger

molecular size. The values for the permeance of N₂ and CH₄ increased as the temperature decreased, which was also caused by a surface diffusion mechanism. However, N₂ and CH₄ showed a gentler slope in the temperature dependence compared with that of CO₂, which can be ascribed to Knudsen and/or surface diffusion caused by weak affinity.

The M250-1 membrane showed H₂/C₃H₈ selectivity of 1,350 together with H₂ permeance of 1.27×10^{-6} mol (m² s Pa)⁻¹ at 500 °C. With an increase in the permeation temperature, the permeance of C₃H₈, however, first increased and reached a maximum peak at 100 °C and then decreased. The permeation mechanism of adsorptive C₃H₈ through membrane pores can be described by the balance between diffusivity and adsorption. With an increase in the temperature, the diffusivity increases, but the amount of adsorption decreases. Thus, the maximal permeance can be explained as follows: the number of adsorbed molecules decreases at temperatures higher than the peak (at 100 °C), while adsorption, which is enhanced at temperatures lower than the peak, causes a decrease in mobility (liquidlike diffusion of pore-filling molecules) [44]. The maximum C₃H₈ permeance was also observed at 100 °C through silicalite-1 [45] and organosilica [44] membranes.

Based on the detailed characterizations thus far, the PCS membranes demonstrate good potential for low-temperature separation of CO₂ (e.g., CO₂/CH₄) and high-temperature separation of H₂ (e.g., H₂/N₂ and H₂/C₃H₈).

2.3.2.4 Separation performance of PCS-derived membranes

Substantial efforts have been made to develop H₂-permselective membranes. The separation of H₂ and C₃H₈ is one of the most important and attractive processes in the petrochemical industry. The use of membranes and/or membrane reactors to remove hydrogen in-situ is well known to be more effective in the direct dehydrogenation of propane to propylene at high temperature, in which the unreacted hot propane can be recycled to the reaction without a cooling process, which promises to save energy consumption. Furthermore, conversion enhancement by the removal of the hydrogen produced in this equilibrium-limited reaction can lead to significantly enhanced productivity.

Fig. 2-20 illuminates the separation performances of a typical PCS membrane (M250-4) as a function of test time at 500 °C for both single gases and an equimolar H₂/C₃H₈ mixture. Those results clearly show that the PCS membrane demonstrated a very stable separation performance (including the permeance and selectivity) for both single gases and the mixture during more than 12 h of measurement. Before and after testing the gas mixture for 6 h, the H₂ and C₃H₈ permeance and H₂/C₃H₈ selectivity of the single gases remained almost unchanged, indicating that the PCS membrane possesses excellent stability due to its stable structure. Interestingly, the permeance and selectivity of the mixture was approximately the same as those of the single gases, that is, the components of the mixture permeate the membrane independently of each other, probably due to no adsorption effect for gas components at a temperature of 500 °C. Thus, the separation mechanism for PCS membranes was ascribed to

molecular sieving, and the separation performance of the $\text{H}_2/\text{C}_3\text{H}_8$ mixture could be predicted according to the single-gas permeation properties.

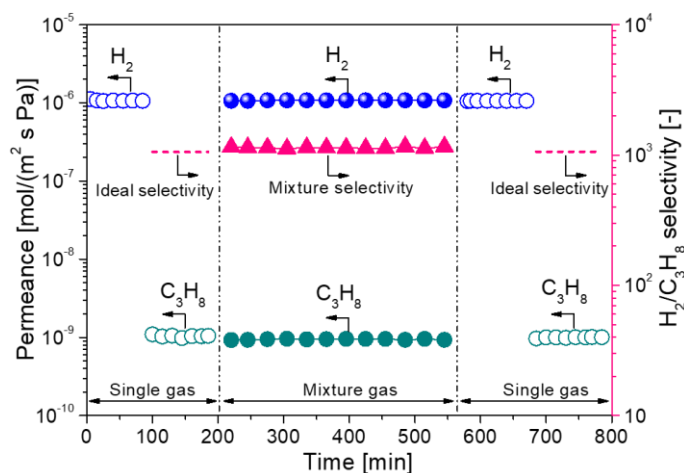


Fig. 2-20 Permeance and selectivity through PCS membrane M250-4 as a function of test time at 500 °C. The solid and open symbols represent data for the gas mixture and for the single gases, respectively. The mixture was an equimolar $\text{H}_2/\text{C}_3\text{H}_8$; the feed pressure was 250 kPa (absolute); the permeate pressure was 100 kPa.

Fig. 2-21 shows the selectivity of $\text{H}_2/\text{C}_3\text{H}_8$ at 20-650 °C as a function of H_2 permeance for various types of membranes, which include zeolite, silica, mixed-matrix, and SiC-based (SiC, SiOC and SiNC) membranes [46]. For example, silica membranes derived from tetraethoxysilane (TEOS) with a pore size of 0.3 nm showed $\text{H}_2/\text{C}_3\text{H}_8$ selectivities of 70-90 together with a low H_2 permeance of $\sim 1.4 \times 10^{-7} \text{ mol (m}^2 \text{ s Pa)}^{-1}$ at 500 °C due to the high resistance caused by the small pores [47]. An ultrathin mixed-matrix membrane (ZIF-8/CNT) has shown H_2 permeance of $2.87 \times 10^{-5} \text{ mol (m}^2 \text{ s Pa)}^{-1}$ with a $\text{H}_2/\text{C}_3\text{H}_8$ selectivity of 950.1 at 20 °C [48]. However,

a major problem is how to control the grain boundary defects for the metal-organic framework layers, which may limit its further application on a large scale, and a more important and critical issue is its limited application at high temperatures ($> 400\text{ }^{\circ}\text{C}$) due to decomposition of the organic framework [48, 49]. Recently, an emerging novel Mxene membrane has been receiving an increasing amount of attention. For example, Ding et al. [50] reported a 2D laminar MXene membrane for H_2 separation, in which, the membrane showed H_2 permeance of $4 \times 10^{-7}\text{ mol (m}^2\text{ s Pa)}^{-1}$ with H_2/N_2 selectivity of 129 and $\text{H}_2/\text{C}_3\text{H}_8$ selectivity of 2024 at $25\text{ }^{\circ}\text{C}$. However, this type of membrane is easily oxidized under oxidizing gases such as O_2 and CO_2 at high temperature [51]. Under high temperatures, most current nanoporous H_2 permeation membranes either demonstrate considerably lower levels of permeance, or suffer from low stability. SiC-based membranes with SiC covalent bonds have a high degree of stability [52]. The optimized PCS-derived, SiC-based membranes (M250) showed superior H_2 permeance of $1\text{-}2 \times 10^{-6}\text{ mol (m}^2\text{ s Pa)}^{-1}$ with $\text{H}_2/\text{C}_3\text{H}_8$ selectivity as high as 1,740 that compares favorably with other membranes (zeolite, silica and other SiC-based membranes) across a wide range of temperatures: $20\text{-}650\text{ }^{\circ}\text{C}$. The high level of permselectivity for $\text{H}_2/\text{C}_3\text{H}_8$ was ascribed to the precise and uniform small pores (0.41 nm) that are the result of appropriately cross-linked networks.

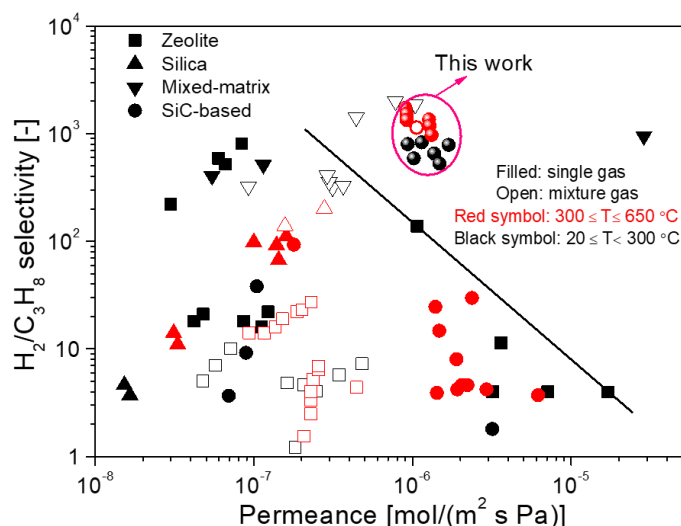


Fig. 2-21 Comparing PCS membranes with zeolite, silica, mixed-matrix, and SiC-based (SiC, SiOC and SiNC) membranes for H_2/C_3H_8 separation performance [46].

In addition to evaluating performance in the separation of H_2/C_3H_8 , the performance of PCS-derived membranes in the separation of H_2/N_2 and CO_2/CH_4 was also evaluated. Fig. 2-22a compares the H_2/N_2 separation performance for silica [19] and SiC-based (SiC, SiOC and SiAlC) membranes [46]. Silica membranes, which were prepared by sol-gel or CVD, generally showed high performance in H_2/N_2 separation because of a narrow pore size, but their performance was reportedly poor under a hydrothermal atmosphere, particularly at high temperatures [19]. As shown in Fig. 2-22a, PCS-derived membranes showed a moderate level of H_2/N_2 selectivity (20-31) with an acceptable H_2 level of permeation ($(1-2) \times 10^{-6} \text{ mol}/(\text{m}^2 \text{ s Pa})$), which showed superior permselectivity compared with other SiC-based membranes.

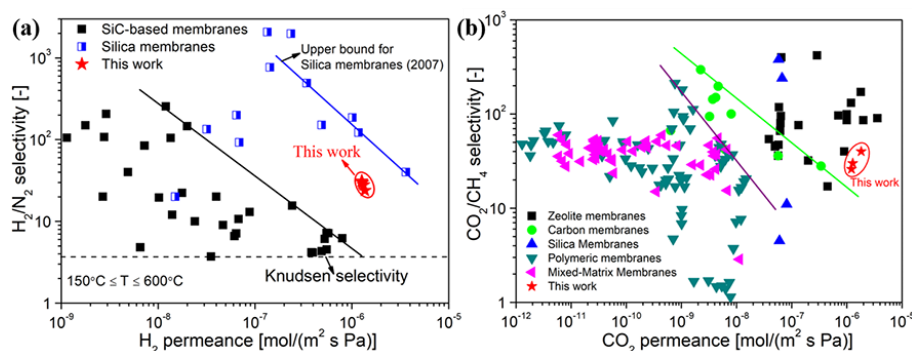


Fig. 2-22 (a) H_2/N_2 ideal selectivity plotted against H_2 permeance for silica [19] and SiC-based (SiC, SiOC and SiAlC) membranes at temperatures ranging from 150-600 °C, (b) CO_2/CH_4 ideal selectivity plotted against CO_2 permeance for different types of membrane systems at or around room temperature [46].

Fig. 2-22b compares PCS-derived membranes with a variety of microporous membranes for CO_2/CH_4 separation at or around room temperature [46]. AEI-type AlPO-18 [53] and CHA-type SAPO-34 [54] zeolite membranes are known to have a pore size of 0.38 nm, which limits the permeation of CH_4 (0.38 nm), and results in high CO_2/CH_4 selectivity together with a high level of CO_2 permeance due to the strong affinity between CO_2 molecules and zeolite frameworks. Compared with various types of membranes, PCS-derived membranes show superior CO_2 permeance of $1.8 \times 10^{-6} \text{ mol}/(m^2 \cdot s \cdot Pa)$ and CO_2/CH_4 selectivity of 40, which far surpasses the upper bounds of carbon membranes, polymeric membranes, or mixed-matrix membranes (MOFs), which may provide a competitive option for membrane materials applicable to the separation of CO_2/CH_4 .

2.4 Conclusions

In this study, the physicochemical properties and microstructural variations of

PCS were systematically studied under different curing and pyrolysis temperatures. Cross-linking behavior enhanced the thermal stability of the PCS structure and the polymer-to-ceramic transformation was completed at 750 °C for both cured and uncured PCS. The cross-linking remarkably increased the inter-chain spacing, which resulted in uniform networks. Either excessive or insufficient cross-linking by air curing tends to cause the collapse or disappearance of micropores of the resulting ceramic material at high temperatures. Furthermore, the elemental composition and microstructure can be precisely tailored via thermal oxidation curing. CO₂ adsorption revealed that PCS-derived ceramics cured at 250 °C possess a stable and uniform microporous structure that is ascribed to appropriately cross-linked networks. The PCS-derived membranes demonstrated high thermal stability and oxidation resistance at 500 °C. The optimized membrane had excellent permeation properties (H₂/N₂ selectivity of 31 and H₂/C₃H₈ selectivity as high as 1,740 together with high H₂ permeance of $1-2 \times 10^{-6}$ mol/(m² s Pa) at 500 °C, and CO₂ permeance of 1.8×10^{-6} mol/(m² s Pa) at room temperature with a CO₂/CH₄ selectivity of 40). Moreover, the separation performance in an equimolar H₂/C₃H₈ mixture at 500 °C were approximately the same as those in single gases, in which, the separation mechanism could be ascribed to molecular sieving. This study is the first to propose the concept of tailoring the microstructure and permeation properties of SiC-based membranes via controlling the thermal-oxidative curing process, which is a novel method for the design of SiC-based membranes.

References

- [1] L. Meng, X. Yu, T. Niimi, H. Nagasawa, M. Kanezashi, T. Yoshioka, T. Tsuru, Methylcyclohexane dehydrogenation for hydrogen production via a bimodal catalytic membrane reactor, *AIChE J.*, 61 (2015) 1628-1638.
- [2] H.M. Williams, E.A. Dawson, P.A. Barnes, B. Rand, R.M. Brydson, The development and stability of porosity formed during the pyrolysis of polyborodiphenylsiloxane, *Microporous Mesoporous Mater.*, 99 (2007) 261-267.
- [3] H.M. Williams, E.A. Dawson, P.A. Barnes, B. Rand, R.M.D. Brydson, A.R. Brough, High temperature ceramics for use in membrane reactors: the development of microporosity during the pyrolysis of polycarbosilanes, *J. Mater. Chem.*, 12 (2002) 3754-3760.
- [4] A.R. Maddocks, D.J. Cassidy, A.S. Jones, A.T. Harris, Synthesis of nanoporous silicon carbide via the preceramic polymer route, *Mater. Chem. Phys.*, 113 (2009) 861-867.
- [5] B. Elyassi, W.X. Deng, M. Sahimi, T.T. Tsotsis, On the Use of Porous and Nonporous Fillers in the Fabrication of Silicon Carbide Membranes, *Industrial & Engineering Chemistry Research*, 52 (2013) 10269-10275.
- [6] S.C. Kim, H.J. Yeom, Y.W. Kim, I.H. Song, J.H. Ha, Processing of alumina-coated glass-bonded silicon carbide membranes for oily wastewater treatment, *International Journal of Applied Ceramic Technology*, 14 (2017) 692-702.
- [7] K. König, V. Boffa, B. Buchbjerg, A. Farsi, M.L. Christensen, G. Magnacca, Y.

- Yue, One-step deposition of ultrafiltration SiC membranes on macroporous SiC supports, *J. Membr. Sci.*, 472 (2014) 232-240.
- [8] M. Herrmann, G. Standke, S. Höhn, G. Himpel, T. Gestrich, High-temperature corrosion of silicon carbide ceramics by coal ashes, *Ceram. Int.*, 40 (2014) 1471-1479.
- [9] F. Han, Z. Zhong, Y. Yang, W. Wei, F. Zhang, W. Xing, Y. Fan, High gas permeability of SiC porous ceramics reinforced by mullite fibers, *J. Eur. Ceram. Soc.*, 36 (2016) 3909-3917.
- [10] Y.A. Kim, J.H. Choi, J. Scott, K. Chiang, R. Amal, Preparation of high porous Pt–V₂O₅–WO₃/TiO₂/SiC filter for simultaneous removal of NO and particulates, *Powder Technol.*, 180 (2008) 79-85.
- [11] Q. Wang, Y. Kawano, L. Yu, H. Nagasawa, M. Kanezashi, T. Tsuru, Development of high-performance sub-nanoporous SiC-based membranes derived from polytitanocarbosilane, *J. Membr. Sci.*, 598 (2020) 117688.
- [12] B. Elyassi, M. Sahimi, T.T. Tsotsis, A novel sacrificial interlayer-based method for the preparation of silicon carbide membranes, *J. Membr. Sci.*, 316 (2008) 73-79.
- [13] G. Barroso, Q. Li, R.K. Bordia, G. Motz, Polymeric and ceramic silicon-based coatings—a review, *Journal of Materials Chemistry A*, 7 (2019) 1936-1963.
- [14] J. Hong, K.Y. Cho, D.G. Shin, J.I. Kim, D.H. Riu, Iodine diffusion during iodine-vapor curing and its effects on the morphology of polycarbosilane/silicon carbide fibers, *J. Appl. Polym. Sci.*, 132 (2015).

- [15] R.A. Wach, M. Sugimoto, M. Yoshikawa, Formation of Silicone Carbide Membrane by Radiation Curing of Polycarbosilane and Polyvinylsilane and its Gas Separation up to 250°C, *J. Am. Ceram. Soc.*, 90 (2007) 275-278.
- [16] A. Takeyama, M. Sugimoto, M. Yoshikawa, Gas Permeation Property of SiC Membrane Using Curing of Polymer Precursor Film by Electron Beam Irradiation in Helium Atmosphere, *Materials Transactions*, advpub (2011) 1276-1280.
- [17] Y.L. Li, H. Fan, D. Su, C. Fasel, R. Riedel, Synthesis, structures, and properties of bulk Si(O)C ceramics from polycarbosilane, *J. Am. Ceram. Soc.*, 92 (2009) 2175-2181.
- [18] S. Yajima, Y. Hasegawa, K. Okamura, T. Matsuzawa, Development of high tensile strength silicon carbide fibre using an organosilicon polymer precursor, *Nature*, 273 (1978) 525-527.
- [19] T. Tsuru, Silica-Based Membranes with Molecular-Net-Sieving Properties: Development and Applications, *J. Chem. Eng. Jpn.*, 51 (2018) 713-725.
- [20] X. Yu, H. Nagasawa, M. Kanezashi, T. Tsuru, Improved thermal and oxidation stability of bis (triethoxysilyl) ethane (BTESE)-derived membranes, and their gas-permeation properties, *Journal of Materials Chemistry A*, 6 (2018) 23378-23387.
- [21] L. Yu, M. Kanezashi, H. Nagasawa, M. Guo, N. Moriyama, K. Ito, T. Tsuru, Tailoring Ultramicroporosity To Maximize CO₂ Transport within Pyrimidine-Bridged Organosilica Membranes, *ACS Applied Materials &*

- Interfaces*, 11 (2019) 7164-7173.
- [22] L. Yu, M. Kanezashi, H. Nagasawa, J. Oshita, A. Naka, T. Tsuru, Pyrimidine-bridged organoalkoxysilane membrane for high-efficiency CO₂ transport via mild affinity, *Sep. Purif. Technol.*, 178 (2017) 232-241.
- [23] Q. Wang, A. Wu, S. Zhong, B. Wang, R. Zhou, Highly (*h0h*)-oriented silicalite-1 membranes for butane isomer separation, *J. Membr. Sci.*, 540 (2017) 50-59.
- [24] M. Shibuya, T. Yamamura, Characteristics of a continuous Si-Ti-C-O fibre with low oxygen content using an organometallic polymer precursor, *JMatS*, 31 (1996) 3231-3235.
- [25] L. Anhua, C. Jianming, D. Shaonan, Y. Yanbo, L. Ling, L. Fengping, C. Lifu, Processing and characterization of cobalt silicide nanoparticle-containing silicon carbide fibers through a colloidal method and their underlying mechanism, *Journal of Materials Chemistry C*, 2 (2014) 4980-4988.
- [26] J. Hong, K.-Y. Cho, D.-G. Shin, J.-I. Kim, S.-T. Oh, D.-H. Riu, Low-temperature chemical vapour curing using iodine for fabrication of continuous silicon carbide fibres from low-molecular-weight polycarbosilane, *Journal of Materials Chemistry A*, 2 (2014) 2781-2793.
- [27] Y. Fang, M. Huang, Z. Yu, H. Xia, L. Chen, Y. Zhang, L. Zhang, Synthesis, Characterization, and Pyrolytic Conversion of a Novel Liquid Polycarbosilane, *J. Am. Ceram. Soc.*, 91 (2008) 3298-3302.
- [28] H. Li, L. Zhang, L. Cheng, Y. Wang, Z. Yu, M. Huang, H. Tu, H. Xia, Effect of the polycarbosilane structure on its final ceramic yield, *J. Eur. Ceram. Soc.*, 28

- (2008) 887-891.
- [29] H. Li, L. Zhang, L. Cheng, Y. Wang, Z. Yu, M. Huang, H. Tu, H. Xia, Polymer–ceramic conversion of a highly branched liquid polycarbosilane for SiC-based ceramics, *JMatS*, 43 (2008) 2806-2811.
- [30] J. Hong, K.-Y. Cho, D.-G. Shin, S.H. Kim, D.-H. Riu, Structural evolution of silicon carbide phase from the polycarbosilane cured with iodine: NMR Study, *Journal of Inorganic and Organometallic Polymers and Materials*, 28 (2018) 2221-2230.
- [31] M.S. Bazarjani, M.M. Muller, H.J. Kleebe, C. Fasel, R. Riedel, A. Gurlo, In situ formation of tungsten oxycarbide, tungsten carbide and tungsten nitride nanoparticles in micro- and mesoporous polymer-derived ceramics, *Journal Of Materials Chemistry A*, 2 (2014) 10454-10464.
- [32] M. Guo, M. Kanezashi, H. Nagasawa, L. Yu, K. Yamamoto, T. Gunji, J. Ohshita, T. Tsuru, Tailoring the microstructure and permeation properties of bridged organosilica membranes via control of the bond angles, *J. Membr. Sci.*, 584 (2019) 56-65.
- [33] G. Lucovsky, M. Mantini, J. Srivastava, E. Irene, Low-temperature growth of silicon dioxide films: a study of chemical bonding by ellipsometry and infrared spectroscopy, *Journal of Vacuum Science & Technology B: Microelectronics Processing and Phenomena*, 5 (1987) 530-537.
- [34] G.H. Koo, J. Jang, Preparation of melting-free poly (lactic acid) by amorphous and crystal crosslinking under UV irradiation, *J. Appl. Polym. Sci.*, 127 (2013)

4515-4523.

- [35] A.V. Janorkar, A.T. Metters, D.E. Hirt, Degradation of poly (L-lactide) films under ultraviolet-induced photografting and sterilization conditions, *J. Appl. Polym. Sci.*, 106 (2007) 1042-1047.
- [36] C.C. Chao, D.S. Tsai, Si-Al-C gas separation membranes derived from polydimethylsilane and aluminum acetylacetonate, *J. Membr. Sci.*, 192 (2001) 209-216.
- [37] C. Schitco, M.S. Bazarjani, R. Riedel, A. Gurlo, NH₃-assisted synthesis of microporous silicon oxycarbonitride ceramics from preceramic polymers: a combined N₂ and CO₂ adsorption and small angle X-ray scattering study, *Journal of Materials Chemistry A*, 3 (2015) 805-818.
- [38] M. Rungta, G.B. Wenz, C. Zhang, L. Xu, W. Qiu, J.S. Adams, W.J. Koros, Carbon molecular sieve structure development and membrane performance relationships, *Carbon*, 115 (2017) 237-248.
- [39] J. Gascón, C. Téllez, J. Herguido, M. Menéndez, Propane dehydrogenation over a Cr₂O₃/Al₂O₃ catalyst: transient kinetic modeling of propene and coke formation, *Applied Catalysis A: General*, 248 (2003) 105-116.
- [40] T. Peters, O. Liron, R. Tschentscher, M. Sheintuch, R. Bredesen, Investigation of Pd-based membranes in propane dehydrogenation (PDH) processes, *Chem. Eng. J.*, 305 (2016) 191-200.
- [41] Q. Wang, L. Yu, H. Nagasawa, M. Kanezashi, T. Tsuru, High-performance molecular-separation ceramic membranes derived from oxidative cross-linked

- polytitanocarbosilane, *J. Am. Ceram. Soc.*, 103 (2020) 4473-4488.
- [42] H.R. Lee, M. Kanezashi, Y. Shimomura, T. Yoshioka, T. Tsuru, Evaluation and fabrication of pore-size-tuned silica membranes with tetraethoxydimethyl disiloxane for gas separation, *AIChE J.*, 57 (2011) 2755-2765.
- [43] H. Nagasawa, T. Niimi, M. Kanezashi, T. Yoshioka, T. Tsuru, Modified gas-translation model for prediction of gas permeation through microporous organosilica membranes, *AIChE J.*, 60 (2014) 4199-4210.
- [44] M. Kanezashi, M. Kawano, T. Yoshioka, T. Tsuru, Organic–inorganic hybrid silica membranes with controlled silica network size for propylene/propane separation, *Industrial & engineering chemistry research*, 51 (2011) 944-953.
- [45] W.J. Bakker, L.J. Van Den Broeke, F. Kapteijn, J.A. Moulijn, Temperature dependence of one-component permeation through a silicalite-1 membrane, *AIChE J.*, 43 (1997) 2203-2214.
- [46] Q. Wang, L. Yu, H. Nagasawa, M. Kanezashi, T. Tsuru, Tuning the microstructure of polycarbosilane-derived SiC(O) separation membranes via thermal-oxidative cross-linking, *Sep. Purif. Technol.*, 248 (2020) 117067.
- [47] H. Weyten, K. Keizer, A. Kinoo, J. Luyten, R. Leysen, Dehydrogenation of propane using a packed-bed catalytic membrane reactor, *AIChE J.*, 43 (1997) 1819-1827.
- [48] E. Shamsaei, X. Lin, L. Wan, Y. Tong, H. Wang, A one-dimensional material as a nano-scaffold and a pseudo-seed for facilitated growth of ultrathin, mechanically reinforced molecular sieving membranes, *Chem. Commun.*, 52 (2016)

13764-13767.

- [49] S. Payra, S. Challagulla, Y. Bobde, C. Chakraborty, B. Ghosh, S. Roy, Probing the photo-and electro-catalytic degradation mechanism of methylene blue dye over ZIF-derived ZnO, *J. Hazard. Mater.*, 373 (2019) 377-388.
- [50] L. Ding, Y. Wei, L. Li, T. Zhang, H. Wang, J. Xue, L.-X. Ding, S. Wang, J. Caro, Y. Gogotsi, MXene molecular sieving membranes for highly efficient gas separation, *Nature communications*, 9 (2018) 1-7.
- [51] Y. Fan, L. Wei, X. Meng, W. Zhang, N. Yang, Y. Jin, X. Wang, M. Zhao, S. Liu, An unprecedented high-temperature-tolerance 2D laminar MXene membrane for ultrafast hydrogen sieving, *J. Membr. Sci.*, 569 (2019) 117-123.
- [52] H. Inde, M. Kanezashi, H. Nagasawa, T. Nakaya, T. Tsuru, Tailoring a Thermally Stable Amorphous SiOC Structure for the Separation of Large Molecules: The Effect of Calcination Temperature on SiOC Structures and Gas Permeation Properties, *ACS Omega*, 3 (2018) 6369-6377.
- [53] B. Wang, F. Gao, F. Zhang, W. Xing, R. Zhou, Highly permeable and oriented AlPO-18 membranes prepared using directly synthesized nanosheets for CO₂/CH₄ separation, *Journal of Materials Chemistry A*, 7 (2019) 13164-13172.
- [54] M.A. Carreon, S. Li, J.L. Falconer, R.D. Noble, Alumina-Supported SAPO-34 Membranes for CO₂/CH₄ Separation, *J. Am. Chem. Soc.*, 130 (2008) 5412-5413.

Chapter 3

Development of high-performance sub-nanoporous SiC-based membranes derived from polytitanocarbosilane: Effect of pyrolysis temperature

3.1 Introduction

Amorphous silica membranes are generally prepared by either CVD or sol-gel processing, and their amorphous structure is a great advantage in the formation of highly permeable thin-films [1, 2]. According to molecular dynamic simulation, conventional amorphous SiO₂ membranes consist of pores ranging from 0.3-0.4 nm, which makes them suitable for the separation of small molecule mixtures such as H₂/N₂ and H₂/CO₂, but may not be suitable for the separation of small-to-medium sized molecules from large molecules such as N₂/SF₆ due to the high resistance caused by the small pores [1-6]. In addition, silica membranes are reportedly densified under a hydrothermal atmosphere, particularly at high temperatures [1-4]. Therefore, the concept of pore size control of silica membranes has been proposed using bridged alkoxysilanes such as bis(triethoxysilyl)ethane, which feature organic functional groups as linking units [7-9]. The pore sizes can be successfully controlled to form a looser structure, and the hydrothermal stability of these membranes has also been improved [7-9]. However, it is still difficult to prepare membranes with large-sized sub-nanopores for the separations of mid-sized molecules such as MeOH and their removal from mixtures. Moreover, organosilica membranes are usually prepared and used at temperatures lower than 300 °C due to decomposition of the organic linking

units at high temperatures [2, 7, 9]. Therefore, to address the above-mentioned issues of organosilica membranes, we have proposed the use of silicon carbide (SiC)-based materials, which are usually processed above 600 °C, to endow the resulting membranes with high levels of hydrothermal stability, thermal shock resistance, biocompatibility, corrosion resistance, and mechanical strength [10-12].

Porous SiC ceramics are essential in a variety of industrial applications such as commercial SiC filtration membranes with meso-/macropores for the filtration of back-wash water, surface water, and water produced from oil and gas industries [13, 14]. These membranes are reported to have high water permeability and to be stable within broad ranges of pH and temperature [13, 14]. However, our interest is in the preparation of sub-nanoporous SiC-based membranes based on the need for the separation of small (e.g., H₂ 0.28 nm) and mid-sized molecules (e.g., N₂ 0.364 nm, and MeOH 0.38 nm) from large ones. This type of membrane would be useful in dehydrogenation membrane reactors such as in methylcyclohexane dehydrogenation, ethylbenzene dehydrogenation, and cyclohexane dehydrogenation; as well as for the recovery of SF₆ from N₂ and for methanol removal from organic solutions by pervaporation (PV). Sub-nanoporous SiC-based membranes are expected to exhibit high performance in a wide range of applications. However, most reports using SiC-based membranes are focused on H₂/N₂ separation. For example, Li *et al.* [15, 16] used polycarbosilane (PCS) as a precursor and polystyrene (PS) as a pore former to prepare SiC-based (Si-O-C) membranes. A membrane prepared by adding 1% PS to the PCS showed H₂ permeance of 4×10^{-8} mol/(m² s Pa) with H₂/N₂ selectivity of 20 [16]. Suda *et al.* [17, 18] prepared SiC-based membranes by dip-coating PCS onto microporous α -alumina tubes. Their cross-linked PCS-derived membranes showed H₂ permeance of $(1-3) \times 10^{-8}$ mol/(m² s Pa) at 100 °C and H₂/N₂ selectivity that ranged

from 90-150 [18]. To date, few reports have focused on sub-nanoporous SiC-based membranes for molecular separation of small/mid-sized molecules from large molecules in gas separation and/or PV.

PCS is the most typical polymeric precursor and has been widely used for SiC ceramic applications since Yajima *et al.* first reported using for SiC fiber with the trade name Nicalon [19, 20]. Nevertheless, PCS-derived materials still have drawbacks in their mechanical properties that cause them to deteriorate at high temperature [21], but a novel Ti-incorporated PCS precursor, polytitanocarbosilane (TiPCS), has recently been developed. This polymer precursor can be synthesized via a reaction with titanium alkoxide using PCS that is synthesized by polydimethylsilane (PMS) and polyborodiphenylsiloxane [20, 22]. Introduction of a small amount (generally $\text{Ti/Si} \leq 0.02$, mol/mol) of titanium components can significantly increase the molecular weight and effectively inhibit the collapse and densification of the micropores during pyrolysis. Using this polymer, a Si-Ti-C-O (TiOSiC) fiber, commercialized under the name Tyranno Fiber and marketed by Ube industries LTD. (Japan), has now been synthesized. The Si-Ti-C-O fiber has many desirable mechanical properties and excellent heat resistance by comparison with SiC fibers obtained from PCS [20]. However, no paper has yet reported the use of TiPCS for the preparation of porous membranes that will be used for molecular separation.

The motivation for the present study was to develop novel sub-nanoporous SiC-based membranes with enhanced permeability using a Ti-incorporated PCS precursor with pore size controlled via pyrolysis temperature, which is intended for use in the separation of small/mid-sized molecules over large molecules. Several papers have characterized TiPCS-derived materials (powders, fibers) and reported their properties when fired under high temperatures, but no study has reported firing

at temperatures as low as 350-800 °C. The present study marks the first use of TiPCS as a separation layer for sub-nanoporous ceramic membranes. The physical and chemical structural variations that constitute the permeation properties of TiPCS-derived membranes were systematically studied under different pyrolysis temperatures. Furthermore, this study marks the first successful application of a SiC-based membrane to a PV process, and the resultant excellent levels of hydrothermal stability were evaluated.

3.2 Experimental

3.2.1 Preparation of TiPCS powders

Commercial polytitanocarbosilane (TiPCS) is a superior heat-resistant paint (Tyranno Coat, TYR-VN100 type, Okitsumo Co., Ltd. Japan) that was used as a pre-ceramic polymeric precursor. The TiPCS content of the paint was ~48 wt% in a mixed solution of xylene, ethylbenzene, and *n*-butanol. TiPCS precursor powder was formed by slowly dropping the paint into pure *n*-butanol under magnetic stirring to form a precipitate. The precipitate was centrifuged and dried in a vacuum oven at 50 °C for 24 h. Next, the TiPCS precursor powders were packed in a glass bottle and stored in a Super-Dry cabinet (0% RH) at room temperature. To study the conversion behavior from an organic polymer to an inorganic amorphous ceramic, the powder sample was treated in the following two steps: initial curing under air at 200 °C for 2 h to promote a cross-linking process in the polymer, and then subsequent pyrolysis under a N₂ flow at selected temperatures up to 1,000 °C for 2 h. The two steps were conducted at a steady flow rate of 500 mL/min.

3.2.2 Fabrication of the TiPCS-derived membranes

A porous α -alumina tube with an average pore size of 1 μm (porosity: 50%, outer diameter: 10 mm, Nikkato Co., Japan) was used as a support. The modification of the supports was similar to a procedure used in our previous work [2, 23]. Briefly, two types of α -alumina particles (average particle diameter: 0.2 μm , 2 μm) were subsequently coated onto the outer surface of the tubes using SiO_2 - ZrO_2 (Si/Zr = 5:5) colloidal sols as a binder, followed by calcination at 750-800 $^\circ\text{C}$ under an air atmosphere for 20 minutes. Each procedure was repeated several times to cover large pores. To minimize the defects in the TiPCS membrane, an intermediate layer with an average pore size of ~ 1 nm was fabricated by coating SiO_2 - ZrO_2 (Si/Zr = 5:5) colloidal sol onto the α -alumina particle layer followed by calcination at 750-800 $^\circ\text{C}$ for 15 min. It is worth noting that the Zr-modified intermediate layer fabricated by SiO_2 - ZrO_2 (Si/Zr = 5:5) colloidal sol showed good hydrothermal stability in our previous work [24, 25].

To synthesize amorphous SiC-based membranes, a TiPCS pre-ceramic polymer was dissolved in xylene to prepare a 3 wt% TiPCS solution and was then coated onto the intermediate layer. Subsequently, the film was cured and cross-linked at 200 $^\circ\text{C}$ for 2 h under an air flow, followed by pyrolysis of the TiPCS film at 350-800 $^\circ\text{C}$ for 0.5 h under a N_2 atmosphere at a heating rate of ~ 35 $^\circ\text{C}/\text{min}$. The air and N_2 flow rates were both set at 500 mL/min. The coating-curing-pyrolysis process was repeated 3 times to reduce possible defects in the SiC-based membranes.

3.2.3 Characterization of TiPCS powders and membranes

Attenuated total reflection Fourier transform infrared spectroscopy (ATR-FTIR)

patterns of the TiPCS powders were collected at room temperature using a FTIR-4100 (JASCO Co., Japan) within a range of 4,000-400 cm^{-1} . The chemical elements of the TiPCS powders were determined via a scanning electron microscope (SEM) equipped with an EX-37001 EDS accessory (JCM 5700, JEOL, Japan). Thermogravimetric-mass spectrometric analysis was performed via TG-MS (TG-DTA-410S, Rigaku Co., Japan) under a helium atmosphere, and the temperature was ramped up at a rate of 10 $^{\circ}\text{C min}^{-1}$ to a level of 1,000 $^{\circ}\text{C}$. Prior to the TG analysis, the sample was cured at 200 $^{\circ}\text{C}$ under a O_2 -He mixed gas (O_2 : 20%, He: 80%) for 2 h to promote cross-linking, and was then switched to a pure He atmosphere; the flow rates were maintained at 300 mL/min. The N_2 adsorption-desorption isotherms for TiPCS powders were measured at 77 K using a BELMAX (BELL Co., Japan); prior to measurement, the samples were pretreated to promote degassing at 200 $^{\circ}\text{C}$ under vacuum for 12 h. The BET surface areas were evaluated using N_2 adsorption data at a relative pressure that ranged from 0.001 to 0.15. The micropore volume was obtained from the amount of nitrogen adsorbed at $P/P_0 = 0.01$ relative to a pore size ≤ 1 nm [26, 27]. The pore size distributions were obtained from the adsorption isotherms using the non-localized density functional theory (NLDFT) method with a slit-pore model. XRD patterns of TiPCS powders were obtained using a D2 PHASER X-ray diffractometer (Bruker, Germany) employing $\text{Cu K}\alpha$ as the X-ray radiation source (1.54 \AA). The cross-sectional morphologies of the resultant membranes were evaluated using the SEM.

3.2.4 Gas permeation and PV measurement

The permeance of single gases with different kinetic diameters (He, 0.26 nm; H_2 , 0.289 nm; CO_2 , 0.33 nm; N_2 , 0.364 nm; CH_4 , 0.38 nm; C_3H_8 , 0.43 nm; CF_4 , 0.48 nm;

and, SF₆, 0.55 nm) was measured using the dead-end (retentate stream blocked) method [28] and an experimental setup that is schematically shown elsewhere [29]. The gas was fed to the outside of a cylindrical membrane at 200 °C. The feed gas was pressurized at ~0.1 MPa using a back-pressure regulator, while the permeate stream was maintained at atmospheric pressure. The selectivity is the permeance ratio of the single gases.

PV dehydration and removal of methanol was performed for binary mixtures composed of various organic solvents (methanol (MeOH), ethanol (EtOH), iso-propanol (IPA), and acetone, methyl acetate (MeOAc)), and an experimental setup that is schematically shown elsewhere [28]. The binary mixture was fed to the outside of the membrane, and the pressure outside and inside the membrane was maintained at atmospheric pressure and at approximately 0 kPa, respectively. A cold trap of liquid nitrogen was used to collect the permeate samples. Before the collection of the vapor permeate, the system was maintained for more than 1 h to ensure that the system was stabilized. The compositions of the feed and permeate samples were analyzed using a GC-14B (Shimadzu, Japan) with a Porapak P column and a TCD detector.

In PV, the values for flux, J [kg/(m² h)], separation factor (α) and permeance of i component, P_i [mol/(m² s Pa)], were calculated using the following equations:

$$J = \frac{Q}{At} \quad (1)$$

$$\alpha_{ij} = \left(\frac{x_i/x_j}{y_i/y_j} \right) \quad (2)$$

$$P_i = \frac{J_i}{p_{1,i} - p_{2,i}} \quad (3)$$

In those equations (1-3), Q (kg) is the total mass that permeates the membrane area, A (m²), over the operation time, t (h); x_i (or x_j) and y_i (or y_j) are the weight

fractions of the i (or j) component in the feed and permeate side, respectively; J_i is the molar flux of the i component [$\text{mol}/(\text{m}^2 \text{ s})$]; the partial pressures p_i (Pa) of component i for the feed side were calculated as $p_i = x_i \gamma_i p_i^0$, where x_i , γ_i and p_i^0 are the weight fraction, activity coefficient and the saturated vapor pressure of component i in the feed side, respectively (γ_i and p_i^0 were obtained using the Wilson and Antoine equations, respectively), while the permeate pressure was assumed to be zero.

3.3 Results and discussion

3.3.1 Physicochemical characterization of the TiPCS precursor

ATR-FTIR spectrum analysis was performed on the TiPCS precursor powder to identify the functional units present, as shown in Fig. 3-1. The absorptions observed at 2,980-2,850 cm^{-1} (CH_n , $n = 1, 2$ or 3); 2,100 cm^{-1} (Si-H); 1,400 cm^{-1} (C-H in Si- CH_3); 1,020 and 1,355 cm^{-1} (CH_2 in Si- CH_2 -Si); 1,259 cm^{-1} (Si- CH_3), and, $\sim 800 \text{ cm}^{-1}$ (Si-C), can be generally ascribed to the contribution of a typical PCS-based chemical structure [22, 29-31]. In addition, other absorption peaks of 695, 716, 740 cm^{-1} and at 1,124 and 1,430 cm^{-1} can be ascribed to the Si(phenyl) $_2$ O and Si-phenyl groups, respectively, due to the presence of the Ti-OSi(phenyl) $_2$ structure in TiPCS [31, 32]. It is worth noting that the peak of a Ti-O-Si bond, which was generally reported at $\sim 900 \text{ cm}^{-1}$, was not observed in this work probably due to the very small amount of Ti and/or overlapping by the stronger absorption of Si-C ($\sim 800 \text{ cm}^{-1}$) [31, 33]. Based on the above analysis and previous research [30, 31, 34], a possible main structure for

TiPCS is shown in Fig. 3-1.

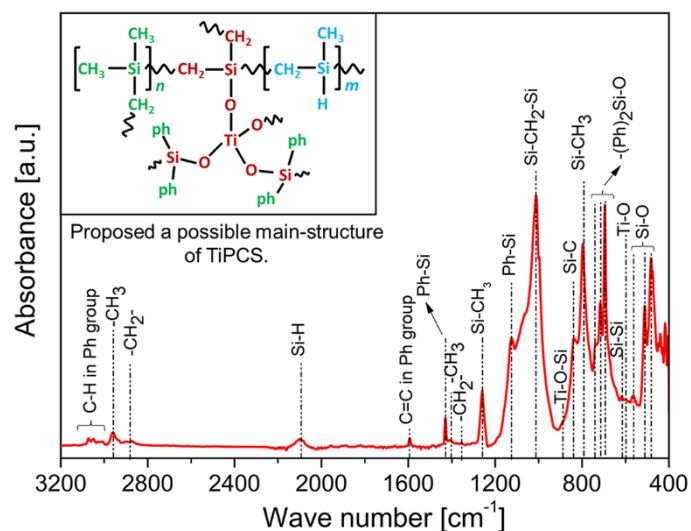


Fig. 3-1 ATR-FTIR spectra of TiPCS precursor powders (the proposed main structure of TiPCS is inserted).

After TiPCS precursor powders were air cured followed by firing under N_2 , their color showed a distinct change from yellow-green to orange and finally to black as shown in Fig. 3-2. It should be noted that the cross-linked powder fired under N_2 at 350 °C obviously maintained its polymer state, because the color of the main body of the powder showed no significant change. In general, during the pyrolysis process, polymer precursors are often subject to a series of complicated physical and chemical changes that include cross-linking, bond fission, and rearrangement reactions, which ultimately results in the generation of solid and gas-phase products.

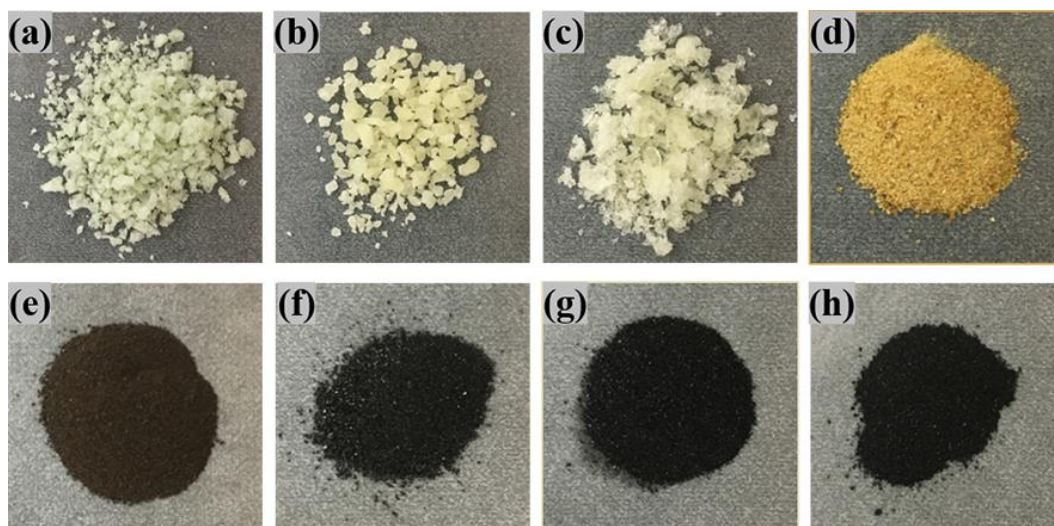


Fig. 3-2 Photos of cross-linked TiPCS powders fired at different temperatures under a N_2 atmosphere together with the precursor powder and air curing powder. (a) precursor powder, (b) air curing powder, (c) 350 °C, (d) 550 °C, (e) 650 °C, (f) 750 °C, (g) 800 °C and (h) 1,000 °C.

To reveal the thermal behavior of cross-linked TiPCS polymers during the pyrolysis process, thermal analysis was conducted using ATR-FTIR and TG-MS, as shown in Fig. 3-3. After air curing at 200 °C, the intensity of Si-H was decreased due to a cross-linking reaction that produced cross-linked structures comprised of Si-O-Si ($1,130\text{-}1,000\text{ cm}^{-1}$) bonds from the reaction between Si-H groups and oxygen. No significant change was observed for absorptions that ranged from $1,130\text{-}1,000\text{ cm}^{-1}$, however, due to overlapping by the stronger absorption of the Si-CH₂-Si ($1,020\text{ cm}^{-1}$) bond.

The ATR-FTIR spectra and TG curve showed that the transformation of a cross-linked TiPCS polymer to a ceramic could be divided into two stages for temperatures that ranged from 300-800 °C with the high ceramic yield of approximately 82 wt% achieved. The first stage (up to 650 °C) can be ascribed to the

decomposition of the organic groups with significant mass loss (15%) due to cross-linking and bonding fission reactions with a release of H_2 ($m/z = 2$), hydrocarbons (such as CH_3 , $m/z = 15$; C_2H_2 , $m/z = 26$; C_3H_3 , $m/z = 39$), and aromatic compounds (such as C_6H_6 , $m/z = 78$), as seen in the results of MS analysis. In this first stage, the intensities of Si-H and phenyl groups decreased above 350 °C and vanished at 550 °C, and the absorptions of Si- CH_3 and Si- CH_2 -Si were also reduced, as shown in the ATR-FTIR spectra.

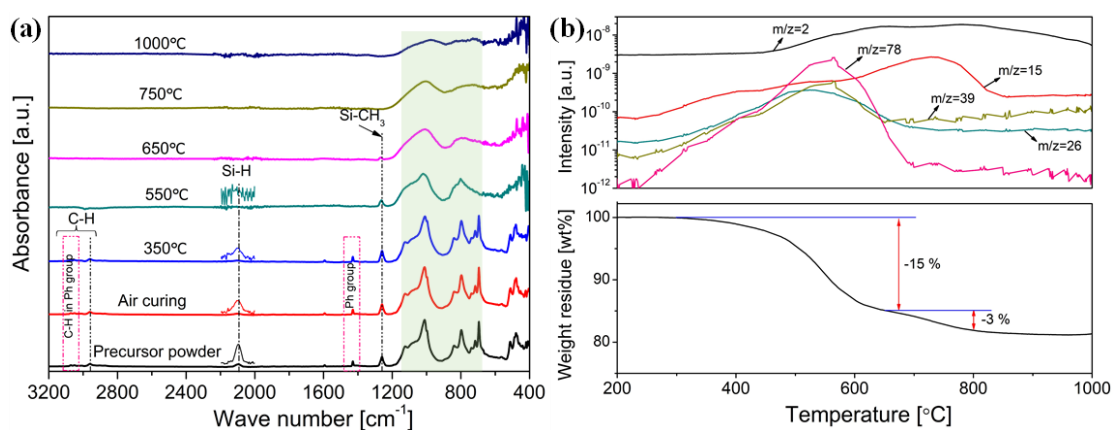


Fig. 3-3 ATR-FTIR spectra of (a) cross-linked TiPCS powders (the enlarged spectra ($\times 10$) of the Si-H is inserted) together with a precursor powder for comparison, (b) TG-MS curves of cross-linked TiPCS powder under a He atmosphere with a heating rate of 10 °C/min to a level of 1,000 °C (before TG analysis, the sample was pretreated for cross-linking at 200 °C under O_2 -He mixed gas (O_2 : 20%, He: 80%) for 2 h).

The second stage featuring a slight mass loss (3 wt%, 650-800 °C) corresponded to the polymer-to-ceramic transformation process, and was attributed to the rearrangement and densification reactions with the release of small molecules such as

CH₃ and H₂. The ATR-FTIR spectra of powders fired up to 750 °C showed that the absorptions of organic groups including Si-CH₂-Si, and Si-CH₃ in particular, mostly disappeared. Meanwhile, the broad peak within a range of from 1,150-700 cm⁻¹ should be assigned to the asymmetric stretching vibrations of Si-O-Si and O-Si-C bonds [35].

The Tyranno Coat was a commercial TiPCS precursor consisting of Si, O, C, and Ti, which was confirmed using the EDS shown in Fig. 3-4. The ratio of O/Si was clearly increased after cross-linking at 200 °C under air. Each ratio of O/Si and C/Si of cross-linked TiPCS was decreased while the ratio of Ti/Si was almost unchanged with the increasing pyrolysis temperature, indicating the mass loss mainly comes from carbon and oxygen during the pyrolysis process. In addition, when the pyrolysis temperature was higher than 750 °C, the elemental composition showed almost no change indicating the polymer-to-ceramic transformation process was completed. It is worth mentioning that after completing the polymer-to-ceramic transformation, the mass fraction of carbon and oxygen was reduced by 16 and 4%, respectively, which is consistent with the weight residue from TG. Different ceramic compositions would have different structural properties, which will be discussed by N₂ adsorption-desorption isotherms.

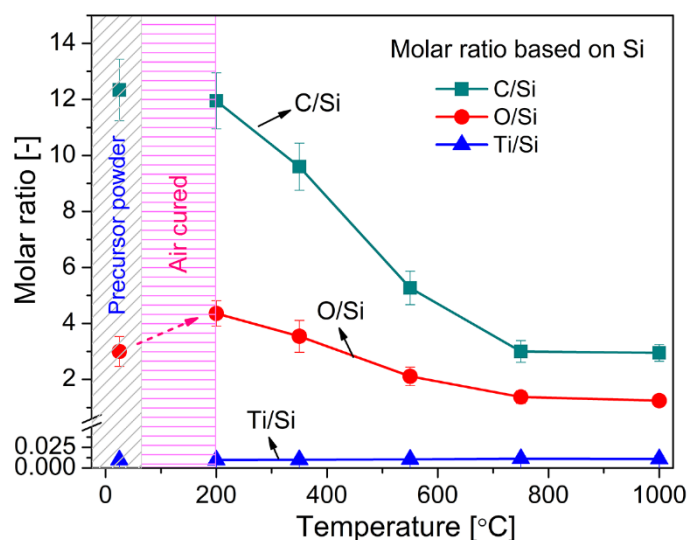


Fig. 3-4 Elemental composition of cross-linked TiPCS powders (analysis with EDS; molar ratio is based on Si and precursor powders for comparison).

Tyranno fibers derived from TiPCS polymers are generally considered amorphous at temperatures (up to 1,400 °C) that are higher than those of the Nicalon fibers derived from PCS (~900 °C) [20, 36-38]. The crystallization behavior of the cross-linked TiPCS powders pyrolyzed at different temperatures ($T \leq 1,000$ °C) was investigated by XRD, and the results appear in Fig. 3-5a. The XRD spectra showed an entirely amorphous structure with no formation of SiC, SiO₂ or TiO₂ nanocrystallites, as expected. A broad peak was observed at $\sim 20^\circ$ below a pyrolysis temperature of 750 °C, and was associated with the amorphous SiO₂/C environment [39, 40]. The peak intensity decreased with temperature, which means the degree of short-range ordering for the organic chemical environment of SiO₂/C was reduced, resulting in a highly disordered structure. Si 2p peaks (Fig. 3-5b) confirmed the presence of mixed units such as Si-H (99.4 eV), Si-C (101 eV), O_xSiC_{4-x} (102 eV), and Si-O (103.1 eV) during the cross-linking, bond fission, and rearrangement reactions [41]. The intensity

of the Si-H bond rapidly decreased and almost vanished at 550 °C, and the Si-C bond also decreased due to the decomposition of Si-CH_n organic groups with the increased pyrolysis temperature, which was in good agreement with the results of ATR-FTIR. By contrast, O_xSiC_{4-x} and Si-O bond intensities increased, which could have been due to the rearrangement reactions of Si-C with Si-O and/or to the reactions with oxygen and moisture that had adsorbed onto the surface of the powders [36]. Also, the mixed binding energy peaks of C 1s were assigned to Si-C (283.4 eV), O_xSiC_{4-x} (284.4 eV), and carbon (285.3 eV) [41], as shown in Fig. 3-5c. The C 1s peaks evolved in a manner similar to that of the Si 2p peaks. With an increase in the pyrolysis temperature, the Si-C bond decreased, and the O_xSiC_{4-x} bond increased, while the peak of carbon (285.3 eV) first decreased and then increased due to the decomposition of phenyl groups (350-550 °C) and to the generation of free carbon (750-1,000 °C) in the system. These results corresponded to a significant shift in the chemical environment of SiO₂/C, as discussed with regard to the XRD patterns.

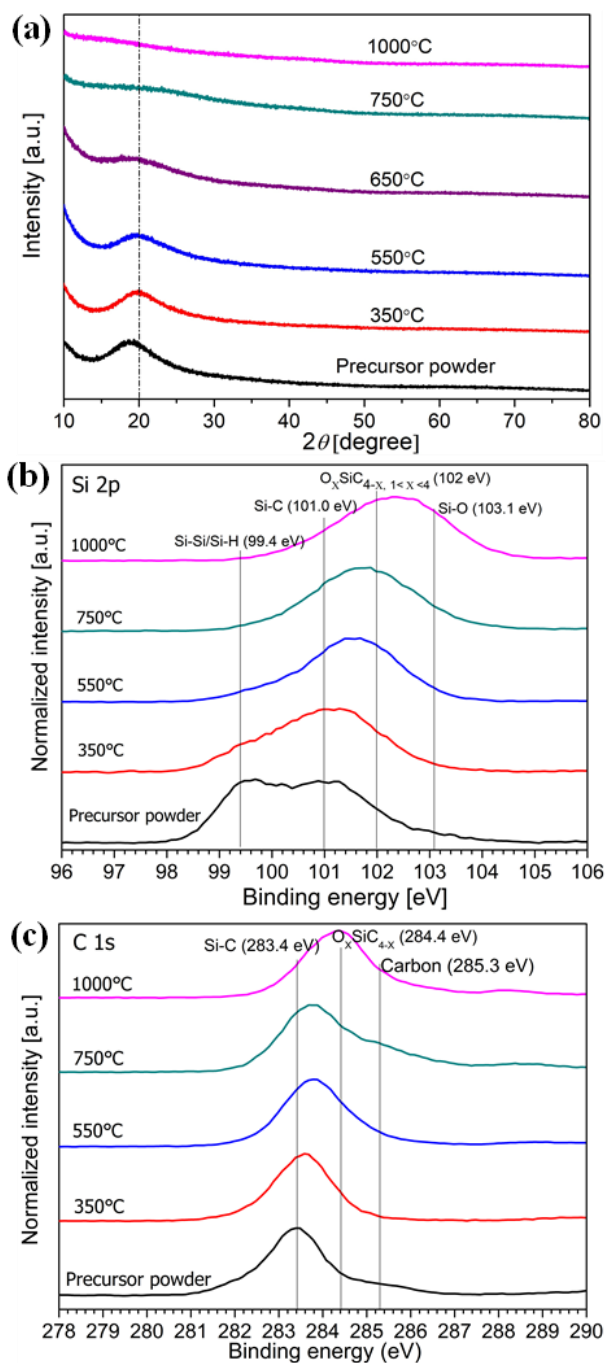


Fig. 3-5 (a) XRD patterns, (b) XPS Si 2p peaks, and (c) XPS C 1s peaks of cross-linked TiPCS powders pyrolyzed at 350-1,000 °C together with a precursor powder for comparison.

The microporous properties, pore structure parameters, BET, micropore volume, and NLDFT pore size distribution curves of the pyrolyzed TiPCS powders were

analyzed via the N₂ adsorption-desorption isotherms, as shown in Fig. 3-6. In the nitrogen adsorption-desorption isotherms (Fig. 3-6a), all samples, with the noted exception of the powder pyrolyzed at 1,000 °C, exhibited steep uptakes at low relative pressures, which indicated the presence of an abundant number of micropores. The micropore volume (at $P/P_0 = 0.01$ relative to a pore size ≤ 1 nm [26, 27]) increased with an increase in the pyrolysis temperature, with the maximum value reaching 0.17 cm³/g at 650 °C and then dropped to 6.6×10^{-5} cm³/g at 1,000 °C. Variations in the BET surface area exactly followed the same increase-then-decrease trend. This trend indicates that an abundant number of micropores was generated at around 650 °C by the decomposition of organic groups, after which the micropores were gradually narrowed due to the rearrangement and densification reactions with increases in the pyrolysis temperature [42]. This increase-then-decrease trend agrees with the results of experiments using PCS [15] and PMS [43] under a similar synthesis process (air-cured at 200 °C and then pyrolysis at 300-950 °C under nitrogen or argon) in previous studies as well as our PCS results shown in **Chapter 2** where the surface area of precursor-derived powders were decreased to approximately 0 m²/g when the pyrolysis temperature reached 700 or 750 °C leading to severe densification. In the present study, TiPCS-derived powders pyrolyzed at 800 °C maintained their microporosity, which is plausibly explained by the titanium components in TiPCS-derived powders inhibiting and/or reducing the densification of network structures.

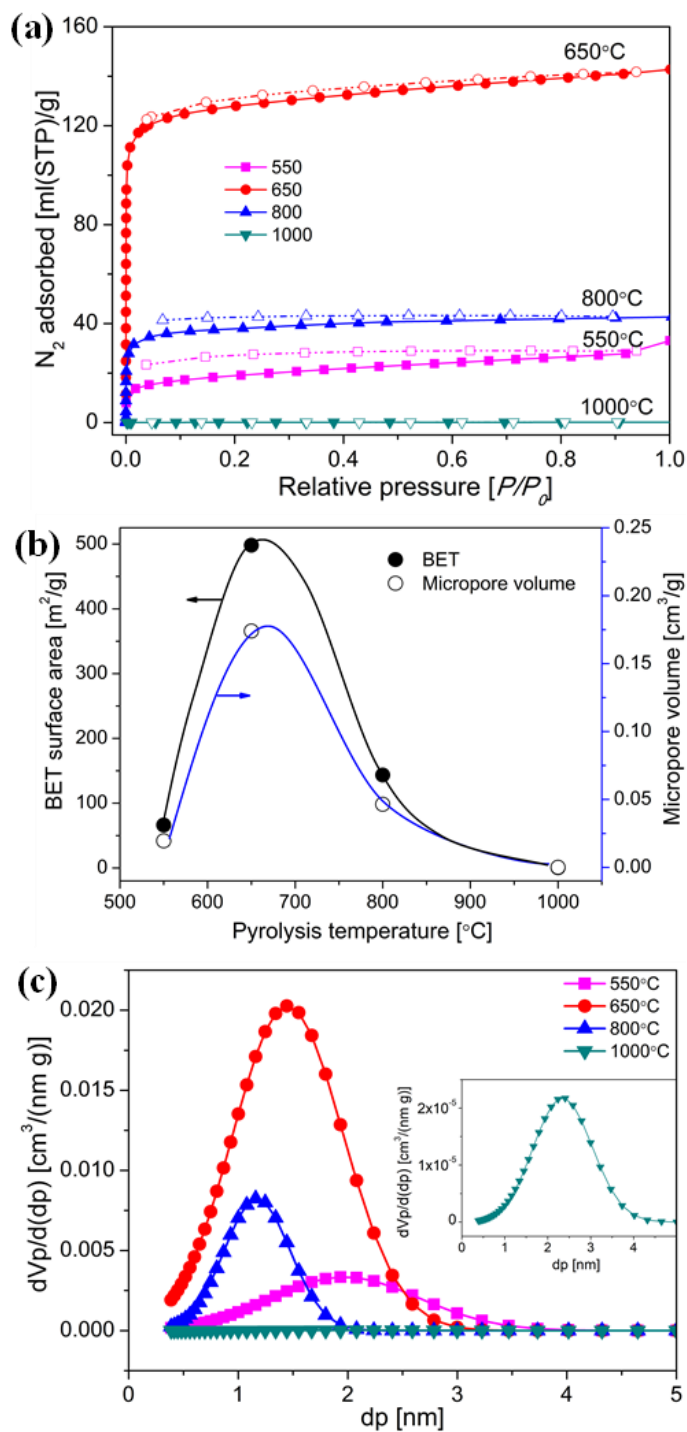


Fig. 3-6 (a) N_2 adsorption-desorption isotherms at 77 K, (b) BET surface area and micropore volume (at a relative pressure of $P/P_0=0.01$, pore size ≤ 1 nm), (c) NLDFT pore size distributions (the insert Fig. is enlarged for cross-linked powder pyrolyzed at 1,000 °C) of pyrolyzed TiPCS powders.

As shown in Fig. 3-6c, NLDFT analysis was used to evaluate the effect of

pyrolysis temperature on the development of the pore size distribution. The average pore diameter was decreased with increases in the pyrolysis temperature. The cumulative micropore volume at 1,000 °C was essentially zero, and it seemed that only a very small number of mesopores (~2.2 nm) existed, which suggests that micropores may have vanished and been replaced by a small number of slit-like pores/defects that formed during densification at elevated temperatures.

Based on the detailed characterization described thus far, the evolution of the network structure in TiPCS fired at various temperatures is schematically illustrated in Fig. 3-7, which consists of the curing for cross-linking and the firing for decomposition as well as the polymer-to-ceramic transformation processes. Generally, TiPCS and PCS require curing under air for cross-linking in the fiber materials and in PCS-derived SiC membranes. The curing process adds oxygen to the system and develops Si-O-Si and Si-O-Ti bonds by the oxidation of Si-Si, Si-H and Ti-OR in the TiPCS structure, which leads to a three-dimensional thermosetting polymer network without melting even at high temperatures [18, 34].

The TiPCS powders fired at a low temperature (≤ 350 °C) tend to form a flexible, dense polymer structure due to the existence of numerous organic groups in the network, as revealed by ATR-FTIR spectra and powder photographs. During the subsequent step where the pyrolysis process is applied at a moderate temperature (350-650 °C), these organic groups are mostly removed by the decomposition reaction with gas evolution, and micropores can be produced to form a loose transitional structure with larger pores. With a further increase in the firing temperature (>

650 °C), such loose transitional structures then shrink to form a relatively denser ceramic structure with narrow pores during the polymer-to-ceramic transformation process via rearrangement and densification reactions. This proposed process of structural evolution is in good agreement with the results of N₂ adsorption-desorption isotherms. Hence, the firing temperature is a key factor in determining the microstructure and pore size distribution of materials derived from ceramic precursor polymers [43], which are expected to affect the gas permeation properties and will be discussed in the next section of the membrane fabrication.

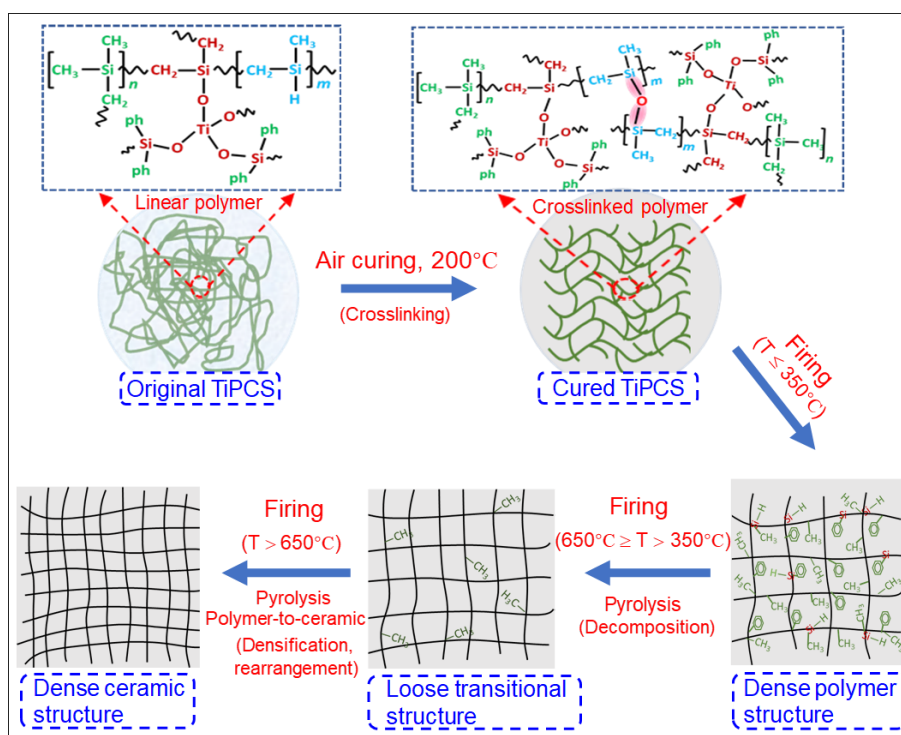


Fig. 3-7 Schematic illustration of the evolution of the network structure of the TiPCS.

3.3.2 Fabrication and reproducibility of TiPCS-derived membranes

The single-gas permeation performance is sensitive to the pore size distribution of the membrane and useful for monitoring the quality of the membrane. TiPCS

membranes were prepared by coating a 3% TiPCS solution onto intermediate layers followed by cross-linking under air at 200 °C and pyrolysis under a N₂ atmosphere at 350, 550, 750 and 800 °C, which hereafter will be used to refer to the membranes: M350, M550, M750, and M800, respectively. Fig. 3-8a shows the relationship between the single-gas permeance at 200 °C with pyrolysis temperatures ranging from 350-800 °C as a function of the molecular size, and Fig. 3-8b shows the H₂/SF₆ and H₂/N₂ selectivity and the H₂ permeance as a function of the pyrolysis temperature. It should be noted that the intermediate layers with large pore sizes, ~1 nm, exhibited high gas permeances and approximately Knudsen selectivity. The H₂ permeance of M550 was 2.74×10^{-6} mol/(m² s Pa), which is approximately 10 times higher than that of M350, while the selectivities of H₂/N₂ and H₂/SF₆ remained low even when the pyrolysis temperature was increased from 350 °C to 550 °C. This was because the M350 network had a dense polymer structure with flexible pores, and the organic segments increased the steric hindrance and consequently increased the resistance to gas permeation [44]. The M550 network, however, had a loose transitional structure with larger pores that significantly increased the gas permeance and lowered the gas selectivity.

When the pyrolysis temperature was increased from 550 °C to 750 °C, the transitional structure was shrunk to form a relatively dense ceramic structure with narrow pores. Therefore, as the H₂ permeance decreased, the selectivity of H₂/N₂ was increased from 4.1 to 8 and the selectivity of H₂/SF₆ was significantly increased from 35 to a maximum value of 16,600, which indicated that the TiPCS membranes were of

high quality with no defects. Moreover, when the pyrolysis temperatures were lower than 750 °C, the permeance of N₂ was lower than that of CH₄ even though N₂ has a smaller molecular size (0.364 nm), which suggests that Knudsen diffusion is dominant and that the membrane layers had loose transitional structures with larger pores. Under pyrolysis temperatures ranging from 750-800 °C, the permeance of CH₄ became lower than that of N₂, which indicated that the pore size of the TiPCS-derived SiC-based membranes was reduced and that the network structure had shrunk, which agrees with the denser ceramic structures in the networks of the membranes. Compared with the M750, the M800 showed smaller values for single-gas permeance, but H₂/N₂ selectivity that had slightly increased from 8 to 11 suggested that the network structure was further densified and narrowed in the membrane via the rearrangement reaction of Si-C and Si-O groups based on the results of XPS.

With an increase in pyrolysis temperature, the network structures of the membranes tended to be dense and the pore size gradually narrowed. A similar trend was reported in a SiC-based (Si-Al-C) membrane [42] that contained aluminum and was prepared under similar conditions (cured under air at 200 °C and then pyrolyzed at 300-900 °C). At pyrolysis temperatures higher than 600 °C, the H₂ permeance was significantly reduced to 1×10^{-9} mol/(m² s Pa) with a H₂/N₂ selectivity of 2.25 (~Knudsen selectivity) at 200 °C. On the other hand, in the present work, when the TiPCS membranes were pyrolyzed at elevated temperatures (750-800 °C), they exhibited a satisfactory H₂ permeance of approximately 10^{-6} mol/(m² s Pa), which is higher than that of either PCS-derived SiC-based membranes [15, 17, 18] ($\sim 10^{-9}$ - 10^{-8}

mol/(m² s Pa)) or Al-Si-C membranes [42]. These results suggest that titanium components in TiPCS membranes could effectively inhibit and/or reduce the densification of network structures.

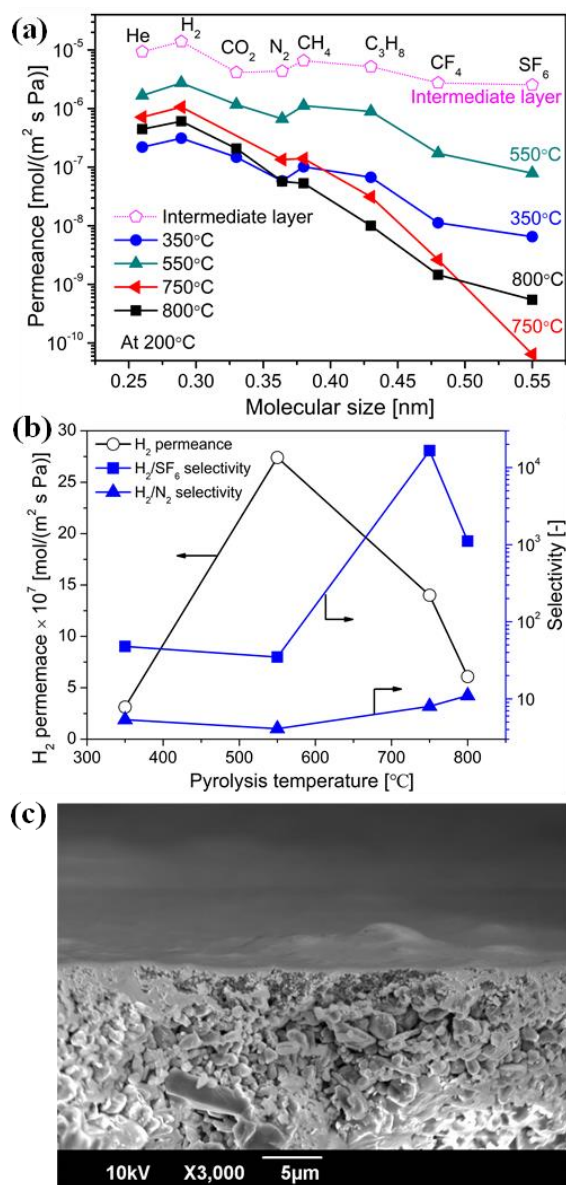


Fig. 3-8 (a) Single-gas permeance as a function of molecular size at 200 °C through TiPCS membranes formed by different pyrolysis temperatures, (b) relationship between the gas permeation performance of TiPCS membranes and pyrolysis temperature, and (c) cross-sectional image of a TiPCS membrane pyrolyzed at 750 °C.

Fig. 3-8c features an SEM image of the cross-section of a TiPCS membrane

pyrolyzed at 750 °C, which was selected as the most promising membrane. The thickness of the separation layer was estimated to be less than 400 nm. No boundary is apparent between the intermediate layer and the top layer, which is similar to the structure of an organosilica membrane reported in a previous study [45], and this was probably due to the thin nature of the coating and/or to the penetration of TiPCS into the SiO₂-ZrO₂ layer during the coating process.

Table 3-1 compares the gas separation performances at 200 °C of different SiC-based membranes [3, 46-48] under similar preparation conditions. TiPCS membranes demonstrated impressive performances as molecular sieving membranes with high levels of permeability (e.g., H₂ permeance $\sim 1 \times 10^{-6}$ mol/(m² s Pa)) and selectivity for small/mid-sized molecules over larger molecules (H₂/C₃H₈, 61; N₂/CF₄, 51; H₂/CF₄, 404; and H₂/SF₆, 16,600), which also emphasizes that the TiPCS membrane consists of sub-nanopores with a quite small number of pinholes. Moreover, the relationship between N₂ permeance and the selectivity of N₂/SF₆ is often used as a benchmark for the separation of mid-sized molecules from large molecules such as methanol/toluene [28, 49], and is also used as an index to evaluate membrane quality [50]. TiPCS membranes clearly showed the permeation properties that dictate better selectivity for N₂/SF₆ (2,110) with high N₂ permeance (1.35×10^{-7} mol/(m² s Pa)) compared with other SiC-based membranes. In addition, five TiPCS membranes prepared at 750 °C were used to confirm that the membrane performance was reproducible (original data are shown in Fig. 3-9).

Table 3-1. Gas-separation performance at 200 °C for different membranes under similar preparation conditions.

Membrane	Pyrolysis Temp. [°C]	Permeance $\times 10^7$ [mol/(m ² s Pa)]			Selectivity			Ref.
		H ₂	N ₂	H ₂ /C ₃ H ₈	H ₂ /CF ₄	N ₂ /SF ₆	H ₂ /SF ₆	
		TiOSiC	750	10.7	1.354	34	404	
SiOC	700	8	1.285	—	636	448	2,920	[3]
SiOC	700	0.1	0.005	—	—	8	152	[46]
SiOC	700	1	—	38	—	—	152	[47]
SiC	700-800	4	0.983	7	—	3	11	[48]

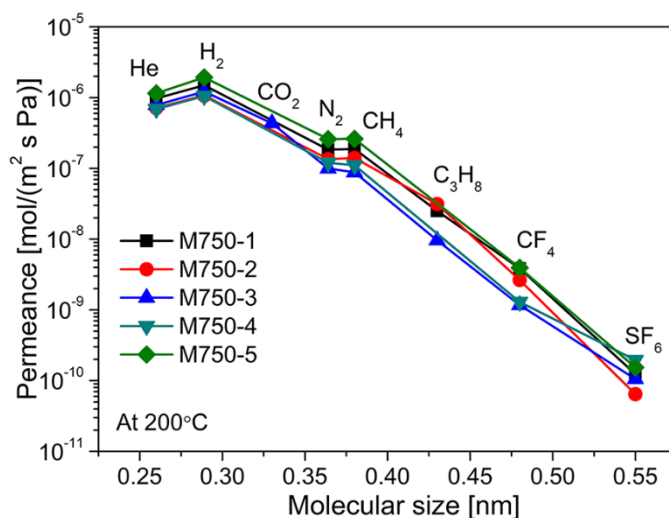


Fig. 3-9. Single-gas permeance as a function of molecular size at 200 °C through TiPCS membranes. TiPCS membranes were prepared by coating a 3% TiPCS solution onto intermediate layers followed by crosslinking under air at 200 °C and pyrolysis under a N₂ atmosphere at 750 °C (the coating-curing-pyrolysis process was repeated 3 times).

3.3.3 PV Performance of the TiPCS-derived membrane

Our previous work proved that PV and gas permeation processes through porous ceramic membranes have similarities in permeation mechanisms such as the molecular-sieving effect [23, 51]. Following the successful construction of the TiPCS-derived SiC-based membrane (M750), PV separation studies were conducted to evaluate the relationships in the permeation performances of gases and liquids (vapor).

Fig. 3-10a shows the dehydration permeance and the separation factor through a M750 membrane in H₂O/MeOH, H₂O/EtOH, H₂O/Acetone, and H₂O/IPA systems at 50 °C with each H₂O concentration in the feed side at 10 wt%. The TiPCS membrane showed H₂O permeance of approximately 1.4×10^{-6} mol/(m² s Pa), irrespective of the separation system. On the other hand, as the molecular size (molecular size: H₂O, 0.2955 nm; MeOH, 0.38 nm; EtOH, 0.4299 nm; acetone, 0.4691 nm; IPA: 0.4699 nm [52]) increased, the permeance of each organic solvent tended to decrease, which significantly increased the separation factor of each system (separation factor of H₂O/MeOH, ~2.3; H₂O/EtOH, ~48; and H₂O/Acetone, 109; and, H₂O/IPA, 216). Fig. 3-10b shows the permeance values for H₂O, MeOH, EtOH, acetone, and IPA as a function of each molecular size together with single-gas permeance at 200 °C. The permeance of dehydration and single-gas permeation through the M750 membrane showed similar dependencies on molecular size, though the permeation temperature differed between PV (50 °C) and single-gas permeation (200 °C). In this case, the

result suggests that the separation mechanism for PV is based mainly on a molecular sieving effect similar to single-gas permeation.

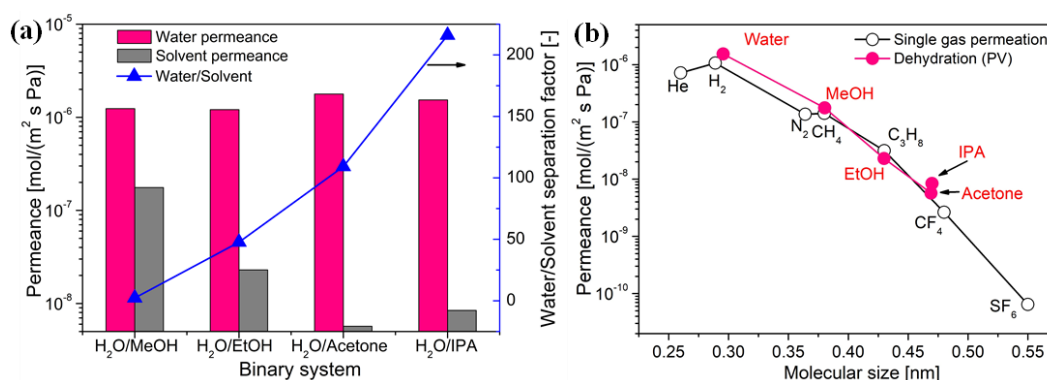


Fig. 3-10. (a) PV dehydration performance in water/x mixtures at 50 °C (water-weight percentage of the feed side maintained at 10 wt%, $x = \text{MeOH}$, EtOH , acetone, and IPA), (b) molecular size dependency of permeance for dehydration PV in binary mixtures at 50 °C with single-gas permeation of TiPCS membrane at 200 °C (the water permeance was from water/IPA PV).

The PV removal of methanol from organic mixtures (MeOH/EtOH, MeOH/IPA, MeOH/MeOAc) with a methanol concentration of 10 wt% at 50 °C for the M750 membrane was also investigated, as shown in Fig. 3-11a. The trend for the performance of PV removal of methanol was similar to that for dehydration, the permeance of MeOH was at a similar level for all mixtures, and the permeance of each organic solvent tended to decrease as the molecular size increased (molecular size of MeOAc is 0.4781 nm [52]). The separation factors for MeOH/EtOH and MeOH/IPA were 4 and 14.6, respectively, and the separation factor for MeOH/MeOAc, which is difficult to separate using polymeric membranes, was as high as 25. Fig. 3-11b shows the permeance for the PV removal of methanol at 50 °C

and for single-gas permeation at 200 °C as a function of the molecular size. Similar to PV dehydration, the PV removal of methanol also showed a trend similar to that of gas permeation, which again confirmed that molecular sieving was the primary mechanism for both gas permeation and PV. Our group reported the similarities between single-gas permeation and PV dehydration on BTESE-derived organosilica membranes, and predicted PV performance based on the gas permeation properties [28, 51], which was confirmed again in the present study, and, in addition, both the performance of PV dehydration and PV removal of methanol were found to be predictable according to the gas permeation properties of sub-nanoporous SiC-based membranes.

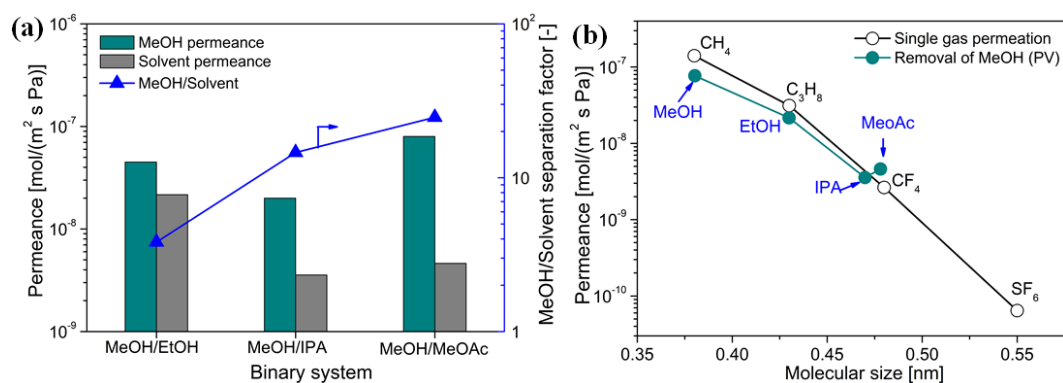


Fig. 3-11. (a) PV removal of methanol performance in MeOH/x mixtures at 50 °C (MeOH weight percentage of the feed side maintained at 10 wt%, x = EtOH, acetone, IPA and MeOAc), and (b) molecular size dependency of permeance for the PV removal of methanol in binary mixtures at 50 °C with single-gas permeation of the TiPCS membrane at 200 °C (the methanol permeance was from methanol/MeOAc PV).

The efficient separation of the methanol/methyl acetate mixture is an important process for industrial applications such as in the production of methyl acetate or

poly(vinyl alcohol), but the issue of separation remains a challenge due to the formation of an azeotrope [53, 54]. Fig. 3-12 shows the permeation flux and separation factors (α) of a M750 membrane for PV separation of a MeOH/MeOAc mixture (10/90 wt%) at temperatures ranging from 30 to 60 °C. With an increase in temperature, the permeate fluxes increased due to the increase of the vapor pressure of both MeOH and MeOAc on the feed side [53]. The flux of small molecular MeOH increased continuously with temperature, which could be attributed to the enhanced driving force for mass transfer associated with activated diffusion through the small pores, which allowed the permeation of only MeOH, but not of MeOAc, that is, penetration of the TiPCS membrane was dominated by molecular sieving. On the other hand, the MeOAc flux only slightly increased with temperature probably because the larger-sized MeOAc permeated larger-sized pores in Knudsen and/or surface diffusion. As a result, the separation factor increased with temperature.

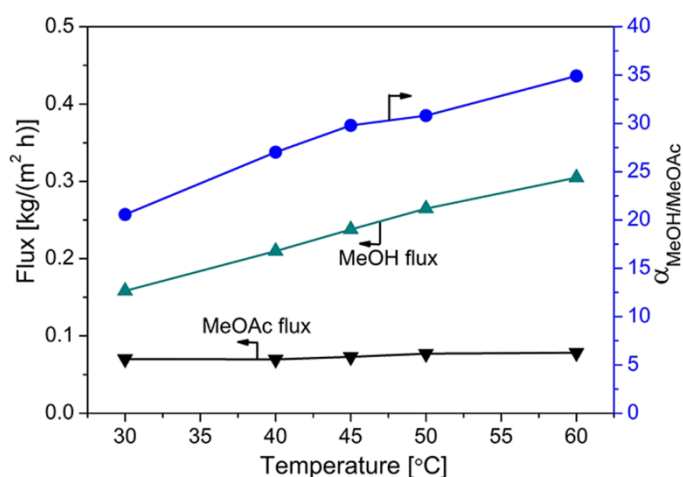


Fig. 3-12. Effect of operating temperature on flux and separation factors (α) for PV separation of MeOH/MeOAc mixtures (10/90 wt%).

Fig. 3-13 summarizes the separation performance of MeOH/MeOAc using TiPCS membranes together with commercial polymer membranes and mixed-matrix membranes under similar test conditions. The TiPCS membrane demonstrated attractive performance in MeOH/MeOAc separation compared with other PV membranes at temperatures ranging from 25 to 60 °C such as a total flux of 0.38 kg/(m² h) with a separation factor of 35 at 60 °C. It is worth noting that two TiPCS membranes (as shown in Table 3-2) had similar separation performance for PV separation of MeOH/MeOAc mixture (10/90 wt%) at 50 °C, which again confirmed the reproducibility of the TiPCS membrane performance.

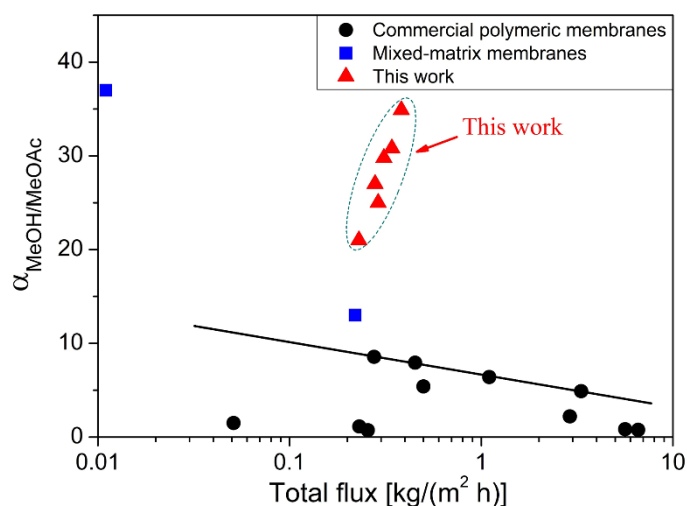


Fig. 3-13 Comparison of the methanol/methyl acetate separation performance under similar test conditions for PV membranes (commercial polymeric membranes [55-58], mixed-matrix membranes [53, 54], and this work; the original data are shown in Table 3-2).

Table 3-2. Summary of methanol/methyl acetate separation performances of different pervaporation membranes under similar test conditions.

Membrane	Feed, MeOH wt %	Temp. [°C]	Total flux [kg/(m ² h)]	Permeate, MeOH wt%	SF.	Ref.
Cuprophane	6	45	0.276	34.9	8.55	[55]
	20	45	0.452	66.3	7.92	
Pervap 2255-40	12	45	2.9	23.3	2.2	
Pervap 2255-50	16	45	1.1	55	6.4	[56]
Pervap 2255-60	15	45	0.5	49	5.4	
Pervap 2255-30	20.7	50	3.32	56.1	4.9	[57]
Pervap TM 4155-80	19	50	0.051	25.8	1.5	
	100	50	0.76	100	~	
Pervap TM 4155-70	10	50	0.256	7.5	0.73	[58]
	15	50	0.231	16.6	1.13	
Pervap TM 4155-30	9	50	5.633	7.7	0.84	
	15	50	6.585	11.9	0.77	
4A/PVA/PVP	10	45	0.011	80.4	37	[53]
PA/ND(3%)	18	25	0.22	74	13	[54]
	<u>10</u>	<u>50</u>	<u>0.29</u>	<u>72.7</u>	<u>25</u>	
TiPCS	10	30	0.23	69.3	21	
	10	40	0.28	75.1	27	This
	10	45	0.31	76.6	30	work
	<u>10</u>	<u>50</u>	<u>0.34</u>	<u>77.5</u>	<u>31</u>	
	10	60	0.38	79.6	35	

SF.= separation factor; Cuprophane and Pervap series are the commercial membranes; 4A/PVA/PVP is zeolite 4A incorporated PVA/PVP membrane; PA/ND(3%) is nanodiamond-modified poly(phenylene isophthalamide) membrane.

Fig. 3-14 shows the time courses for fluxes and the separation factors through TiPCS membranes when used in various binary systems. It should be noted that the separation performance of H₂O/IPA was maintained unchanged (including the fluxes and separation factor) after more than 65 h for different aqueous systems and organic-organic mixture systems, indicating that the TiPCS membrane possesses excellent stability due to a stable TiOSiC network.

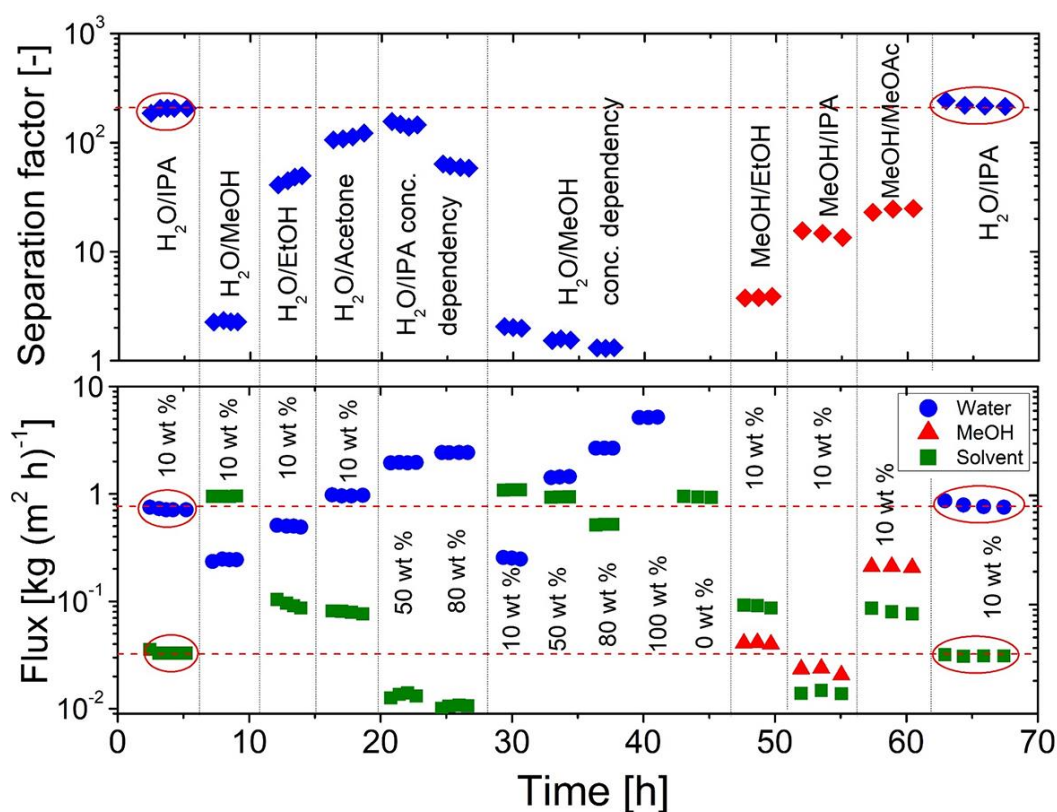


Figure 3-14 Time courses for pervaporation performance in water (or MeOH)/x mixtures at 50 °C (water or MeOH weight percentage (wt%) of the feed side was inserted in the figure, x = IPA, MeOH, EtOH, acetone and methyl acetate; details of the data are shown in Table 3-3)

Table 3-3 Pervaporation performance at 50 °C in terms of total flux and separation factor for a TiPCS membrane prepared at 750 °C

Binary mixture	Feed, solute wt %	Total flux [kg/(m ² h)]	Permeate, solute wt%	Separation factor	Permeance × 10 ⁸ [mol/(m ² s Pa)]	
					Solute	Solvent
H ₂ O/IPA	10 (H ₂ O)	0.75	95.57	216	154	0.84
H ₂ O/IPA	50 (H ₂ O)	1.965	99.33	152	256	0.52
H ₂ O/IPA	80 (H ₂ O)	2.43	99.57	62.4	310	0.48
H ₂ O/MeOH	10 (H ₂ O)	1.19	20.36	2.3	126	17.6
H ₂ O/MeOH	50 (H ₂ O)	2.37	60.57	1.6	256	32.2
H ₂ O/MeOH	80 (H ₂ O)	3.18	83.74	1.3	375	39.7
H ₂ O/EtOH	10 (H ₂ O)	0.588	84.5	47.7	121	2.29
H ₂ O/acetone	10 (H ₂ O)	1.05	92.68	109	178	0.57
MeOH/EtOH	10 (MeOH)	0.13	31.31	3.8	4.45	2.16
MeOH/IPA	10 (MeOH)	0.038	62.16	15.1	1.92	0.36
MeOH/methyl acetate	10 (MeOH)	0.29	72.7	25	7.77	0.446

3.4 Conclusions

This study marks the first fabrication of TiPCS-derived SiC-based membranes with sub-nanopores via the pyrolysis of a commercial polytitanocarbosilane polymer, Tyranno Coat. The pore characteristics and the surface areas of TiPCS-derived ceramic powders were strongly dependent on the pyrolysis temperatures. The

evolution of the network structure of TiPCS during the pyrolysis process began with a dense polymer structure (≤ 350 °C) that was then passed through a loose transitional structure (350-650 °C), and then transformed into a relatively denser ceramic structure (> 650 °C). Additionally, the titanium components in TiPCS effectively inhibited and/or reduced the densification of the network structures. The membrane prepared at 750 °C featured reproducibility and attractive selectivities (H_2/SF_6 , 16,600; and N_2/SF_6 , 2,100) with a high H_2 permeance at a magnitude of 10^{-6} mol/(m^2 s Pa). These SiC-based membrane demonstrated great potential for the separation of small and mid-sized molecules from large molecules such as N_2/SF_6 separation and PV removal of water or methanol from liquid mixtures. The TiPCS membranes exhibited separation performance for methanol/methyl acetate mixtures with a total flux of 0.38 kg/(m^2 h) and a methanol/methyl acetate separation factor of 35 for 10 wt% MeOH in a MeOH/MeOAc binary mixture at 60 °C.

References

- [1] T. Tsuru, Nano/subnano-tuning of porous ceramic membranes for molecular separation, *J. Sol-Gel Sci. Technol.*, 46 (2008) 349-361.
- [2] X. Yu, H. Nagasawa, M. Kanezashi, T. Tsuru, Improved thermal and oxidation stability of bis (triethoxysilyl) ethane (BTESE)-derived membranes, and their gas-permeation properties, *Journal of Materials Chemistry A*, 6 (2018) 23378-23387.
- [3] H. Inde, M. Kanezashi, H. Nagasawa, T. Nakaya, T. Tsuru, Tailoring a Thermally Stable Amorphous SiOC Structure for the Separation of Large Molecules: The Effect of Calcination Temperature on SiOC Structures and Gas Permeation Properties, *ACS Omega*, 3 (2018) 6369-6377.
- [4] N.W. Ockwig, T.M. Nenoff, Membranes for hydrogen separation, *Chem. Rev.*, 107 (2007) 4078-4110.
- [5] K.-S. Chang, T. Yoshioka, M. Kanezashi, T. Tsuru, K.-L. Tung, A molecular dynamics simulation of a homogeneous organic–inorganic hybrid silica membrane, *Chem. Commun.*, 46 (2010) 9140-9142.
- [6] X. Ren, T. Tsuru, Organosilica-Based Membranes in Gas and Liquid-Phase Separation, *Membranes*, 9 (2019) 107.
- [7] G. Li, M. Kanezashi, T. Tsuru, Preparation of organic–inorganic hybrid silica membranes using organoalkoxysilanes: the effect of pendant groups, *J. Membr. Sci.*, 379 (2011) 287-295.

- [8] M. Kanezashi, K. Yada, T. Yoshioka, T. Tsuru, Design of silica networks for development of highly permeable hydrogen separation membranes with hydrothermal stability, *J. Am. Chem. Soc.*, 131 (2009) 414-415.
- [9] M. Kanezashi, K. Yada, T. Yoshioka, T. Tsuru, Organic–inorganic hybrid silica membranes with controlled silica network size: preparation and gas permeation characteristics, *J. Membr. Sci.*, 348 (2010) 310-318.
- [10] M. Kanezashi, H. Sazaki, H. Nagasawa, T. Yoshioka, T. Tsuru, Preparation and gas permeation properties of thermally stable organosilica membranes derived by hydrosilylation, *Journal of Materials Chemistry A*, 2 (2014) 672-680.
- [11] S. Dabir, W.X. Deng, M. Sahimi, T. Tsotsis, Fabrication of silicon carbide membranes on highly permeable supports, *J. Membr. Sci.*, 537 (2017) 239-247.
- [12] R.J. Ciora, B. Fayyaz, P.K.T. Liu, V. Suwanmethanond, R. Mallada, M. Sahimi, T.T. Tsotsis, Preparation and reactive applications of nanoporous silicon carbide membranes, *Chem. Eng. Sci.*, 59 (2004) 4957-4965.
- [13] K. König, V. Boffa, B. Buchbjerg, A. Farsi, M.L. Christensen, G. Magnacca, Y. Yue, One-step deposition of ultrafiltration SiC membranes on macroporous SiC supports, *J. Membr. Sci.*, 472 (2014) 232-240.
- [14] M. Facciotti, V. Boffa, G. Magnacca, L.B. Jørgensen, P.K. Kristensen, A. Farsi, K. König, M.L. Christensen, Y. Yue, Deposition of thin ultrafiltration membranes on commercial SiC microfiltration tubes, *Ceram. Int.*, 40 (2014) 3277-3285.
- [15] L. Zhongyang, K. Kusakabe, S. Morooka, Preparation of thermostable

- amorphous Si-C-O membrane and its application to gas separation at elevated temperature, *J. Membr. Sci.*, 118 (1996) 159-168.
- [16] Z. Li, K. Kusakabe, S. Morooka, Pore Structure and Permeance of Amorphous Si-C-O Membranes with High Durability at Elevated Temperature, *Sep. Sci. Technol.*, 32 (1997) 1233-1254.
- [17] H. Suda, H. Yamauchi, Y. Uchimar, I. Fujiwara, K. Haraya, Structural Evolution during Conversion of Polycarbosilane Precursor into Silicon Carbide-Based Microporous Membranes, *J. Ceram. Soc. Jpn.*, 114 (2006) 539-544.
- [18] H. Suda, H. Yamauchi, Y. Uchimar, I. Fujiwara, K. Haraya, Preparation and gas permeation properties of silicon carbide-based inorganic membranes for hydrogen separation, *Desalination*, 193 (2006) 252-255.
- [19] S. Yajima, Y. Hasegawa, K. Okamura, T. Matsuzawa, Development of high tensile strength silicon carbide fibre using an organosilicon polymer precursor, *Nature*, 273 (1978) 525-527.
- [20] T. Yamamura, T. Ishikawa, M. Shibuya, T. Hisayuki, K. Okamura, Development of a new continuous Si-Ti-C-O fibre using an organometallic polymer precursor, *JMatS*, 23 (1988) 2589-2594.
- [21] S. Yajima, W. Watt, B. Harris, A.C. Ham, Development of ceramics, especially silicon carbide fibres, from organosilicon polymers by heat treatment, *Philosophical Transactions of the Royal Society of London. Series A, Mathematical and Physical Sciences*, 294 (1980) 419-426.

- [22] S. Yajima, T. Iwai, T. Yamamura, K. Okamura, Y. Hasegawa, Synthesis of a polytitanocarbosilane and its conversion into inorganic compounds, *JMatS*, 16 (1981) 1349-1355.
- [23] T. Tsuru, Silica-Based Membranes with Molecular-Net-Sieving Properties: Development and Applications, *J. Chem. Eng. Jpn.*, 51 (2018) 713-725.
- [24] W. Puthai, M. Kanezashi, H. Nagasawa, T. Tsuru, SiO₂-ZrO₂ nanofiltration membranes of different Si/Zr molar ratios: Stability in hot water and acid/alkaline solutions, *J. Membr. Sci.*, 524 (2017) 700-711.
- [25] W. Puthai, M. Kanezashi, H. Nagasawa, T. Tsuru, Nanofiltration performance of SiO₂-ZrO₂ membranes in aqueous solutions at high temperatures, *Sep. Purif. Technol.*, 168 (2016) 238-247.
- [26] M. Thommes, K. Kaneko, A.V. Neimark, J.P. Olivier, F. Rodriguez-Reinoso, J. Rouquerol, K.S.W. Sing, Physisorption of gases, with special reference to the evaluation of surface area and pore size distribution (IUPAC Technical Report), *Pure Appl. Chem.*, 87 (2015) 1051-1069.
- [27] L. Yu, M. Kanezashi, H. Nagasawa, M. Guo, N. Moriyama, K. Ito, T. Tsuru, Tailoring Ultramicroporosity To Maximize CO₂ Transport within Pyrimidine-Bridged Organosilica Membranes, *ACS Applied Materials & Interfaces*, 11 (2019) 7164-7173.
- [28] M. Kanezashi, M. Murata, H. Nagasawa, T. Tsuru, Fluorine Doping of Microporous Organosilica Membranes for Pore Size Control and Enhanced Hydrophobic Properties, *ACS Omega*, 3 (2018) 8612-8620.

- [29] Y. Yu, Y. Guo, X. Cheng, Y. Zhang, Preparation of TiO₂/SiO₂ composite fiber by thermal decomposition of polycarbosilane–tetrabutyl titanate hybrid precursor, *J. Mater. Chem.*, 19 (2009) 5637-5642.
- [30] T. Ishikawa, T. Yamamura, K. Okamura, Production mechanism of polytitanocarbosilane and its conversion of the polymer into inorganic materials, *JMatS*, 27 (1992) 6627-6634.
- [31] Y.C. Song, Y. Hasegawa, S.J. Yang, M. Sato, Ceramic fibres from polymer precursor containing Si-O-Ti bonds, *JMatS*, 23 (1988) 1911-1920.
- [32] P.J. Launer, Infrared analysis of organosilicon compounds: spectra-structure correlations, *Silicone compounds register and review*, ed. B. Arkles, Petrarch Systems (1987) 100-103.
- [33] Z. Yu, J. Zhan, C. Zhou, L. Yang, R. Li, H. Xia, Synthesis and characterization of SiC (Ti) ceramics derived from a hybrid precursor of titanium-containing polycarbosilane, *Journal of Inorganic and Organometallic Polymers and Materials*, 21 (2011) 412-420.
- [34] M. Shibuya, T. Yamamura, Characteristics of a continuous Si-Ti-C-O fibre with low oxygen content using an organometallic polymer precursor, *JMatS*, 31 (1996) 3231-3235.
- [35] M.S. Bazarjani, M.M. Muller, H.J. Kleebe, C. Fasel, R. Riedel, A. Gurlo, In situ formation of tungsten oxycarbide, tungsten carbide and tungsten nitride nanoparticles in micro- and mesoporous polymer-derived ceramics, *Journal Of Materials Chemistry A*, 2 (2014) 10454-10464.

- [36] Z. Yu, L. Yang, H. Min, P. Zhang, A. Liu, R. Riedel, High-ceramic-yield precursor to SiC-based ceramic: A hyperbranched polytitaniumcarbosilane bearing self-catalyzing units, *J. Eur. Ceram. Soc.*, 35 (2015) 851-858.
- [37] A.R. Maddocks, D.J. Cassidy, A.S. Jones, A.T. Harris, Synthesis of nanoporous silicon carbide via the preceramic polymer route, *Mater. Chem. Phys.*, 113 (2009) 861-867.
- [38] W.Y. Chen, J. Zhou, Study on the Pyrolysis Behavior of Polycarbosilane, *Journal Of Wuhan University Of Technology-Materials Science Edition*, 30 (2015) 679-683.
- [39] J. Shen, M. Wang, Y.-n. Wu, F. Li, Preparation of mesoporous carbon nanofibers from the electrospun poly(furfuryl alcohol)/poly(vinyl acetate)/silica composites, *RSC Advances*, 4 (2014) 21089-21092.
- [40] X. Zou, L. Ji, H.-Y. Hsu, K. Zheng, Z. Pang, X. Lu, Designed synthesis of SiC nanowire-derived carbon with dual-scale nanostructures for supercapacitor applications, *Journal of Materials Chemistry A*, 6 (2018) 12724-12732.
- [41] N. Wu, L.Y. Wan, Y. Wang, F. Ko, Conversion of hydrophilic SiOC nanofibrous membrane to robust hydrophobic materials by introducing palladium, *Appl. Surf. Sci.*, 425 (2017) 750-757.
- [42] C.C. Chao, D.S. Tsai, Si-Al-C gas separation membranes derived from polydimethylsilane and aluminum acetylacetonate, *J. Membr. Sci.*, 192 (2001) 209-216.
- [43] L.-L. Lee, D.-S. Tsai, Synthesis and Permeation Properties of

- Silicon–Carbon-Based Inorganic Membrane for Gas Separation, *Industrial & Engineering Chemistry Research*, 40 (2001) 612-616.
- [44] L. Yu, M. Kanezashi, H. Nagasawa, N. Moriyama, T. Tsuru, K. Ito, Enhanced CO₂ separation performance for tertiary amine-silica membranes via thermally induced local liberation of CH₃Cl, *AIChE J.*, 64 (2018) 1528-1539.
- [45] L. Yu, M. Kanezashi, H. Nagasawa, J. Ohshita, A. Naka, T. Tsuru, Fabrication and Microstructure Tuning of a Pyrimidine-Bridged Organoalkoxysilane Membrane for CO₂ Separation, *Industrial & Engineering Chemistry Research*, 56 (2017) 1316-1326.
- [46] R.M. Prasad, Y. Jüttke, H. Richter, I. Voigt, R. Riedel, A. Gurlo, Mechanism of Gas Separation through Amorphous Silicon Oxycarbide Membranes *Adv. Eng. Mater.*, 18 (2016) 721-727.
- [47] Y. Juttke, H. Richter, I. Voigt, R.M. Prasad, M.S. Bazarjani, A. Gurlo, R. Riedel, Polymer Derived Ceramic Membranes for Gas Separation, *Chemical Engineering Transactions*, 32 (2013) 1891-1896.
- [48] B.-K. Sea, K. Ando, K. Kusakabe, S. Morooka, Separation of hydrogen from steam using a SiC-based membrane formed by chemical vapor deposition of triisopropylsilane, *J. Membr. Sci.*, 146 (1998) 73-82.
- [49] M. Drobek, J. Motuzas, M. van Loon, R.W.J. Dirrix, R.A. Terpstra, A. Julbe, Coupling microwave-assisted and classical heating methods for scaling-up MFI zeolite membrane synthesis, *J. Membr. Sci.*, 401 (2012) 144-151.
- [50] Q. Wang, A. Wu, S. Zhong, B. Wang, R. Zhou, Highly (h0h)-oriented silicalite-1

- membranes for butane isomer separation, *J. Membr. Sci.*, 540 (2017) 50-59.
- [51] N. Moriyama, H. Nagasawa, M. Kanezashi, T. Tsuru, Pervaporation dehydration of aqueous solutions of various types of molecules via organosilica membranes: Effect of membrane pore sizes and molecular sizes, *Sep. Purif. Technol.*, 207 (2018) 108-115.
- [52] M.E. van Leeuwen, Derivation of Stockmayer potential parameters for polar fluids, *Fluid Phase Equilib.*, 99 (1994) 1-18.
- [53] X. Tong-Hu, X. Xiao-Li, Q. Hai-Jiao, Y. Xiao-Gang, Z. Rui-Feng, Zeolite 4A-Incorporated Polymeric Membranes for Pervaporation Separation of Methanol-Methyl Acetate Mixtures, *Journal of Inorganic and Organometallic Polymers and Materials*, 21 (2011) 816-822.
- [54] N.V. Avagimova, A.M. Toikka, G.A. Polotskaya, Nanodiamond-modified polyamide evaporation membranes for separating methanol-methyl acetate mixtures, *Petroleum Chemistry*, 55 (2015) 276-282.
- [55] S. Sain, S. Dinçer, Ö.T. Savaşçı, Pervaporation of methanol–methyl acetate binary mixtures, *Chemical Engineering and Processing: Process Intensification*, 37 (1998) 203-206.
- [56] S. Steinigeweg, J. Gmehling, Transesterification processes by combination of reactive distillation and pervaporation, *Chemical Engineering and Processing: Process Intensification*, 43 (2004) 447-456.
- [57] D. Gorri, R. Ibáñez, I. Ortiz, Comparative study of the separation of methanol–methyl acetate mixtures by pervaporation and vapor permeation using a

commercial membrane, *J. Membr. Sci.*, 280 (2006) 582-593.

- [58] S. Lux, T. Winkler, M. Forstinger, S. Friesenbichler, M. Siebenhofer, Pervaporative Separation of Methanol-Methyl Acetate Mixtures with Commercial PVA Membranes, *Sep. Sci. Technol.*, 50 (2015) 2920-2929.

Chapter 4

Study on the effect of oxidative cross-linking on the structure and performance of polytitanocarbosilane-derived SiC-based membranes

4.1 Introduction

Polymeric membranes dominate membrane-based separation technologies that are now widely used in fields such as water treatment, foods, pharmaceuticals, and gas separation processes [1-3], although ceramic membranes have higher thermal and mechanical resistance. In particular, silicon carbide-based (SiC and SiC-related) membranes have shown great potential for separation processes since they possess high levels of mechanical strength, structural stability, biocompatibility, and demonstrate long lifetimes at elevated temperatures, and have been applied to water-filtration technologies [4-6]. Only a limited number of studies have focused on the preparation of SiC-based membranes for molecular separation, however, and even fewer have examined the separation of mid-sized molecules (e.g., N₂ 0.364 nm, and MeOH 0.38 nm) from large ones.

The use of silicon-containing preceramic precursors is a very convenient way to prepare SiC-based (SiC and SiC-related) materials. High-quality SiC-based materials are generally prepared via a curing process that promotes cross-linking and a subsequent high-temperature pyrolysis to achieve the polymer-to-ceramic transformation. In the fabrication of both SiC fibers and SiC-based membranes, the formation of cross-linking is a critical step before the transformation into ceramics [7, 8]. The cross-linking process converts thermoplastic polymers into a thermosetting polymer under a series of reactions that includes dehydrogenation and oxidation of

Si-H groups in order to preserve the shape of the object during pyrolysis [7, 8]. Additionally, a high ceramic yield is a general requirement for the precursor polymer, and cross-linking is known to promote high ceramic yields from polymer precursors following pyrolysis [9, 10].

Cross-linking methods that have historically been used to produce SiC-based membranes from preceramic polymers include ultraviolet irradiation [10], electron beam irradiation [11, 12], and conventional thermal (oxidation) cross-linking [7, 9, 13]. Wach *et al.* [11, 14] reported the preparation of a SiC-based (Si-O-C) membrane via the electron-beam irradiation curing of a polycarbosilane (PCS) and polyvinylsilane blend. Their membrane achieved H₂ permeance of 10⁻¹⁰-10⁻⁸ mol/(m² s Pa) and excellent H₂/N₂ selectivity of 254 at 250 °C [14]. Li *et al.* [15] used PCS as a precursor to prepare SiC-based (Si-O-C) membranes via thermal-oxidative cross-linking (i.e., cured at 200 °C under air atmosphere). The Li membrane showed a H₂ permeance of 10⁻⁸ mol/(m² s Pa) with a H₂/N₂ selectivity of 18-63. The Tsotsis group [16, 17] used an intramolecular thermal cross-linking method via allyl groups (C=C-C) without oxygen in allyl-hydridopolycarbosilane (AHPCS) to produce a SiC-based membrane. The Tsotsis membrane showed an ideal He/Ar separation factor of ~1,100 with He permeance of ~1 × 10⁻⁸ mol/(m² s Pa) at 200 °C [17]. The thermal-oxidative cross-linking method adds oxygen to the network of SiC-based materials and is commonly used in the preparation of SiC fibers and SiC-based membranes because it is considered more economical and convenient than the radiation method [13, 18].

Si-based precursors have recently received a great amount of research focus, and the chemical structure of PCS is now being chemically modified by the incorporation of transition metallic elements such as Al, Ti, and Zr in order to improve the heat

resistance, structure stability, and electrical properties of the final ceramic product [19, 20]. Our group was the first to report the fabrication of Ti-incorporated sub-nanoporous SiC-based membranes derived from polytitanocarbosilane (TiPCS) [21], which is commercially available and used as a precursor for the fabrication of Si-Ti-C-O (TiOSiC) fibers (Tyranno) with high mechanical and thermal properties. In that study, the effect of the pyrolysis temperature on the physical and chemical structures was systematically studied. The titanium components in TiPCS effectively inhibited and/or reduced the densification of the network structures at high temperatures (≥ 800 °C), which affected the permeation properties of TiPCS-derived membranes. On the other hand, most SiC-related ceramic materials lost the microporosity at the pyrolysis temperature of 700-750 °C due to the severe densification and pore shrinkage, and this was particularly true for the PCS-derived pure SiC and SiOC ceramic materials [9, 15, 22]. Thus, most of the SiC-based dense ceramic membranes were used to separate mixtures of small-sized molecules such as H₂/N₂ rather than for the separation of small/mid-sized molecules over large ones such as methanol/methyl acetate via pervaporation (PV). These membranes have shown a low level of H₂ permeance ranging from $\sim 10^{-9}$ - 10^{-7} mol/(m² s Pa) with high H₂/N₂ selectivities. Another important aspect of that work involved investigation into the PV dehydration and PV removal of methanol, for which the TiPCS membranes demonstrated a great potential for the separation of methanol/methyl acetate mixtures.

No study, however, has described the effect of thermal-oxidative treatment for cross-linking on the pore-formation behavior of TiPCS, although it is expected to affect the permeation properties. In the present work, thermal-oxidative cross-linking was studied for its effect on the ceramic yield, thermal stability, and microstructure of TiPCS ceramics. Moreover, the influence of the concentration of the TiPCS precursor

coating solution was also optimized, and the oxidation resistance and hydrothermal stability of the membranes at high temperatures were also evaluated. Furthermore, PV removal of methanol from organic solvents was further extended to other new challenging azeotropic mixtures. The most promising version of a TiPCS membrane demonstrated great performance in the PV removal of methanol in both MeOH/butyl acetate and MeOH/toluene azeotropic systems, and as an air-drying contactor, these membranes also showed excellent dehumidification performance in H₂O/N₂ systems at high temperatures.

4.2 Experimental

4.2.1 Preparation of cross-linked TiPCS powders

Commercial polytitanocarboxylic silane (TiPCS) is a superior heat-resistant paint (Tyranco Coat, TYR-VN100 type, Okitsumo Co., Ltd. Japan) that consists of ~48 wt% TiPCS in a mixed solvent of xylene, ethylbenzene, and *n*-butanol. The TiPCS precursor powder was prepared via dropping the paint into pure *n*-butanol to form a precipitate, which was then centrifuged, followed by drying in a vacuum oven at 50 °C for 24 h. To study the effect that cross-linking exerts on the evolution of TiPCS-derived products during the pyrolysis process, fresh powdered samples with and without an air curing process (i.e., under air at 200 °C for 2 h) were pyrolyzed at a series of temperatures (350-1000 °C) for 2 h under a N₂ flow, where the same heating rate of ~35 °C/min was employed.

4.2.2 Fabrication of a TiPCS-derived membrane

A porous α -alumina tube (porosity, 50%; average pore size, 1 μ m; outer diameter, 10 mm; Nikkato, Co., Japan) was used as a support. The support was modified in a

manner similar to that described in our previous work [3, 23, 24]. Briefly, two types of α -alumina particles (0.2 μm and 2 μm) with 1 wt% $\text{SiO}_2\text{-ZrO}_2$ (Si/Zr = 5: 5) colloidal sol as a binder were coated onto the outer surface of the tubes followed by calcination at 750-800 $^\circ\text{C}$ for 20 min under air. Subsequently, a 0.5 wt% $\text{SiO}_2\text{-ZrO}_2$ (Si/Zr = 5: 5) colloidal sol was coated onto the α -alumina particle layer followed by calcination at 750-800 $^\circ\text{C}$ for 15 min to obtain an intermediate layer. Each procedure was repeated several times.

A TiPCS precursor solution (1-5 wt% in xylene) was coated onto the intermediate layer followed by air curing at 200 $^\circ\text{C}$ and then pyrolysis at 750 $^\circ\text{C}$ under N_2 for 0.5 h with a heating rate of ~ 35 $^\circ\text{C}/\text{min}$. A non-cross-linked membrane was also prepared without the air curing process as a control. During the curing and pyrolysis processes, the gas flow rates were set at 500 mL/min. The coating-pyrolysis process of all TiPCS-derived membranes was repeated 3 times.

4.2.3 Characterization of TiPCS powders and membranes

The pyrolysis process was assessed via thermogravimetric analysis (TGA) using a Shimadzu TGA-50 with a steady N_2 flow rate of 50 mL/min. ATR-FTIR spectra of the TiPCS powders, and FT-IR spectra of the films coated onto KBr plates were collected using an FTIR-4100 (JASCO Co., Japan). N_2 (-196 $^\circ\text{C}$) and CO_2 (25 $^\circ\text{C}$) adsorption-desorption isotherms for TiPCS powders were carried out using BELMAX equipment (BELL Co., Japan). Prior to the measurement, all powder samples were degassed at 200 $^\circ\text{C}$ under vacuum for 12 h. The BET surface area was evaluated using N_2 adsorption data at a relative pressure (P/P_0) of between 0.001 and 0.15, and the micropore volume was calculated from the amount of N_2 adsorbed at $P/P_0 = 0.01$, which corresponds to a pore size of less than 1 nm [24, 25]. The micropore size

distributions were obtained from the CO₂ adsorption isotherms via the non-localized density functional theory (NLDFT) method with a slit-pore model. The chemical elements of the TiPCS powders and morphologies of the membranes were examined using a scanning electron microscope (SEM) equipped with an EX-37001 EDS accessory (JCM 5700, JEOL, Japan).

4.2.4 Single-gas permeation, pervaporation, and H₂O/N₂ separation

measurements

The permeation performances of the TiPCS-derived membranes were evaluated at 200 °C with a single gas using a schematic experimental apparatus shown in a previous publication [26]. The permeate steam (inside of the cylindrical membrane) was maintained at atmospheric pressure, while the pressure drop across the membrane was maintained at ~100 kPa. The permeate flux was measured via a soap-film meter.

Pervaporation (PV) removal of methanol was performed for the azeotropic mixtures of both MeOH/toluene and MeOH/butyl acetate (BuAcO). The MeOH weight percentages of the feed sides were maintained at 10 wt%. The binary mixtures were fed to the outsides of the membranes, and the pressures inside and outside the membranes were maintained at approximately 0 kPa and at atmospheric pressure, respectively. The permeate samples were collected via cold traps. Before the collection of the samples, the system was maintained for more than 1 h to ensure that a steady state was reached. The compositions were determined using a Shimadzu GC-14B with a Porapak P column. Values for flux and separation factor in PV were calculated using equations shown in our previous work [21].

An equimolar H₂O/N₂ mixture (50 kPa: 50 kPa) separation was conducted at 300 °C, using the experimental apparatus schematically shown in our previous work

[27, 28]. The H₂O/N₂ mixture was fed to the outside (upstream) of a cylindrical membrane at atmospheric pressure, while the permeate side (downstream) was evacuated using a vacuum pump. Permeate H₂O was collected by a cold trap for a specified time interval, and the flow rate of the permeant N₂ was calculated using the observed pressure value via a calibrated critical nozzle located between the permeation cell and a vacuum pump [28]. After the measurement of H₂O/N₂ separation, the membrane was dried completely under a N₂ flow at 500 °C for ~3 h. A log-mean pressure drop was used to calculate the permeance [29], and the ratio for the permeance of H₂O and N₂ was served as the selectivity.

4.3 Results and Discussion

4.3.1 Cross-linking behavior of the TiPCS polymer

Thermal-oxidative cross-linking generally involves curing under air at a moderate temperature (160-220 °C) [7, 13]; as the curing temperature increases, the reactivity of Si-H increases, which can significantly reduce the reaction time. However, when the cross-linking process is carried out at a much higher temperature (e.g., 300 °C), significant amounts of the volatile oligomer will be lost leading to a reduction in the ceramic yield [30]. In this section, the thermal-oxidative cross-linking process of TiPCS powders was therefore carried out at 200 °C. The cross-linking behavior of the TiPCS precursor was characterized via TGA and FT-IR, as shown in Fig. 4-1. The weight of the TiPCS was increased by 4% when it was air cured at 200 °C for ~90 min, at which point it reached a stable value, while the weight of

TiPCS treated under N₂ in the same manner was unchanged (Fig. 4-1a). Fig. 4-1b and c show the FT-IR spectrum analysis and the absorbance ratio of Si-H/Si-CH₃ with the corresponding cross-linking degree of TiPCS precursor for different curing times, respectively. The characteristics of TiPCS are described in a recent publication [21], and the main absorption peaks are included: 2,100 cm⁻¹ (Si-H); 1,020 cm⁻¹ (Si-CH₂-Si); 1,259 cm⁻¹ (Si-CH₃); and, ~800 cm⁻¹ (vs, Si-C stretching). The absorbance ratio of Si-H/Si-CH₃ and the cross-linking degree were determined using the following equation [31]:

$$D_{Si-H} = \frac{(A_{2100}/A_{1259})_{uncured} - (A_{2100}/A_{1259})_{cured}}{(A_{2100}/A_{1259})_{uncured}}$$

The intensity of Si-H groups and the absorbance ratio of Si-H/Si-CH₃ were reduced with an increase in the air curing time, which suggested that the Si-H group was consumed via an oxidation reaction. The cross-linking degree gradually increased from 0 to 26.5% during curing for 1 h and reached a stable maximum of 39% after curing for 2 h. This finding implies that some oxygen was introduced into the TiPCS polymer during the thermal-oxidative cross-linking and that the linear structure of the thermoplastic polymer was converted into a 3-D thermosetting polymer network structure [8], as shown by the schematic drawing in Fig. 4-1c. The Si-H bonds reacted with oxygen to develop Si-O-Si (1,000-1,130 cm⁻¹) bonds, although no significant change was observed in the FT-IR spectra due to overlapping by the stronger absorption of the Si-CH₂-Si (1,020 cm⁻¹) bond [32].

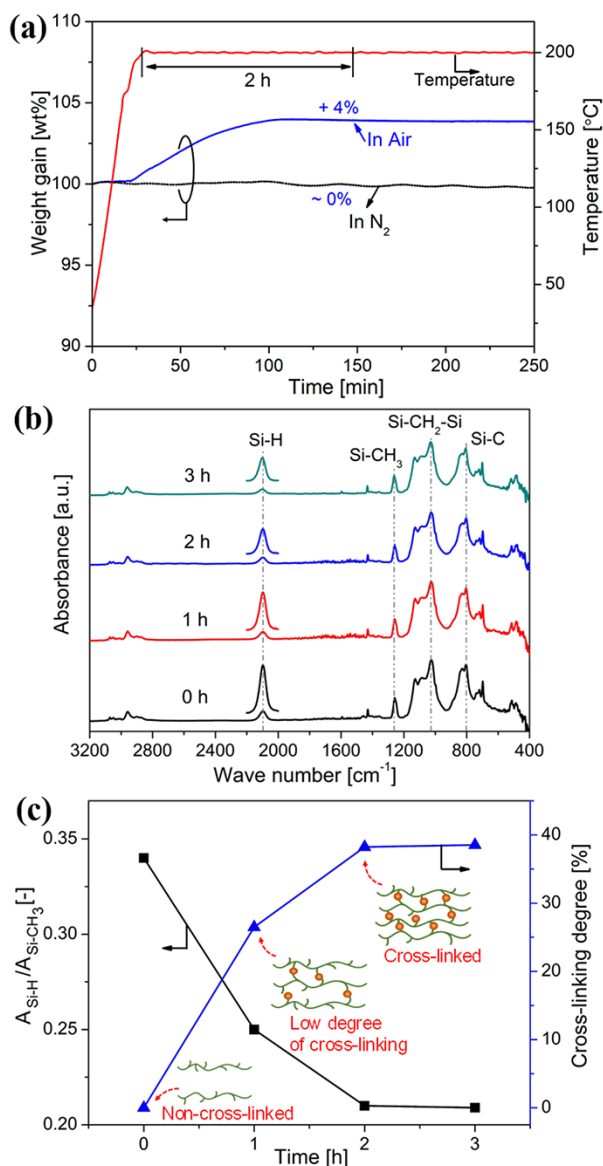


Fig. 4-1. (a) Time course of weight gains for TiPCS precursor powders at 200 °C under either an N₂ or an air atmosphere via TG analysis; (b) FT-IR spectra on substrates of KBr plate (the enlarged spectra ($\times 5$) of the Si-H is inserted), and (c) the absorbance ratio of Si-H/Si-CH₃ and the corresponding cross-linking degree with different curing times for the TiPCS precursor.

4.3.2 Characterization of TiPCS powders fired at different temperatures

TGA was used to explain the effect that cross-linking exerts on the thermal

behavior of TiPCS during the pyrolysis process, as shown in Fig. 4-2. The cured powders were pre-treated under air at 200 °C for 2 h to promote cross-linking, and for the sake of convenience, the residue weights were normalized according to the weights at 200 °C (i.e., weight gain was deducted for cured powders) for the comparison between cured and uncured TiPCS powders.

Fig. 4-2a shows the TG analysis with a heating rate of 10 °C/min to a level of 1,000 °C for cured and uncured TiPCS powders with residue weights of 80.4% and 78.4%, respectively. Examination of the uncured TiPCS powder revealed that the mass loss started at ~230 °C, while mass loss for the cured version started at 300 °C or higher. These results indicate that the cross-linking process improved the thermal stability and inhibited/reduced the degradation of TiPCS, and, thus, the ceramic yield increased. This result agrees with the results of experiments using PCS under a similar process in a previous study [22] as well as our study shown in **Chapter 2**.

Fig. 4-2b shows the weights of the residue as a function of time at a heating rate of 35 °C/min, which approximated that of membrane fabrication that reached a level of 750 °C for both cured and uncured TiPCS powders. Clearly, the cured powders had a higher level of thermal stability than the non-cross-linked versions even at a higher heating rate of 35 °C/min, and it also is evident that the two curves for residue weights reached plateaus after being pyrolyzed for ~15 min at 750 °C. Fig. 4-2b also shows the contact angle images for water droplets on TiPCS films pyrolyzed at 750 °C. These images show that the water contact angle of the cured (cross-linked) TiPCS film (29.6°) was lower than that of the uncured (non-cross-linked) version

(40.4°), probably due to the higher number of Si-O bonds with higher hydrophilicity in the cross-linked film. Moreover, Fig. 4-3 shows the residue weight curves (normalized at 200 °C) of cured and uncured TiPCS powders pyrolyzed at different temperatures for 2 h. The weights of the residue in the cured TiPCS were always higher than that in the uncured version during the pyrolysis process, which again confirmed that the cross-linking behavior suppresses the loss of polymer fragments, which plays a vital role in obtaining a high ceramic yield.

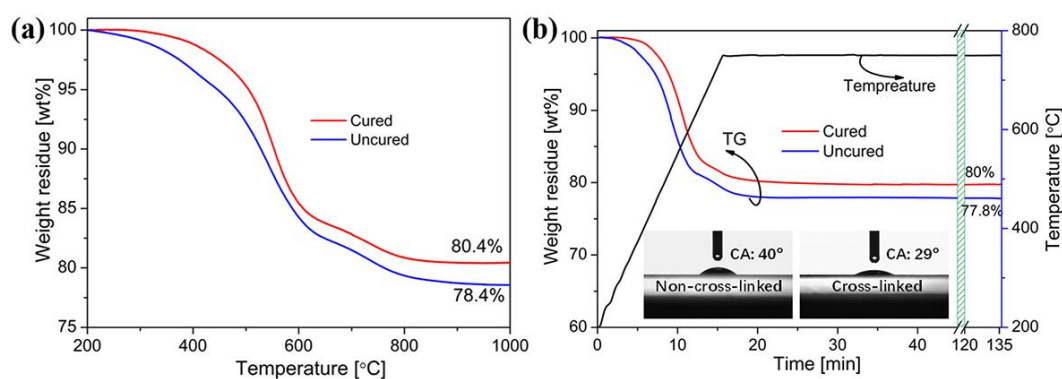


Fig. 4-2. (a) TGA curves of the thermal decomposed behavior for cured and uncured TiPCS powders under a N₂ atmosphere with a heating rate of 10 °C/min to a level of 1,000 °C; (b) the residue weights as a function of time with a heating rate of 35 °C/min to a level of 750 °C after being held for 2 h (the temperature history is also shown on the right y-axis, contact angle images for water droplets on TiPCS films are inserted). The cured powders were pre-treated under air at 200 °C for 2 h, while the uncured powders were not. The weights of the residue were normalized according to the weight at 200 °C for the convenience of comparison.

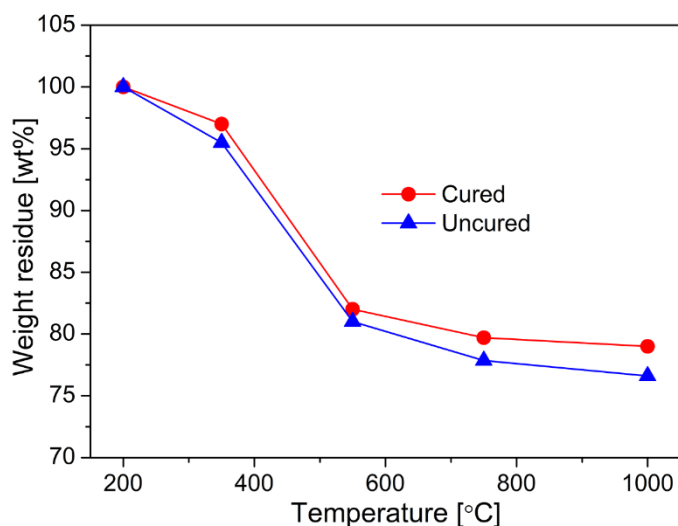


Fig. 4-3. Weight residue of cured and uncured TiPCS powders pyrolyzed for 2 h under a N_2 atmosphere with a heating rate of $35\text{ }^\circ\text{C}/\text{min}$. The cured powders were pre-treated under air at $200\text{ }^\circ\text{C}$ for 2 h, while the uncured powders were not. The weight residues were normalized according to the weight at $200\text{ }^\circ\text{C}$ (i.e., weight gain was deducted for cured powders) for the convenience of comparison.

Fig. 4-4 shows the ATR-FTIR spectra of cured and uncured TiPCS powders pyrolyzed at different temperatures for 2 h under a N_2 flow. With an increase in pyrolysis temperature, the absorption of organic groups such as Si- CH_3 ($1,259\text{ cm}^{-1}$; $\sim 800\text{ cm}^{-1}$, Si-C stretch in Si- CH_n) and Si- CH_2 -Si ($1,020\text{ cm}^{-1}$) was decreased, and these groups had vanished at $750\text{ }^\circ\text{C}$. The final powders only displayed absorption bands at $1,150\text{--}700\text{ cm}^{-1}$, which was attributed to the asymmetric stretching vibrations of Si-O-Si and O-Si-C mixture linkages ($1,150\text{--}900\text{ cm}^{-1}$) and Si-C ($\sim 800\text{ cm}^{-1}$) [33, 34]. This is also consistent with the results of XPS in our previous work [21]. When the pyrolysis temperature was further increased ($T \geq 750\text{ }^\circ\text{C}$), the peaks of uncured TiPCS were significantly decreased, while that of cross-linked TiPCS had decreased only slightly, which also indicated that the structure of the cross-linked TiPCS was

more stable than that of the non-cross-linked version.

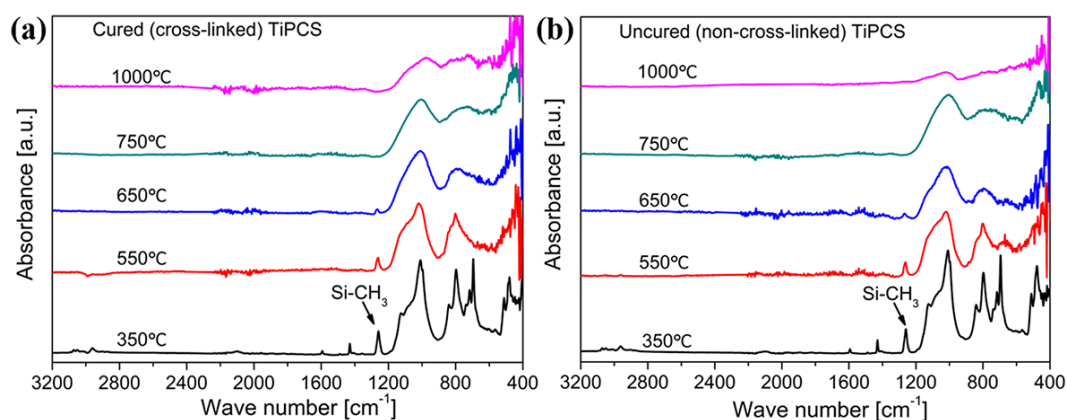


Fig. 4-4. ATR-FTIR spectra of (a) cured and (b) uncured TiPCS powders with and without the air curing process (under air at 200 °C for 2 h) following pyrolysis under a N₂ flow for 2 h at different temperatures.

Fig. 4-5 shows the EDS analysis of the elemental composition ratios (molar ratio based on Si) for cured and uncured TiPCS powders pyrolyzed at different temperatures. The ratio of O/Si increased after thermal-oxidative cross-linking at 200 °C, which matches well with the TGA data (Fig. 4-1a). Every reading for the ratio of O/Si and C/Si for cross-linked TiPCS was higher than that of the non-cross-linked version at the same pyrolysis temperature. The ratio of Ti/Si in each cross-linked and non-cross-linked TiPCS was almost unchanged due to the stable Ti-O bonds. In addition, when the pyrolysis temperature was higher than 750 °C for both cross-linked and non-cross-linked TiPCS, the elemental composition curves tended to be flat. This result was consistent with both the residue weight data shown in Fig. 4-3 and the disappearance of the organic segment, particularly that of the Si-CH₃ group, at 750 °C via ATR-FTIR spectra (Fig. 4-4). These findings all indicated that the

polymer-to-ceramic transformation process was complete at 750 °C for both cured and uncured versions. It is worth noting that the cross-linked and non-cross-linked samples pyrolyzed at 750 °C gave a composition of approximately $\text{SiO}_{1.4}\text{C}_3\text{Ti}_{0.01}$ and $\text{SiO}_{1.06}\text{C}_2\text{Ti}_{0.01}$, respectively. The existence of Si-C and O-Si-C bonds in addition to Si-O-Si bonds clearly shows the difference with silica (SiO_2), which also was confirmed by the ATR-FTIR (Fig. 4-4) and XPS investigations in our previous work [21]. Different ceramic compositions and residue yields would have different structure properties, which will be discussed according to the N_2 and CO_2 adsorption-desorption isotherms.

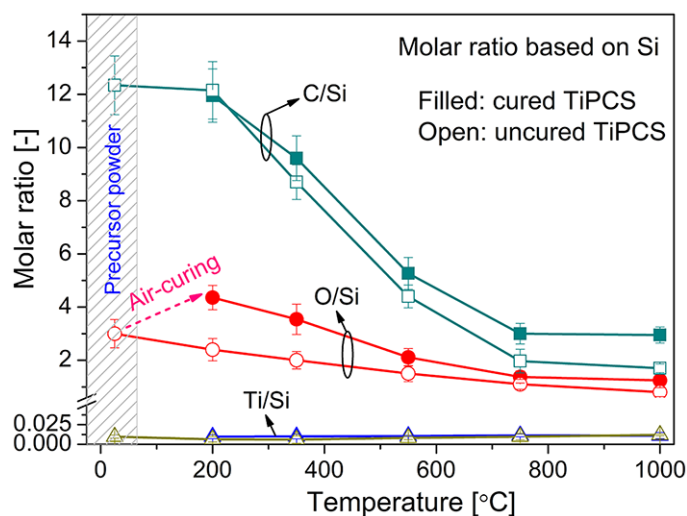


Fig. 4-5. Elemental composition (analysis with EDS, molar ratio based on Si, together with precursor powders for comparison) for cured and uncured TiPCS powders pyrolyzed for 2 h under a N_2 atmosphere with a heating rate of 35 °C/min. The cured powders were pre-treated under air at 200 °C for 2 h, while the uncured powders were not.

Fig. 4-6 displays the N_2 adsorption-desorption isotherms at -196 °C for both

cured and uncured TiPCS powders pyrolyzed under a N_2 flow for 2 h at different temperatures. Also shown are the microstructure parameters in terms of BET surface area and micropore volume (at $P/P_0 = 0.01$ relative to pore size ≤ 1 nm) analyzed via the N_2 adsorption-desorption isotherms in Table 4-1.

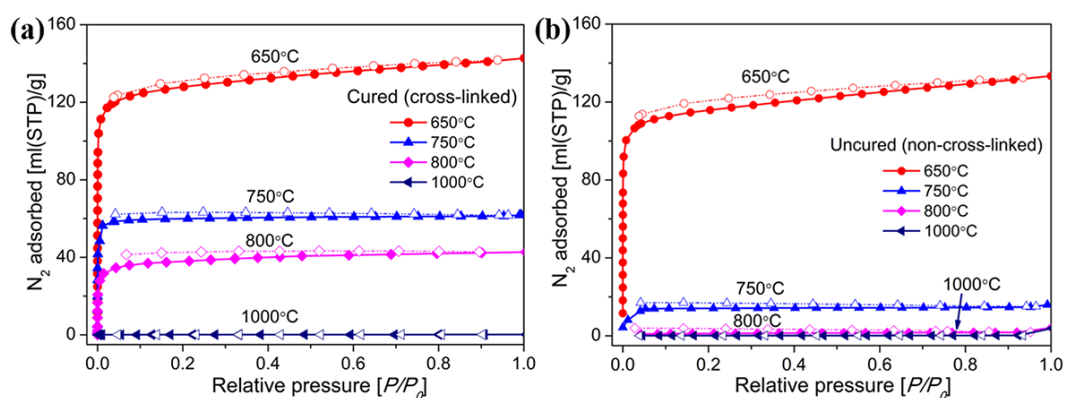


Fig. 4-6. N_2 adsorption-desorption isotherms at -196 °C of (a) cured and (b) uncured TiPCS powders with and without the air curing process (under air at 200 °C for 2 h) followed by pyrolysis under a N_2 flow for 2 h at different temperatures.

Table 4-1. N_2 adsorption results for both cured and uncured TiPCS powders.

Pyrolysis temp. [°C]	BET [m^2/g]		Micropore volume [$cm^3/g, \leq 1$ nm]	
	Air curing	No curing	Air curing	No curing
650	498	452	0.174	0.157
750	245.7	56.7	0.084	0.013
800	143.1	4.2	0.046	~ 0
1000	0.4	0.3	~ 0	~ 0

Although 650 °C is lower than the temperature of complete polymer-to-ceramic transformation (750 °C), both the cured and uncured TiPCS powders showed the

highest microstructure parameter values for N₂ adsorption capacity, BET surface area, and micropore volume for a temperature range of 650-1,000 °C. Those results agree with the finding in our previous work whereby a loose transitional structure with large-sized pores was obtained by the decomposition of a larger number of organic groups at a moderate pyrolysis temperature (350-650 °C) [21]. When the TiPCS samples were pyrolyzed at the temperature of a complete polymer-to-ceramic transformation of 750 °C, however, the microstructure parameter values (BET, 245.7 m²/g, micropore volume, 0.084 cm³/g) of the cured TiPCS were significantly higher than those of the uncured version (BET, 56.7 m²/g, micropore volume, 0.013 cm³/g). With further increases in the pyrolysis temperature to 800 °C, the BET surface area of cured TiPCS was gradually reduced to 143.1 m²/g with a micropore volume of 0.046 cm³/g, and no microporosity was exhibited at 1,000 °C due to the rearrangement and densification reactions. For the uncured TiPCS, the BET surface area decreased sharply and fell to less than 5 m²/g with a micropore volume of essentially zero (0.001 cm³/g) at 800 °C. These results indicated that the cross-linking behavior enhanced the thermal stability of the TiPCS network structure and reduced the influence of densification at high temperature [18]. This result agrees with the findings of experiments using PCS [9, 15, 22] and PMS [35] under a similar synthesis process (with and without air curing at 200 °C). When the pyrolysis temperature rose to 700-750 °C, however, the microporosity of the cross-linked precursor (PCS and PMS)-derived materials was lost due to the severe densification and pore shrinkage. In this case, the cross-linked TiPCS-derived powders pyrolyzed at 800 °C maintained

their microporosity, which probably was due to the Ti components inhibiting and/or reducing densification of the network structures.

Micropores can be classified into ultra-micropores (pores < 0.7 nm) and super-micropores (pores between 0.7-2 nm) [36]. Generally, N_2 adsorption-desorption isotherms at -196 °C create difficulties in evaluating the ultra-micropores, because of the diffusion problems with N_2 molecules, which cannot access those pores at extremely low temperatures. By contrast, the smaller CO_2 molecules have a higher boiling point (-78 °C) than that of N_2 and are able to enter the ultra-micropores at high temperatures (25 °C) with a high level of kinetic energy [24, 25, 36]. Thus, CO_2 adsorption analysis can provide additional information about the microstructure. CO_2 adsorption-desorption isotherms at 25 °C and at pressures up to 1 atm were measured for the final cured and uncured TiPCS ceramic powders, which were pyrolyzed at 750 °C. As shown in Fig. 4-7, the CO_2 uptake of uncured TiPCS was lower than that of the cured version within a pressure range of 60-100 kPa, probably due to the existence of large pores that could not be filled by CO_2 in the uncured TiPCS [36]. Fig. 4-8a shows the NLDFT pore size distribution curves based on the CO_2 adsorption-desorption isotherms data. The pore size distribution of cross-linked TiPCS showed a narrow peak centered at 0.536 nm, while that of the non-cross-linked version showed a very broad peak centered at 0.573 nm. These results indicate that the micropores in the cross-linked TiPCS were uniform, while the non-cross-linked version showed a broad peak consisting of both small and large micropores. This trend was expected to affect the permeation properties of the membrane, which will

be discussed in the next section.

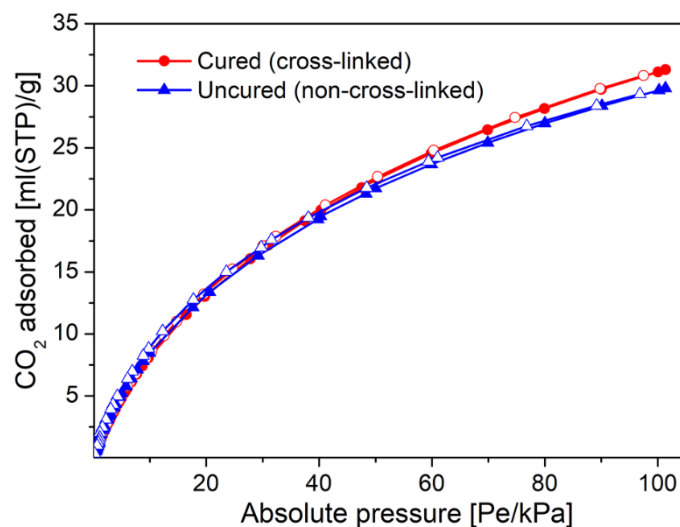


Fig. 4-7. CO₂ adsorption-desorption isotherms at 25 °C of cross-linked and non-cross-linked TiPCS powders pyrolyzed at 750 °C.

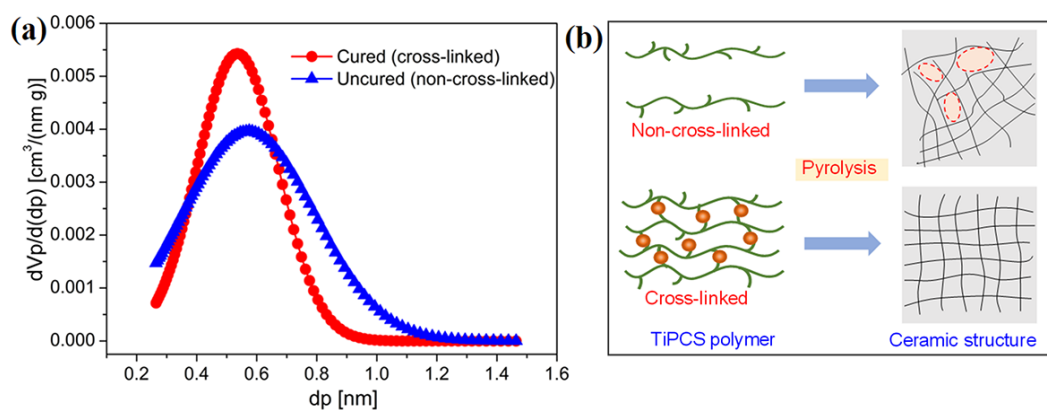


Fig. 4-8. (a) NLDFT pore size distribution curves based on the CO₂ adsorption-desorption isotherms at 25 °C; and, (b) schematic illustration of the network structure for cured and uncured TiPCS powders with and without the air curing process (under air at 200 °C for 2 h) and pyrolyzed at 750 °C for 2 h under a N₂ flow.

The network structures of both the cross-linked and non-cross-linked versions of TiPCS pyrolyzed at 750 °C are schematically illustrated in Fig. 4-8b, which is based

on the characteristics described thus far. During the polymer-to-ceramic transformation processes, the structure of the cross-linked flexible polymer was shrunk via the decomposition of organic groups caused by the evolution of gases, which formed a denser ceramic structure of narrow and uniform micropores. On the other hand, the structure of the non-cross-linked polymer could have evolved from a linear precursor with stacks of random “strands” and small micropores that formed due to weak cross-linking caused by the dehydrogenation between Si-H groups. Also, large “slit-like” micropores were possibly formed by the imperfect packing of the aforementioned strands, which is similar to the formation of pores in carbon molecular sieve materials [37].

4.3.3 Membrane fabrication

4.3.3.1 Effect of cross-linking

TiPCS membranes were fabricated by coating a 3% TiPCS solution onto intermediate layers followed by air curing for 0 (non-cross-linked), 0.5 and 2 h at 200 °C, followed by pyrolysis at 750 °C under a N₂ atmosphere, which hereafter will be referred to by the membrane designations: M-3%-0, M-3%-0.5, and M-3%-2, respectively. Single-gas permeation performance is sensitive to the pore size distribution of the membrane, and is used here as a simple method to characterize the quality of the membrane [38].

Fig. 4-9a shows the relationship between the single-gas permeance of TiPCS membranes with curing times ranging from 0 to 2 h as a function of the molecular size,

and Fig. 4-9b shows the H₂ and N₂ permeance as well as the H₂/N₂ and H₂/SF₆ selectivities as functions of the curing time. Both H₂ (0.289 nm) and N₂ (0.364 nm) permeance gradually decreased when the curing time was increased from 0 to 2 h, and the permeance of N₂ with a larger molecular size was decreased more rapidly than that of H₂, which led to a H₂/N₂ selectivity increase of from 4.6 to 8.3. Moreover, with curing times of 0 and 0.5 h, the CH₄ (0.38 nm) permeance was higher than that of N₂ (0.364 nm) even though CH₄ has a larger molecular size, which indicates that Knudsen diffusion was dominant through the large pores or defects in the uncured membrane network. When the curing time was increased to 2 h, which led to a higher degree of cross-linking, the CH₄ permeance became lower than that of N₂. Those results suggested that the pore size of the TiPCS membranes had been reduced and the network structure was narrowed with the curing time. Similar to the selectivity of H₂/N₂, with an increase in the curing time of from 0 to 2 h, the selectivity of H₂/SF₆ was also increased from 557 to 12,000 because it was more affected by the existence of large pores. This result indicates that the number of defects was small enough, and the quality of the membranes had increased with an increase in the cross-linking degree. In addition, the non-cross-linking approach made it more difficult to obtain a defect-free SiC-based film/membrane compared with that of the cross-linking version. The effect of cross-linking on membrane performance was consistent with the results of pore size distribution (Fig. 4-8a). The M-3%-2 corresponded to well-oxidative cross-linking and showed the highest H₂/SF₆ selectivity of 12,000, N₂/SF₆ selectivity of 1500, H₂/N₂ selectivity of 8.3, and exhibited a satisfactory H₂ permeance of 1.49×10^{-6} mol/(m² s Pa), which indicated that the membrane consisted of sub-nanopores with a quite small number of pinholes.

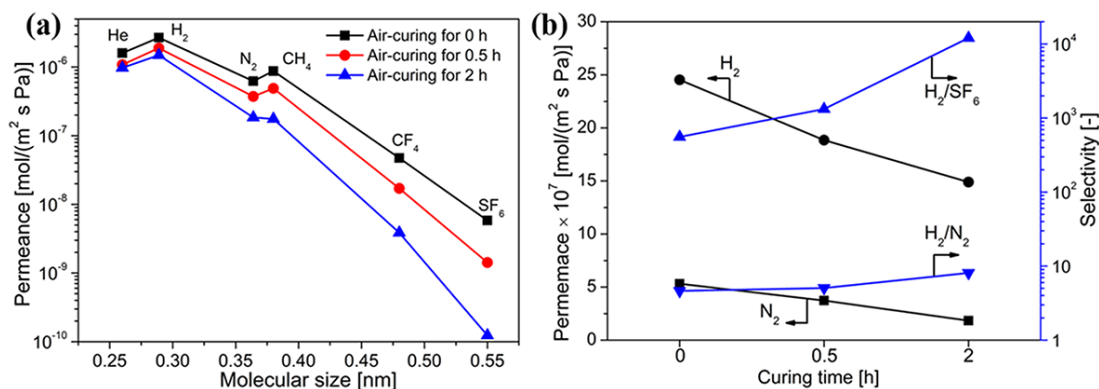


Fig. 4-9. (a) Effect of curing time on single-gas permeance at 200 °C as a function of the molecular size; and, (b) relationship between the gas permeation performance of TiPCS membranes and curing time. The curing process for cross-linking was implemented under air at 200 °C for different times before pyrolysis. The membranes were pyrolyzed at 750 °C under N₂.

4.3.3.2 Effect of TiPCS concentration

The precursor concentration of the coating solution is another important factor that directly affects the thickness and morphology of membranes, and could ultimately affect their permeation performance and quality. Therefore, the coating concentration was also optimized with 1, 3 and 5 wt% TiPCS in this study, and the corresponding membranes were prepared via air curing for 2 h followed by pyrolysis at 750 °C under N₂, which hereafter will be referred to by the membrane designations: M-1%-2, M-3%-2, and M-5%-2. Fig. 4-10 shows the single-gas permeance at 200 °C as a function of the molecular size for TiPCS membranes prepared using different concentrations of TiPCS, and Fig. 4-11 shows the SEM images of the cross-sections and surfaces of those TiPCS membranes. With an increase in the TiPCS concentration,

the H_2 permeance of TiPCS membranes decreased significantly, which was probably due to the increased thickness of the membranes. When the precursor concentration was increased from 1 wt% to 3 wt%, the N_2/SF_6 selectivity quickly increased from 6 to 1,500, but a further increase in the TiPCS concentration to 5 wt% significantly decreased the N_2/SF_6 selectivity to 20. This could have been the result of the inability of a 1 wt% coating layer to cover the large pores and/or some of the bulges in the intermediate layers, which would result in many defects. A 5 wt% solution, however, would have resulted in a thicker separation layer (up to $2.3 \mu\text{m}$) that would be prone to the formation of cracks and defects during the pyrolysis process, as shown in Fig. 4-11. On the other hand, the M-3%-2 as the optimized membrane with a thickness of less than 400 nm exhibited a uniform, un-cracked layer that adhered well to the intermediate layer.

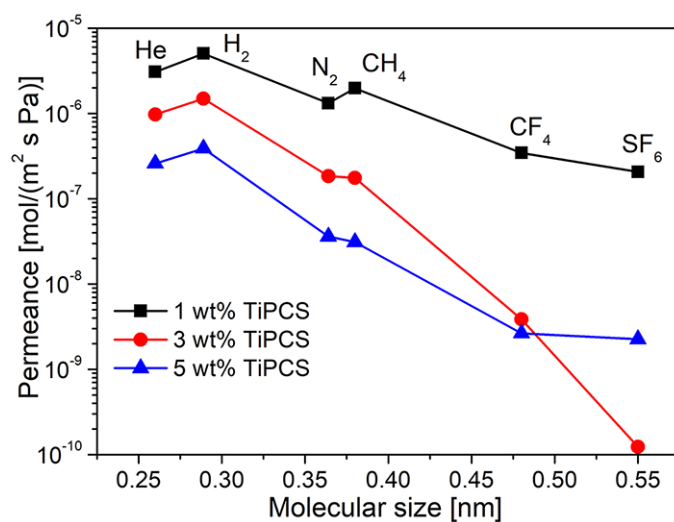


Fig. 4-10. Effect of TiPCS concentration on single-gas permeance at 200 °C as a function of the molecular size. The curing process for cross-linking was implemented under air at 200 °C for 2 h. The membranes were pyrolyzed at 750 °C under N_2 .

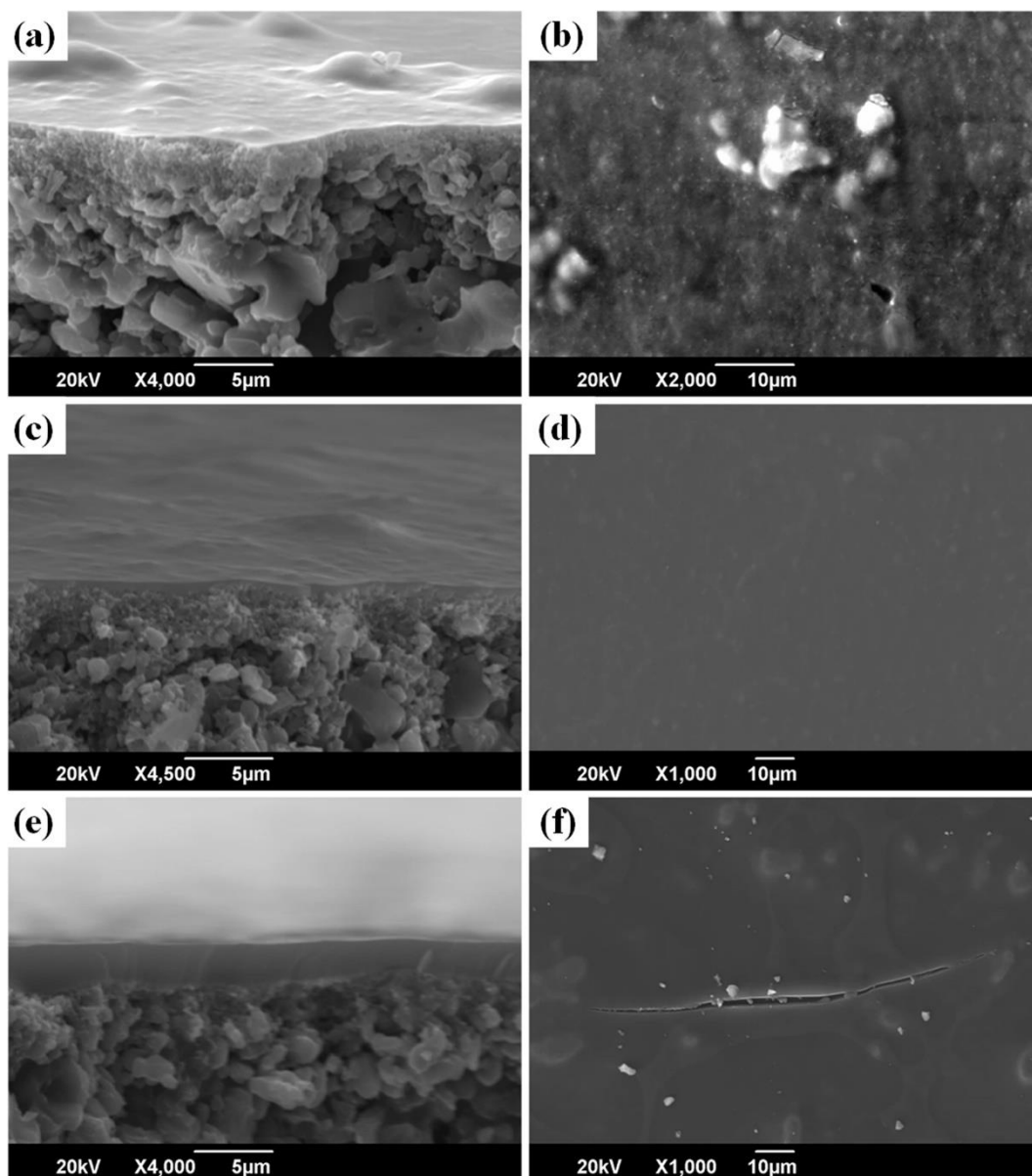


Fig. 4-11. SEM images of the cross-sections and surfaces of TiPCS membranes derived from different concentrations of TiPCS coating solutions: (a,b) 1 wt% TiPCS; (c,d) 3 wt% TiPCS; and, (e,f) 5 wt% TiPCS.

4.3.3.3 Membrane reproducibility

Fig. 4-12 a and b summarizes the H_2 and N_2 permeance versus the selectivity of H_2/N_2 and N_2/SF_6 of TiPCS membranes (M-3%-2) prepared under the same optimized

conditions together with other SiC-based membranes and MFI membranes (pore size, ~ 0.55 nm) for comparison. SF_6 , which is the gas with the largest molecular size, is often used for evaluating the existence of large pores, and N_2/SF_6 is used as a benchmark for the separation of mid-sized molecules from large molecules such as the removal of methanol from organic mixtures [39, 40], and is also used as an index to evaluate membrane quality [41]. Fig. 4-12 clearly shows that the four TiPCS membranes of M-3%-2 have very similar qualities and permeation behaviors, which demonstrates the reproducibility of the membrane properties and preparation. TiPCS membranes showed rather low H_2/N_2 selectivity (~ 10) due to relatively large pore sizes (sub-nanopores), but revealed permeation properties that dictate better permselectivity for N_2/SF_6 compared with other SiC-based membranes. These membranes also displayed high N_2 permeance with excellent selectivity compared with their MFI counterparts. This result also emphasizes that the TiPCS membrane consists of sub-nanopores with a quite small number of pinholes.

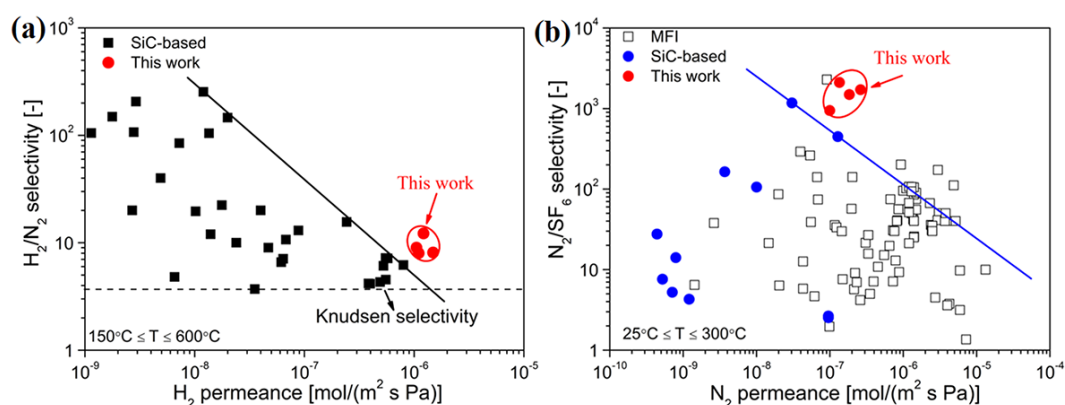


Fig. 4-12. Comparison of the selectivities for (a) H_2/N_2 and (b) N_2/SF_6 of various membranes (SiC-based membranes found in the literature[11, 14, 15, 28, 35, 42-50] and TiPCS membranes (M-3%-2) in this work, as well as MFI membranes[40, 41, 51, 52]).

4.3.3.4 Oxidation resistance

In order to evaluate the effect of cross-linking behavior on the oxidation resistance of membranes, values for the time courses of air flux at 300 °C under a pressure difference of 50 kPa for typical cured (M-3%-2) and uncured (M-3%-0) membranes were recorded, as shown in Fig. 4-13a. Obviously, the air flux of the uncured membrane increased significantly (by more than twice) after 12 h, while that of the cured membrane showed almost stable permeance during the air treatment. Fig. 4-13b shows the single-gas permeance as a function of the molecular size at 200 °C for cured and uncured TiPCS membranes before and after air treatment for 12 h. For the uncured membrane, the permeance of all permeation gases was increased significantly after air treatment; for example, the H₂ permeance increased from 2.7×10^{-6} mol/(m² s Pa) to 3.9×10^{-6} mol/(m² s Pa), and conversely, the selectivity of H₂/SF₆ decreased from 460 to 90, which indicates the pore sizes of the uncured membrane were enlarged. The cured membranes showed a slight increase in gas permeance after air treatment, with almost no change in the selectivity of the membrane, particularly to the selectivity of N₂/SF₆, which suggests that the pore structure of the cross-linked membranes is stable.

Free carbon was believed to have been generated in SiC-based (SiC and SiC-related) materials [53-55]. Yue *et al.* [53] reported PCS-derived SiC-based fibers prepared by thermal-oxidative cross-linking, and a longer cross-linking time gave the fibers less free carbon, which resulted in higher tensile strength and oxidation

resistance. In this case, the structure of the non-cross-linked membrane could contain a larger amount of free carbons, most of which were packed into the non-cross-linked TiOSiC network. These free carbons were easily burned off, which resulted in larger pores that greatly reduced the selectivity [54, 55]. On the contrary, the structure of the cross-linked membrane contained numerous molecules of oxygen but a low content of free carbons since most of the carbons constituted the network chains of the TiOSiC structure, which is considered highly resistant to oxidation [53, 56]. This indicates that the cross-linked membranes have higher levels of oxidation resistance than the non-cross-linked versions.

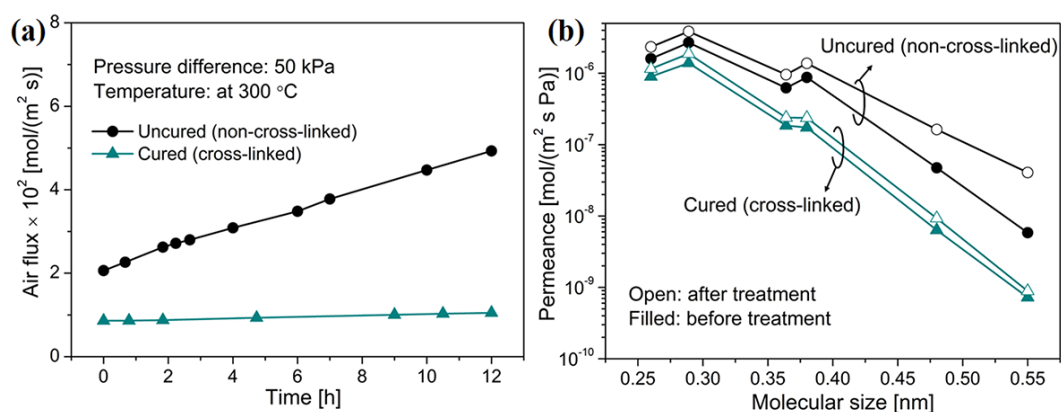


Fig. 4-13. (a) Time course of air flux for cured (M-3%-2) and uncured (M-3%-0) TiPCS membranes at 300 °C with a pressure difference of 50 kPa; and, (b) single-gas permeance at 200 °C of cured (M-3%-2) and uncured (M-3%-0) TiPCS membranes before and after air treatment at 300 °C for 12 h.

4.3.4 Pervaporation performance of cross-linked TiPCS membranes

An optimized, TiPCS-derived SiC-based, M-3%-2 membrane was successfully

prepared. PV removal of methanol in MeOH/BuAcO and MeOH/toluene mixtures was used to evaluate the membrane performance. Some physical properties of MeOH, butyl acetate (BuAcO), and toluene (together with water for comparison) are listed in Table 4-2. Methanol, BuAcO, and toluene are widely used in the petrochemical and medicinal fields [57, 58]. The efficient separation of methanol from MeOH/BuAcO mixtures in transesterification reactions and from MeOH/toluene mixtures in alkylation reactions of benzene with methanol are important manufacturing processes for industrial applications [59, 60], but separation via membranes remains a challenge since a membrane must be able to withstand harsh solvents and provide good flux and selectivity.

Table 4-2. Various properties of penetrants.

Name	MW (g/mol)	Stokes diameter (nm) [61-63]	Solubility parameter (MPa ^{0.5}) [64]	Polarity (MPa ^{0.5}) [64, 65]
Water	18	0.296	47.8	16
MeOH	32.04	0.38	29.6	12.3
BuAcO	116.16	0.524	17.4	3.7
Toluene	92.14	0.91 [0.59]	18.2	1.4

Fig. 4-14 shows the time courses for fluxes and separation factors through the optimized TiPCS membrane (M-3%-2) in MeOH/BuAcO, and MeOH/toluene systems at 50 °C under PV. Each flux and separation factor under different binary systems was nearly constant over a course of 10 h confirming the stable PV performance of TiPCS membranes. Additionally, the TiPCS membrane showed a

MeOH flux of 0.63 kg/(m² h) and a MeOH/toluene separation factor of 410, both of which were higher than what is typically achieved with a MeOH/BuAcO system (MeOH flux, 0.21 kg/(m² h); MeOH/BuAcO separation factor, 79). This may have been due to the fact that the linear-shaped molecules of BuAcO (0.524 nm) could enter and plug some pores of the membrane, which could form steric hindrance that would inhibit/reduce the penetration of MeOH, while it was difficult for the large ring-shaped molecules of toluene (0.59 nm) to enter the pores of the membrane. Moreover, operating temperatures are considered an important factor that affects PV performance. Fig. 4-15 shows the PV performance of a M-3%-2 membrane in MeOH/BuAcO (10/90, wt%) and MeOH/toluene (9/91, wt%) mixtures at temperatures ranging from 30 to 60 °C. The flux of small molecular MeOH increased continuously with temperature in both MeOH/BuAcO and MeOH/toluene mixtures, which could be attributed to the enhanced driving force for mass transfer associated with activated diffusion through the small pores, which allowed the permeation of only MeOH, but not of BuAcO and toluene. Either BuAcO or toluene flux slightly decreased with temperature in each system probably because the larger BuAcO and toluene molecules tended to permeate through the larger pores via surface diffusion, which was decreased with increases in temperature. As a result, the separation factors of both MeOH/BuAcO and MeOH/toluene increased several-fold with temperature.

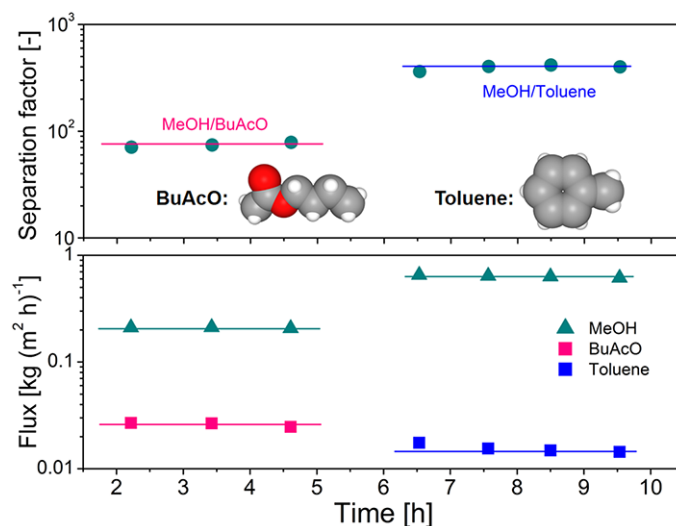


Fig. 4-14. Performance of the PV removal of methanol from MeOH/x mixtures at 50 °C (MeOH weight percentage of feed side maintained at 10%, x = BuAcO and toluene).

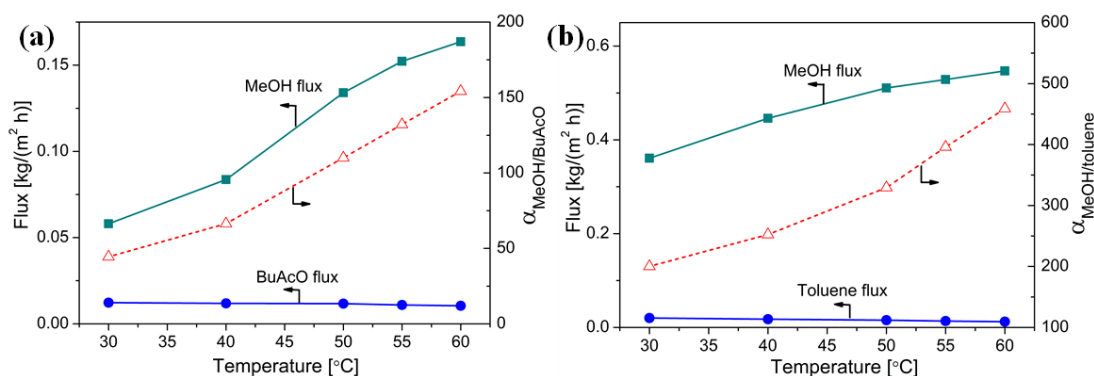


Fig. 4-15. Effect of operating temperature on fluxes and separation factors (α) for PV separation of (a) MeOH/BuAcO (10/90, wt%) and (b) MeOH/toluene (9/91, wt%) mixtures

Fig. 4-16 summarizes the PV separation performance of MeOH/BuAcO and MeOH/toluene using TiPCS membranes together with polymeric membranes under similar test conditions. Our TiPCS membranes displayed attractive performance in the separation of MeOH/BuAcO mixture systems (e.g., total flux = 0.18 kg/(m² h), α = 154 at 60 °C) and MeOH/toluene mixture systems (e.g., total flux = 0.56 kg/(m² h), α

= 460 at 60 °C) compared with the polymeric membranes. The TiPCS membrane has a unique and stable TiOSiC sub-nanopore structure and proved to be a promising candidate for methanol separation from organic solvent systems. It is worth noting that two TiPCS membranes had similar separation performances for the PV separation of MeOH/BuAcO and MeOH/toluene mixtures at 50 °C as shown in Table 4-3, which again confirmed the reproducibility of the TiPCS membrane performance.

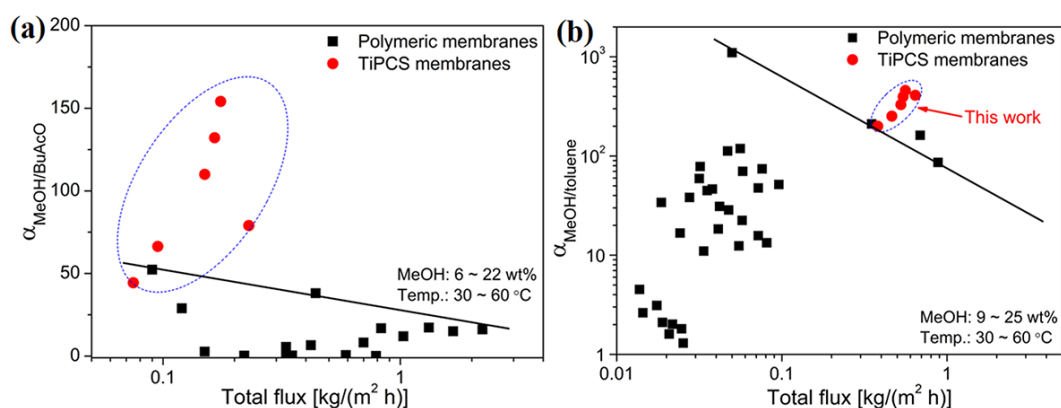


Fig. 4-16. Comparing the separations of (a) MeOH/BuAcO and (b) MeOH/toluene under similar test conditions for PV membranes (polymeric membranes [57, 59, 66-71] and this work).

Table 4-3 Pervaporation performance at 50 °C in terms of total flux and separation factor for TiPCS membranes.

Membrane	MeOH/BuAcO system			MeOH/Toluene system		
	MeOH in feed [wt%]	Total flux [kg/(m ² h)]	Separation factor	MeOH in feed [wt%]	Total flux [kg/(m ² h)]	Separation factor
TiPCS-1	10	0.24	79	10	0.643	410
TiPCS-2	10	0.15	110	9	0.526	330

4.3.5 H₂O/N₂ separation at high temperature

The H₂O/N₂ separation is an interesting and challenging issue, particularly under high temperatures, since the membrane must be able to withstand these harsh conditions. Silica (SiO₂) microporous membranes have been extensively investigated and have generally shown high performance, but their performances have been poor under a hydrothermal atmosphere since only a few hours of exposure in steam caused severe densification, particularly at high temperatures [3]. Recently, our group reported an organosilica membrane (BTESE) for the separation of steam/non-condensable gas mixtures at moderate temperatures ranging from 80 to 200 °C. When used at high temperatures, however, the effectiveness of organosilica membranes is limited due to decomposition of the organic linking units [29]. SiC-based membranes are expected to be more hydrothermally stable than SiO₂ and organosilica membranes due to the incorporation of carbon elements in the silica structure [27].

TiPCS membranes have good hydrothermal stability under moderate temperatures, which is a hallmark of PV performance. Hydrothermal stability of membranes at high temperature, however, is a significant and challenging issue. Fig. 4-17a shows the time courses of gas permeance and H₂O/N₂ selectivity for a cured TiPCS membrane (M-3%-2) under hydrothermal conditions (300 °C, an equimolar H₂O/N₂ mixture (50 kPa: 50 kPa)). During the initial ~3.5 h period, the permeance of H₂O slightly increased from 1.36×10^{-6} mol/(m² s Pa) to $\sim 1.64 \times 10^{-6}$ mol/(m² s Pa),

while the permeance of N₂ gradually decreased from 1.33×10^{-7} mol/(m² s Pa) to $\sim 4 \times 10^{-8}$ mol/(m² s Pa). As a result, the selectivity of H₂O/N₂ increased significantly from 14 to 40, and then both the permeance and selectivity reached a steady state. The decrease in N₂ permeance can be ascribed to capillary-condensed water and/or surface hydroxylation. As is well known, capillary condensation is prone to occur at low temperatures or under a high relative pressure of water vapor. At higher temperatures, therefore, a larger partial pressure of water is required. In this case, the decreased N₂ permeance at a high temperature of 300 °C and the low partial pressure (50 kPa) of water was likely caused by the gradual generation of -OH (Si-OH) groups on the surface of the membrane pores, which would increase the affinity and permeance of small H₂O molecule (0.296 nm), but N₂ (0.36 nm) permeation through the pores was inhibited by the Si-OH groups and/or the adsorbed H₂O [27, 72]. In the absence of water, the N₂ permeance was slightly decreased due to the presence of hydroxyl, and after the membrane was dried at 500 °C for 3 h, the N₂ permeance had almost completely recovered, which suggests the pore structure of the membrane was unchanged. This indicates that -OH (Si-OH) groups could be removed following the high-temperature drying process [72]. This result agrees with the findings in experiments using carbonized-template molecular sieve silica membranes (CTMSS, a carbon modified membrane) under hydrothermal conditions (400 °C, steam: 34 kPa) [72, 73], in which, the gas permeance was recovered after a drying (regeneration) process of the membranes at 500 °C by the removal of -OH groups [73]. In this case, the hydrothermal stability was also confirmed by measuring the molecular size

dependence of gas permeance before and after the “steam-treatment-then-drying” process, as shown in Fig. 4-17b. The gas permeance showed almost no change, which again suggested that there was no significant change in the pore channels of the TiPCS membranes that have a structure densification that differs from that of silica membranes. The cross-linked TiPCS membranes have stable hydrothermal stability, which is assisted by the inherent stability of the TiOSiC network structure. Moreover, our TiPCS membrane could be a promising candidate for gas dehumidification for use in membrane contactor systems since it meets the requirements for an air-drying contactor: [29, 74] high water-vapor permeability, high H₂O/N₂ selectivity, high hydrothermal stability, and mechanical stability.

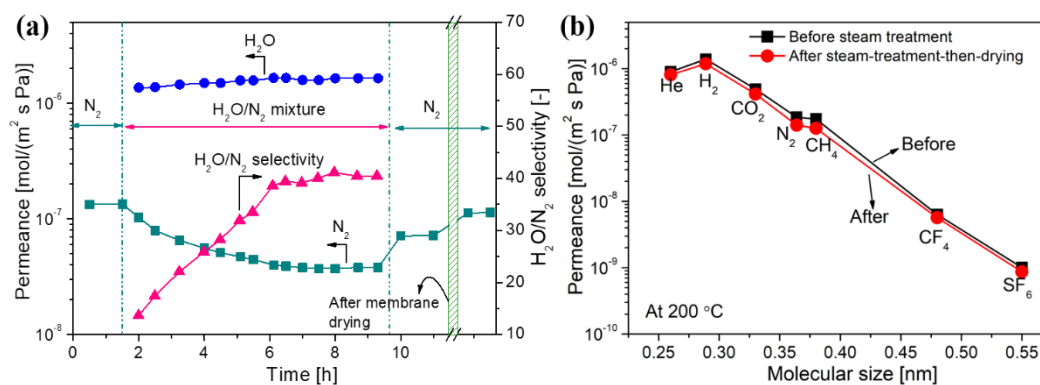


Fig. 4-17. (a) Time course of H₂O steam treatment for a cured TiPCS membrane (M-3%-2) in an equimolar H₂O/N₂ mixture (50 kPa: 50 kPa) at 300 °C, (b) comparing the single-gas permeance at 200 °C of the cured TiPCS membrane (M-3%-2) before and after the “steam-treatment-then-drying” process.

4.4 Conclusions

TiPCS-derived membranes were fabricated using a superior commercial heat-resistant precursor, polytitanocarboasilane. The effects that thermal-oxidative cross-linking exerted on the ceramic yield, thermal stability, oxidation resistance, and microstructure of TiPCS were investigated. We found that the pore formation behavior induced by the cross-linking process of TiPCS chains was closely related to the gas permeation properties in SiC-based membranes. Moreover, the influence of the concentration of the TiPCS precursor coating solution was also studied to optimize the performance of the membrane. The main conclusions are as follows:

- (1) The cross-linking degree reached a maximum value following air curing for 2 h, and the cross-linked powders showed a ceramic yield and thermal stability that were both higher than that of the non-cross-linked versions. The cross-linking behavior enhanced the stability of the pore structure.
- (2) The cross-linked TiPCS membranes had excellent permeation properties (such as H₂/SF₆ selectivity, >10,000, and N₂/SF₆, 1,500, together with high H₂ permeance of 1.49×10⁻⁶ mol/(m² s Pa)) and showed a higher level of oxidation resistance than the non-cross-linked versions. Furthermore, the cross-linked membrane with sub-nanopores demonstrated great performance for the PV removal of methanol from both MeOH/BuAcO and MeOH/toluene systems.
- (3) The cross-linked membranes showed high hydrothermal stability together with an H₂O permeance of 1.64×10⁻⁶ mol/(m² s Pa) and a high H₂O/N₂ selectivity of 40 in

an equimolar H₂O/N₂ mixture (50 kPa: 50 kPa) at 300 °C, and the surface hydroxylation in membrane pores could be the dominant factor to enhance H₂O permeance and block N₂. The cross-linked TiPCS membrane is a promising candidate for gas dehumidification in membrane contactor systems that must operate at high temperatures.

References

- [1] N. Moriyama, H. Nagasawa, M. Kanezashi, T. Tsuru, Pervaporation dehydration of aqueous solutions of various types of molecules via organosilica membranes: Effect of membrane pore sizes and molecular sizes, *Sep. Purif. Technol.*, 207 (2018) 108-115.
- [2] A. Kayvani Fard, G. McKay, A. Buekenhoudt, H. Al Sulaiti, F. Motmans, M. Khraisheh, M. Atieh, Inorganic membranes: Preparation and application for water treatment and desalination, *Materials*, 11 (2018) 74.
- [3] T. Tsuru, Silica-Based Membranes with Molecular-Net-Sieving Properties: Development and Applications, *J. Chem. Eng. Jpn.*, 51 (2018) 713-725.
- [4] M. Kanezashi, H. Sazaki, H. Nagasawa, T. Yoshioka, T. Tsuru, Preparation and gas permeation properties of thermally stable organosilica membranes derived by hydrosilylation, *Journal of Materials Chemistry A*, 2 (2014) 672-680.
- [5] V. Proust, M.C. Bechelany, R. Ghisleni, M.-F. Beaufort, P. Miele, S. Bernard, Polymer-derived Si-C-Ti systems: From titanium nanoparticle-filled polycarbosilanes to dense monolithic multi-phase components with high hardness, *J. Eur. Ceram. Soc.*, 36 (2016) 3671-3679.
- [6] M. Facciotti, V. Boffa, G. Magnacca, L.B. Jørgensen, P.K. Kristensen, A. Farsi, K. König, M.L. Christensen, Y. Yue, Deposition of thin ultrafiltration membranes on commercial SiC microfiltration tubes, *Ceram. Int.*, 40 (2014) 3277-3285.
- [7] M. Shibuya, T. Yamamura, Characteristics of a continuous Si-Ti-C-O fibre with

- low oxygen content using an organometallic polymer precursor, *JMatS*, 31 (1996) 3231-3235.
- [8] T.-E. Kim, K.-E. Khishigbayar, K.Y. Cho, Effect of heating rate on the properties of silicon carbide fiber with chemical-vapor-cured polycarbosilane fiber, *Journal of Advanced Ceramics*, 6 (2017) 59-66.
- [9] H.M. Williams, E.A. Dawson, P.A. Barnes, B. Rand, R.M.D. Brydson, A.R. Brough, High temperature ceramics for use in membrane reactors: the development of microporosity during the pyrolysis of polycarbosilanes, *J. Mater. Chem.*, 12 (2002) 3754-3760.
- [10] X. Zhong, X. Pei, Y. Miao, L. He, Q. Huang, Accelerating the crosslinking process of hyperbranched polycarbosilane by UV irradiation, *J. Eur. Ceram. Soc.*, 37 (2017) 3263-3270.
- [11] R.A. Wach, M. Sugimoto, M. Yoshikawa, Formation of Silicone Carbide Membrane by Radiation Curing of Polycarbosilane and Polyvinylsilane and its Gas Separation up to 250°C, *J. Am. Ceram. Soc.*, 90 (2007) 275-278.
- [12] A. Takeyama, M. Sugimoto, M. Yoshikawa, Gas Permeation Property of SiC Membrane Using Curing of Polymer Precursor Film by Electron Beam Irradiation in Helium Atmosphere, *Materials Transactions*, advpub (2011) 1276-1280.
- [13] Y.L. Li, H. Fan, D. Su, C. Fasel, R. Riedel, Synthesis, structures, and properties of bulk Si(O)C ceramics from polycarbosilane, *J. Am. Ceram. Soc.*, 92 (2009) 2175-2181.

- [14] R.A. Wach, M. Sugimoto, A. Idesaki, M. Yoshikawa, Molecular sieve SiC-based membrane for hydrogen separation produced by radiation curing of preceramic polymers, *Materials Science and Engineering: B*, 140 (2007) 81-89.
- [15] L. Zhongyang, K. Kusakabe, S. Morooka, Preparation of thermostable amorphous Si-C-O membrane and its application to gas separation at elevated temperature, *J. Membr. Sci.*, 118 (1996) 159-168.
- [16] B. Elyassi, W.X. Deng, M. Sahimi, T.T. Tsotsis, On the Use of Porous and Nonporous Fillers in the Fabrication of Silicon Carbide Membranes, *Industrial & Engineering Chemistry Research*, 52 (2013) 10269-10275.
- [17] S. Dabir, W.X. Deng, M. Sahimi, T. Tsotsis, Fabrication of silicon carbide membranes on highly permeable supports, *J. Membr. Sci.*, 537 (2017) 239-247.
- [18] J. Hong, K.-Y. Cho, D.-G. Shin, J.-I. Kim, D.-H. Riu, Room temperature reaction of polycarbosilane with iodine under different atmospheres for polymer-derived silicon carbide fibres, *RSC Advances*, 5 (2015) 83847-83856.
- [19] T. Ishikawa, H. Yamaoka, Y. Harada, T. Fujii, T. Nagasawa, A general process for in situ formation of functional surface layers on ceramics, *Nature*, 416 (2002) 64-67.
- [20] K. Suzuki, K. Kumagawa, T. Kamiyama, M. Shibuya, Characterization of the medium-range structure of Si-Al-C-O, Si-Zr-C-O and Si-Al-C Tyranno fibers by small angle X-ray scattering, *JMatS*, 37 (2002) 949-953.
- [21] Q. Wang, Y. Kawano, L. Yu, H. Nagasawa, M. Kanezashi, T. Tsuru, Development of high-performance sub-nanoporous SiC-based membranes derived from

- polytitanocarbosilane, *J. Membr. Sci.*, 598 (2020) 117688.
- [22] X. Zhen, X. Pei, Y. Wang, X. Zhong, L. He, Z. Chai, Z. Huang, Q. Huang, Crosslinking kinetics of polycarbosilane precursor in ozone atmosphere and the formation mechanism of continuous hollow SiC fiber, *J. Eur. Ceram. Soc.*, 39 (2019) 2028-2035.
- [23] X. Yu, H. Nagasawa, M. Kanezashi, T. Tsuru, Improved thermal and oxidation stability of bis (triethoxysilyl) ethane (BTESE)-derived membranes, and their gas-permeation properties, *Journal of Materials Chemistry A*, 6 (2018) 23378-23387.
- [24] L. Yu, M. Kanezashi, H. Nagasawa, M. Guo, N. Moriyama, K. Ito, T. Tsuru, Tailoring Ultramicroporosity To Maximize CO₂ Transport within Pyrimidine-Bridged Organosilica Membranes, *ACS Applied Materials & Interfaces*, 11 (2019) 7164-7173.
- [25] M. Thommes, K. Kaneko, A.V. Neimark, J.P. Olivier, F. Rodriguez-Reinoso, J. Rouquerol, K.S.W. Sing, Physisorption of gases, with special reference to the evaluation of surface area and pore size distribution (IUPAC Technical Report), *Pure Appl. Chem.*, 87 (2015) 1051-1069.
- [26] L. Yu, M. Kanezashi, H. Nagasawa, J. Oshita, A. Naka, T. Tsuru, Pyrimidine-bridged organoalkoxysilane membrane for high-efficiency CO₂ transport via mild affinity, *Sep. Purif. Technol.*, 178 (2017) 232-241.
- [27] M. Kanezashi, H. Sazaki, H. Nagasawa, T. Yoshioka, T. Tsuru, Evaluating the gas permeation properties and hydrothermal stability of organosilica membranes

- under different hydrosilylation conditions, *J. Membr. Sci.*, 493 (2015) 664-672.
- [28] H. Inde, M. Kanezashi, H. Nagasawa, T. Nakaya, T. Tsuru, Tailoring a Thermally Stable Amorphous SiOC Structure for the Separation of Large Molecules: The Effect of Calcination Temperature on SiOC Structures and Gas Permeation Properties, *ACS Omega*, 3 (2018) 6369-6377.
- [29] N. Moriyama, H. Nagasawa, M. Kanezashi, T. Tsuru, Selective water vapor permeation from steam/non-condensable gas mixtures via organosilica membranes at moderate-to-high temperatures, *J. Membr. Sci.*, 589 (2019) 117254.
- [30] Z. Yu, L. Yang, H. Min, P. Zhang, A. Liu, R. Riedel, High-ceramic-yield precursor to SiC-based ceramic: A hyperbranched polytitaniumcarbosilane bearing self-catalyzing units, *J. Eur. Ceram. Soc.*, 35 (2015) 851-858.
- [31] S. Yajima, T. Iwai, T. Yamamura, K. Okamura, Y. Hasegawa, Synthesis of a polytitanocarbosilane and its conversion into inorganic compounds, *JMatS*, 16 (1981) 1349-1355.
- [32] M. Narisawa, T. Kawai, S. Watase, K. Matsukawa, A. Iwase, Synthesis of photoluminescent Si–O–C(–H) ceramics from oxidation-cured polycarbosilane by hydrogen decarbonization, *Mater. Lett.*, 110 (2013) 49-52.
- [33] M.S. Bazarjani, M.M. Muller, H.J. Kleebe, C. Fasel, R. Riedel, A. Gurlo, In situ formation of tungsten oxycarbide, tungsten carbide and tungsten nitride nanoparticles in micro- and mesoporous polymer-derived ceramics, *Journal Of Materials Chemistry A*, 2 (2014) 10454-10464.

- [34] S. Yajima, J. Hayashi, M. Omori, Continuous silicon carbide fiber of high tensile strength, *Chem. Lett.*, 4 (1975) 931-934.
- [35] L.-L. Lee, D.-S. Tsai, Synthesis and Permeation Properties of Silicon–Carbon-Based Inorganic Membrane for Gas Separation, *Industrial & Engineering Chemistry Research*, 40 (2001) 612-616.
- [36] C. Schitco, M.S. Bazarjani, R. Riedel, A. Gurlo, NH₃-assisted synthesis of microporous silicon oxycarbonitride ceramics from preceramic polymers: a combined N₂ and CO₂ adsorption and small angle X-ray scattering study, *Journal of Materials Chemistry A*, 3 (2015) 805-818.
- [37] M. Rungta, G.B. Wenz, C. Zhang, L. Xu, W. Qiu, J.S. Adams, W.J. Koros, Carbon molecular sieve structure development and membrane performance relationships, *Carbon*, 115 (2017) 237-248.
- [38] G. Li, H.R. Lee, H. Nagasawa, M. Kanezashi, T. Yoshioka, T. Tsuru, Pore-size evaluation and gas transport behaviors of microporous membranes: An experimental and theoretical study, *AIChE J.*, 61 (2015) 2268-2279.
- [39] M. Kanezashi, M. Murata, H. Nagasawa, T. Tsuru, Fluorine Doping of Microporous Organosilica Membranes for Pore Size Control and Enhanced Hydrophobic Properties, *ACS Omega*, 3 (2018) 8612-8620.
- [40] M. Drobek, J. Motuzas, M. van Loon, R.W.J. Dirrix, R.A. Terpstra, A. Julbe, Coupling microwave-assisted and classical heating methods for scaling-up MFI zeolite membrane synthesis, *J. Membr. Sci.*, 401 (2012) 144-151.
- [41] Q. Wang, A. Wu, S. Zhong, B. Wang, R. Zhou, Highly (*h0h*)-oriented silicalite-1

- membranes for butane isomer separation, *J. Membr. Sci.*, 540 (2017) 50-59.
- [42] H. Suda, H. Yamauchi, Y. Uchimaru, I. Fujiwara, K. Haraya, Structural Evolution during Conversion of Polycarbosilane Precursor into Silicon Carbide-Based Microporous Membranes, *J. Ceram. Soc. Jpn.*, 114 (2006) 539-544.
- [43] B.-K. Sea, K. Ando, K. Kusakabe, S. Morooka, Separation of hydrogen from steam using a SiC-based membrane formed by chemical vapor deposition of triisopropylsilane, *J. Membr. Sci.*, 146 (1998) 73-82.
- [44] R.M. Prasad, Y. Jüttke, H. Richter, I. Voigt, R. Riedel, A. Gurlo, Mechanism of Gas Separation through Amorphous Silicon Oxycarbide Membranes *Adv. Eng. Mater.*, 18 (2016) 721-727.
- [45] C.C. Chao, D.S. Tsai, Si-Al-C gas separation membranes derived from polydimethylsilane and aluminum acetylacetonate, *J. Membr. Sci.*, 192 (2001) 209-216.
- [46] Z. Li, K. Kusakabe, S. Morooka, Pore Structure and Permeance of Amorphous Si-C-O Membranes with High Durability at Elevated Temperature, *Sep. Sci. Technol.*, 32 (1997) 1233-1254.
- [47] L.-L. Lee, D.-S. Tsai, A Hydrogen-Permeable Silicon Oxycarbide Membrane Derived from Polydimethylsilane, *J. Am. Ceram. Soc.*, 82 (1999) 2796-2800.
- [48] T. Nagano, K. Sato, T. Saitoh, Y. Iwamoto, Gas Permeation Properties of Amorphous SiC Membranes Synthesized from Polycarbosilane without Oxygen-Curing Process, *J. Ceram. Soc. Jpn.*, 114 (2006) 533-538.
- [49] C.L. Chen, D.S. Tsai, Permeation properties of microporous membranes prepared

- via coating of evaporated polydimethylsilane, *J. Membr. Sci.*, 237 (2004) 163-165.
- [50] K. Kusakabe, Z. Yan Li, H. Maeda, S. Morooka, Preparation of supported composite membrane by pyrolysis of polycarbosilane for gas separation at high temperature, *J. Membr. Sci.*, 103 (1995) 175-180.
- [51] V. Sebastian, R. Mallada, J. Coronas, A. Julbe, R.A. Terpstra, R.W.J. Dirrix, Microwave-assisted hydrothermal rapid synthesis of capillary MFI-type zeolite–ceramic membranes for pervaporation application, *J. Membr. Sci.*, 355 (2010) 28-35.
- [52] Y. Sugiyama, S. Ikarugi, K. Oura, A. Ikeda, E. Matsuyama, R. Ono, M. Nomura, H. Tawarayama, T. Saito, K. Kuwahara, MFI Zeolite Membranes Prepared on Novel Silica Substrates, *J. Chem. Eng. Jpn.*, 48 (2015) 891-896.
- [53] Y. Yue, Synthesis of silicon carbide fibers from polycarbosilane by electrospinning method, (2014).
- [54] H.M. Williams, E.A. Dawson, P.A. Barnes, B. Rand, R.M. Brydson, The development and stability of porosity formed during the pyrolysis of polyborodiphenylsiloxane, *Microporous Mesoporous Mater.*, 99 (2007) 261-267.
- [55] H.Q. Ly, R. Taylor, R. Day, F. Heatley, Conversion of polycarbosilane (PCS) to SiC-based ceramic Part II Pyrolysis and characterisation, *JMatS*, 36 (2001) 4045-4057.
- [56] J. Lipowitz, H. Freeman, R. Chen, E. Prack, Composition and structure of ceramic fibers prepared from polymer precursors, *Advanced Ceramic*

Materials;(USA), 2 (1987).

- [57] N. Avagimova, G. Polotskaya, N. Saprykina, A. Toikka, Z. Pientka, Mixed Matrix Membranes Based on Polyamide/Montmorillonite for Pervaporation of Methanol–Toluene Mixture, *Sep. Sci. Technol.*, 48 (2013) 2513-2523.
- [58] X. Tong-Hu, X. Xiao-Li, Q. Hai-Jiao, Y. Xiao-Gang, Z. Rui-Feng, Zeolite 4A-Incorporated Polymeric Membranes for Pervaporation Separation of Methanol-Methyl Acetate Mixtures, *Journal of Inorganic and Organometallic Polymers and Materials*, 21 (2011) 816-822.
- [59] P. Luis, J. Degrève, B. Van der Bruggen, Separation of methanol–n-butyl acetate mixtures by pervaporation: potential of 10 commercial membranes, *J. Membr. Sci.*, 429 (2013) 1-12.
- [60] J. Abraham, T. Jose, G. Moni, S.C. George, N. Kalarikkal, S. Thomas, Ionic liquid modified multiwalled carbon nanotube embedded styrene butadiene rubber membranes for the selective removal of toluene from toluene/methanol mixture via pervaporation, *Journal of the Taiwan Institute of Chemical Engineers*, 95 (2019) 594-601.
- [61] M.E. van Leeuwen, Derivation of Stockmayer potential parameters for polar fluids, *Fluid Phase Equilib.*, 99 (1994) 1-18.
- [62] B. Van der Bruggen, J. Schaep, D. Wilms, C. Vandecasteele, Influence of molecular size, polarity and charge on the retention of organic molecules by nanofiltration, *J. Membr. Sci.*, 156 (1999) 29-41.
- [63] F. Zheng, C. Li, Q. Yuan, F. Vriesekoop, Influence of molecular shape on the

- retention of small molecules by solvent resistant nanofiltration (SRNF) membranes: A suitable molecular size parameter, *J. Membr. Sci.*, 318 (2008) 114-122.
- [64] J. BURKE, Solubility parameters-Theory and application, *The AIC book and paper group annual*, 3 (1984) 13-58.
- [65] C.M. Hansen, Hansen solubility parameters: a user's handbook, CRC press, 2002.
- [66] P. Garg, R.P. Singh, V. Choudhary, Pervaporation separation of organic azeotrope using poly(dimethyl siloxane)/clay nanocomposite membranes, *Sep. Purif. Technol.*, 80 (2011) 435-444.
- [67] J. Tang, K.K. Sirkar, S. Majumdar, Permeation and sorption of organic solvents and separation of their mixtures through an amorphous perfluoropolymer membrane in pervaporation, *J. Membr. Sci.*, 447 (2013) 345-354.
- [68] M. Zhou, M. Persin, J. Sarrazin, Methanol removal from organic mixtures by pervaporation using polypyrrole membranes, *J. Membr. Sci.*, 117 (1996) 303-309.
- [69] N.R. Singha, S.K. Ray, Separation of Toluene-Methanol Mixtures by Pervaporation Using Semi-IPN Polymer Membranes, *Sep. Sci. Technol.*, 45 (2010) 2298-2307.
- [70] R.Y.M. Huang, G.Y. Moon, R. Pal, N-acetylated chitosan membranes for the pervaporation separation of alcohol/toluene mixtures, *J. Membr. Sci.*, 176 (2000) 223-231.
- [71] N.R. Singha, S.B. Kuila, P. Das, S.K. Ray, Separation of toluene-methanol

- mixtures by pervaporation using crosslink IPN membranes, *Chemical Engineering and Processing: Process Intensification*, 48 (2009) 1560-1565.
- [72] M.C. Duke, J.D. Da Costa, D.D. Do, P.G. Gray, G.Q. Lu, Hydrothermally robust molecular sieve silica for wet gas separation, *Adv. Funct. Mater.*, 16 (2006) 1215-1220.
- [73] M. Duke, J.D. Da Costa, G.M. Lu, M. Petch, P. Gray, Carbonised template molecular sieve silica membranes in fuel processing systems: permeation, hydrostability and regeneration, *J. Membr. Sci.*, 241 (2004) 325-333.
- [74] V. Usachov, N. Laguntsov, A. Okunev, V. Teplyakov, S. Glukhov, Experimental study of the membrane contactor systems for gas dehumidification, *Ars Separatoria Acta*, (2003) 36-46.

Chapter 5

Conclusions

5.1 Summary of this study

The overall of this dissertation research is focused on the development and microstructure tuning of SiC-based membranes for gas separation and PV application. Two types of preceramic precursors; PCS and TiPCS were chosen for the fabrication of SiC-based membranes and Ti-containing SiC-based membranes, respectively. Conventional SiC-based membranes derived from PCS are mainly used for H₂/N₂ separation due to their narrow and small pore sizes. However, few studies have investigated the microporosity of ceramic products pyrolyzed at moderate temperatures (350-800 °C), and the relationship between the microporous structure and curing process for molecular separation remains unclear. In addition, Ti-containing SiC-based ceramics have many superior properties, however, the research on them is limited to fibers and bulk ceramics at high temperatures ($\geq 1,000$ °C). Here, we are the first to propose the fabrication of SiC-based membranes to obtain sub-nanopores by doping with Ti for molecular separation of small/mid-sized molecules from large molecules.

The main conclusions in this thesis were summarized according to each chapter as follows:

First, we started from the most commonly preceramic polymer of PCS for the

formation of SiC-based membranes. The main interest was focused on tuning the microstructure of the PCS-derived membranes via air-curing temperature. The elemental composition and microstructure of the final ceramic material could be precisely tailored via the air curing process. The most promising PCS-derived membranes, which were cured at 250 °C and then pyrolyzed at 750 °C, had high thermal stability and oxidation resistance at 500 °C in addition to excellent permeation properties: H₂ permeance of $1-2 \times 10^{-6}$ mol/(m² s Pa) at 500 °C with H₂/N₂ selectivity of 31 and H₂/C₃H₈ selectivity of 1,740; and, CO₂ permeance of 1.8×10^{-6} mol/(m² s Pa) at 27 °C with CO₂/CH₄ selectivity of 40. This is the first study to propose the concept of tailoring the microstructure of SiC-based membranes by controlling the curing process.

Based on the investigation and experience of PCS-derived membranes, we describe the first use of Ti-incorporated PCS precursor (TiPCS), which is known as a precursor of continuous Si-Ti-C-O fibers (Tyranno), in the preparation of titanium-incorporated SiC-based membranes for the gas separation and PV removal of water or methanol. The dependence of the polymer-to-ceramic transformation process of TiPCS on pyrolysis temperature was systematically investigated. The pore characteristics and the surface areas of TiPCS-derived ceramic powders were strongly dependent on the pyrolysis temperatures. The evolution of the network structure of TiPCS during the pyrolysis process began with a dense polymer structure (≤ 350 °C) that was then passed through a loose transitional structure (350-650 °C), and then transformed into a relatively denser ceramic structure (> 650 °C). Additionally, the

titanium components in TiPCS effectively inhibited and/or reduced the densification of the network structures at elevated temperatures. The network structure of TiPCS-derived SiC-based membranes showed trends similar to those of TiPCS-derived ceramic powders. The membrane prepared at 750 °C featured sub-nanopores, reproducibility, and attractive selectivities (H_2/SF_6 , 16,600; and N_2/SF_6 , 2,100) with a high H_2 permeance at a magnitude of $10^{-6} \text{ mol}/(\text{m}^2 \text{ s Pa})$. These SiC-based membranes demonstrated great potential for the separation of small and mid-sized molecules from large molecules such as N_2/SF_6 separation and PV removal of water or methanol from liquid mixtures. The TiPCS membranes exhibited separation performance for methanol/methyl acetate mixtures with a total flux of $0.38 \text{ kg}/(\text{m}^2 \text{ h})$ and a methanol/methyl acetate separation factor of 35 for 10 wt% MeOH in a MeOH/MeOAc binary mixture at 60 °C.

Additionally, special attention was focused on a process of thermal-oxidative curing that was used to induce cross-linking and the effect of this process on the ceramic yield, thermal stability, oxidation resistance, and microstructure of TiPCS. The cross-linked TiPCS powders showed a ceramic yield and thermal stability that were higher than that from the non-cross-linked version. In addition, the cross-linked TiPCS with uniform micropores showed higher levels of N_2 and CO_2 adsorption capacity, BET surface area, and micropore volume than the non-cross-linked versions, and the cross-linking process enhanced the stability of the pore structure at high temperatures. The pore formation behavior induced by the cross-linking process of TiPCS chains was closely related to the gas permeation properties in SiC-based

membranes. The cross-linked TiPCS membranes showed higher oxidation resistance than their non-cross-linked counterparts at 300 °C under air. Furthermore, the influence of the concentration of the TiPCS precursor coating solution was optimized. The cross-linked, optimized membranes demonstrated great performance for the pervaporation removal of methanol in binary azeotropic systems of either MeOH/butyl acetate or MeOH/toluene. Moreover, the membranes showed high hydrothermal stability together with an H₂O permeance of 1.64×10^{-6} mol/(m² s Pa) and a high H₂O/N₂ selectivity of 40 in an equimolar H₂O/N₂ mixture (50 kPa: 50 kPa) at 300 °C. The TiPCS membrane is a promising candidate for gas dehumidification in membrane contactor systems that must operate at high temperatures.

5.2 Recommendations

Membrane separation process has become one of the emerging technologies that undergo a rapid growth for the past few decades. The development of advanced membranes for molecular separation with excellent separation performances, a simple fabrication process, and low-cost is always being pursued by membrane developers. The main interest of this thesis was focused on tuning the microstructure and development of SiC-based membranes. For the conventional SiC-based membranes derived from PCS, this is the first study to propose the concept of tailoring the microstructure of SiC-based membranes by controlling the curing process. The optimized PCS-derived membranes achieved satisfactory separation performance,

which is not limited to H_2/N_2 separation but also revealed superior separation performance for the H_2/C_3H_8 and CO_2/CH_4 separations. Furthermore, we describe the first use of Ti-incorporated PCS precursor (TiPCS) in the preparation of titanium-incorporated SiC-based membranes that consisted of sub-nanopores for the gas separation and PV removal of water or methanol. The effects of pyrolysis temperature and air curing on the evolution of the pore structures as well as the physicochemical properties of TiPCS were thoroughly investigated. The optimized Ti-containing membranes with sub-nanopores demonstrated great performance for the pervaporation removal of methanol or water and it also showed high hydrothermal stability with excellent dehumidification performance under high temperatures.

This thesis has contributed an interesting topic about that the high separation performance which could be obtained by adjusting the pore size of the SiC-based membranes, could make SiC-based membranes suitable for separation not limited to H_2/N_2 separation but also in the separation of small and mid-sized molecules from large molecules.

Based on the results and conclusions derived from this thesis, the recommendations for further work are given as follows:

(1) High-performance SiC-based membranes derived from traditional PCS have been developed, but the detailed separation properties of different systems are not yet clear, such as CO_2/CH_4 separation and PV dehydration, etc. Furthermore, the application of PCS-derived membranes in membrane reactors such as propane dehydrogenation is a topic worthy of further investigation.

(2) Ti-containing SiC-based membranes derived from TiPCS demonstrated great potential for the separation of small and mid-sized molecules from large molecules, however, the separation of high-temperature steam by TiPCS-derived membranes requires more extensive investigation. Moreover, this work also provides a reference for the development of SiC-based membranes doped with different metal elements.

List of Publications

Published Papers:

- [1] **Qing Wang**, Yuta Kawano, Liang Yu, Hiroki Nagasawa, Masakoto Kanezashi, Toshinori Tsuru*, Development of high-performance sub-nanoporous SiC-based membranes derived from polytitanocarbosilane, *Journal of Membrane Science*, 2020;598:117688.
- [2] **Qing Wang**, Liang Yu, Hiroki Nagasawa, Masakoto Kanezashi, Toshinori Tsuru*, High-performance molecular-separation ceramic membranes derived from oxidative cross-linked polytitanocarbosilane, *Journal of the American Ceramic Society*, 2020;103:4473-4488.
- [3] **Qing Wang**, Liang Yu, Hiroki Nagasawa, Masakoto Kanezashi, Toshinori Tsuru*, Tuning the microstructure of polycarbosilane-derived SiC(O) separation membranes via thermal-oxidative cross-linking, *Separation and Purification Technology*, 2020;248:117067.
- [4] **Qing Wang**, Makato Yokoji, Hiroki Nagasawa, Masakoto Kanezashi, Toshinori Tsuru*, Microstructure evolution and enhanced permeation of SiC membranes derived from allylhydridopolycarbosilane, *Journal of Membrane Science*, in press; doi.org/10.1016/j.memsci.2020.118392.
- [5] Guanying Dong, Hiroki Nagasawa, Liang Yu, **Qing Wang**, Kazuki Yamamoto, Joji Ohshita, Masakoto Kanezashi, Toshinori Tsuru*, Pervaporation removal of methanol from methanol/organic azeotropes using organosilica membranes: experimental and modeling. *Journal of Membrane Science*, 2020;610:118284

Conference:

- [1] **Qing Wang**, Hiroki Nagasawa, Masakoto Kanezashi, Toshinori Tsuru*, Preparation and gas permeation properties of a novel SiC-based membrane, 2018 Membrane Symposium of the Membrane Society of Japan, November 13-14, 2018, Kobe, Japan. (**Poster, Best Presentation Award**)
- [2] **Qing Wang**, Mirai short course for Phd-Sustainability: “Membranes for a sustainable water cycle”, October 14-18, 2018, Hiroshima, Kyoto and Tokyo, Japan. (**Best Presentation Award**)

Acknowledgements

First and foremost, I would like to express my deep and sincere gratitude to my supervisors, Prof. Toshinori Tsuru, for his continues guidance, inspiration and encouragement throughout my PhD study. He has offered me valuable suggestions in the academic studies, and spent much time reading my drafts and provided me with inspiring advice. His encouragement and unwavering support have sustained me through frustration and depression. Moreover, he is a distinguished expert in both chemical engineering and membrane science and I am always touched and benefit a lot from his professional dedication, great enthusiasm and profound understanding in scientific research. Under his leadership, I have learned a lot not only in scientific research itself but also in the way they do scientific research and the way they deal with everyday things, which I think will provide me with lifetime benefits.

I would like to express my heartfelt gratitude to Prof. Masakoto Kanezashi, Prof. Hiroki Nagasawa, and Prof. Liang Yu for their kind assistant in my experiments, insightful discussion on my research work, and valuable suggestions in organization of journal articles. I also would like to express my sincere gratitude to Prof. Kunihiro Fukui and Prof. Takashi Ogi in my dissertation committee for reviewing my thesis in their busy schedule.

I wish to thank my tutor, Mr. Norihiro Moriyama, for his warm-hearted assistance in my research work and daily life, when I came to Japan. My sincere gratitude also goes to my colleague PhD friends, Dr. Xin Yu, Dr. Jing Xu, Dr. Guanying Dong, and Dr. Meng Guo. I would also like to thank all other group membranes in Separation Technology Lab, for their sustained help and all the good moments we spent together.

I gratefully acknowledge the financial support of the China Scholarship Council (CSC No. 201708320371), who covers my maintenance in Japan for this PhD project.

Lastly, I would like to thank my family members, and my beloved girlfriend, Mengmeng Sun, for their endless support and encouragements through the entire three-year journey.